Order Number 9432354

A computational study of the long term stability of total hip implants

Luo, Gangming, Ph.D.

City University of New York, 1994

U·M·I
300 N. Zeeb Rd.
Ann Arbor, MI 48106

A COMPUTATIONAL STUDY OF THE LONG TERM STABILITY OF TOTAL HIP IMPLANTS

BY

GANGMING LUO

A dissertation submitted to the Graduate Faculty in Engineering
in partial fulfillment of the requirements for the degree of
Doctor of Philosophy, The City University of New York

1994

This manuscript has been read and accepted for the Graduate Faculty in Engineering in satisfaction of the dissertation requirement for the degree of Doctor of Philosophy.

April 26, 1994
Date

Stephen C. Cowin
Chair of Examining Committee

4/27/94
Date

Gerard G. Stowell
Executive Officer

Professor Stephen C. Cowin

Professor Ali M. Sadegh

Dr. Harold Alexander

Professor Noshir Langrana

Professor Sheldon Weinbaum

Professor Mark C. Zimmerman

Supervisory Committee

THE CITY UNIVERSITY OF NEW YORK

ABSTRACT

A COMPUTATIONAL STUDY OF THE LONG TERM STABILITY OF TOTAL HIP IMPLANTS

by

Gangming Luo

Adviser: Professor Stephen C. Cowin and Ali M. Sadegh

The total hip replacement is the most commonly performed joint replacement. Although the technology of joint replacement has progressively evolved in the last thirty years, the problem of the long term stability (10 years or more) of hip and knee implants has not been solved. The objective of this research is to evaluate the influence of local bone remodeling at the bone-implant interface on the long term stability and load carrying capacity of the implant. The effect of the interactive temporal evolution of bone remodeling on all surfaces, the bone-implant interface as well as the periosteum and portions of the endosteum that do not contact the implant, on the long term stability of the implant is studied computationally. A set of interchangeable local computational models of contact surface structures that permit the modeling of different interfaces, such as a screw face, a sintered bead or wire mesh face, is developed. The applicability

of the model is demonstrated by applying it to basic implant designs seeking conceptual insights into the changing structural behavior of the bone implant system over time due to progressive bone remodeling.

The comparison of the numerical results and clinical observations shows that the models predict many phenomena widely observed in the clinic, such as calcar resorption, cortical bone thickening and so on.

The method of predicting the long term stability of a bone prosthesis will contribute significantly to the improved design of these prostheses and improved surgical placement procedures for implants.

ACKNOWLEDGEMENTS

I wish to express my sincere and deep appreciation to my mentors, Professor Stephen C. Cowin and Professor Ali M. Sadegh. I am truly indebted to their constant guidance, encouragement and assistance.

I would like to thank Dr. Harold Alexander for his valuable comments and suggestions on this research, as well as the members of my supervisory committee for their interests. To Robert Siffert M.D. and Dr John L. Ricci, I express my appreciation for their providing valuable information.

The financial support received from the National Science Foundation under Grants No. BSC 88-22401 and 91-03236 is gratefully appreciated.

TABLE OF CONTENTS

1. INTRODUCTION	1 - 11
1.1 Interference, initial ingrowth and micromotion	3 - 4
1.2 Methods for total hip implant studies	4 - 9
1.3 A new approach for total hip implant stability	9 - 11
2. BACKGROUND TOPICS	12 - 26
2.1 Historical notes on modeling the bone-implant interface	12 - 16
2.2 Historical notes on computational stability studies	16 - 19
2.3 Surface bone remodeling theory	20 - 26
3. STUDY OF LOCAL MODELS	27 - 40
3.1 Local models	27 - 29
3.2 Boundary conditions and initial ingrowth	29 - 34
3.3 Stress concentration near a sharp corner	34 - 37
3.4 The effect of loading on final ingrowth	38 - 40
4. LOCAL-GLOBAL FEEDBACK MODEL	41 - 58
4.1 General introduction to the model	41 - 41
4.2 Local models and databases	42 - 46
4.3 Global models	46 - 47
4.4 Conceptual framework of the local-global feedback mechanism	47 - 53
4.5 Computational implementation of the local-global	

feedback mechanism 53 - 58

5. GLOBAL MODELS EMPLOYED IN THE DISSERTATION 59 - 71

5.1 Axisymmetric global model 61 - 62

5.2 Pseudo 3-D global model without abductor force 62 - 63

5.3 Pseudo 3-D global model with abductor force 63 - 64

5.4 Dimensions in pseudo 3-D global models 64 - 68

5.5 Meshes of global models 68 - 71

6. RESULTS 72 - 94

6.1 Results of the axisymmetric global model 72 - 73

6.2 Results of the pseudo 3-D global model without abductor force 73 - 77

6.3 Results of the pseudo 3-D global model with abductor force 77 - 78

6.4 Comments on these global models 78 - 79

7. COMPARISONS WITH ANIMAL EXPERIMENTS AND CLINICAL OBSERVATIONS 95 -112

7.1 Comparisons of local models 95 - 99

7.2 Comparisons of global models 100-103

8. DISCUSSION 113-116

REFERENCES 117-122

LIST OF TABLES

Table 1:	The value of the final ingrowth distance of bone for the slot model	33
Table 2:	The numbers of elements and nodes for screw thread mode	42
Table 3:	The numbers of elements and nodes for bead thread mode	45
Table 4:	The head and abductor forces	63
Table 5:	The dimensions of pseudo 3-D global models	68
Table 6:	The three cases of screw thread interface for the axisymmetric global models	73
Table 7:	A list of thirteen cases and figure numbers for the pseudo 3-D global model without abductor force	75
Table 8:	A list of five cases and figure numbers for the pseudo 3-D global model with abductor force	76

LIST OF CHARTS AND FIGURES

Chart 1:	The local-global feedback model	50
Chart 2:	Feedback process programming	55
Figure 1:	Cross-section of a hip arthroplasty	2
Figure 2:	Schematic illustration of various idealized boundary conditions at the bone-implant interface	13
Figure 3:	The simulation of the 3-D cylindrical geometry by a 2-D model	16
Figure 4:	A plot of surface bone remodeling equation	25
Figure 5:	The screw thread model, a local model	27
Figure 6:	The slot model, a local model	28
Figure 7:	The bead or wire model, a local model	28
Figure 8:	(a) An illustration of the fixed boundary condition corresponding to zero relative displacement in the plane of the bone-implant interface	30
	(b) An illustration of the free boundary condition corresponding to zero shear stress in the plane of the bone-implant interface	30
Figure 9:	Illustrations of the bone remodeling in the slot for the fixed boundary condition at the wall with initial ingrowth of (a) 0.01 mm, (b) 0.05 mm and (c) 0.1 mm	31
Figure 10:	Illustrations of bone remodeling in a slot with initial ingrowth of 0.1 mm (a) fixed and (b) free boundary condition	32

Figure 11: An illustration of the models used to study the effect of stress concentration

(a) a perfectly sharp right angle external corner 35

(b) a rounded right angle external corner 35

Figure 12: An illustration of the depth of bony ingrowth between the screw threads 39

Figure 13: Plots of the curves representing the non-dimensionalized final ingrowth between the screw threads as a function of the applied stress σ 40

Figure 14: (a) A plot of bone ingrowth into a screw thread against time for an indentation of 0.02 mm 44

(b) A plot of bone resorption from a screw thread against time for an indentation of 0.48 mm 44

Figure 15: The maximum shear force test model 52

Figure 16: The axisymmetric global model including illustration of the loading and boundary conditions 59

Figure 17: Pseudo 3-D global model without abductor force 60

Figure 18: Pseudo 3-D global model with an abductor force 61

Figure 19: The cross-sections of a real 3-D model and a pseudo 3-D model 65

Figure 20: A coarse global mesh

(a) the mesh of bone and implant 69

(b) the mesh of side plates 69

Figure 21: A finer global mesh

(a) the mesh of bone and implant 69

(b) the mesh of side plates 69

Figure 22: Stress distribution along the medial interface of both the coarse mesh and finer mesh 70

Figure 23: Stress distribution along the lateral interface of both the coarse mesh and finer mesh 70

Figure 24: The global FEM mesh used in the dissertation

(a) mesh of bone and implant 71

(b) mesh of side plate 71

Figure 25: An illustration of the terms used in the Results section 74

Figure 26-28:

The results of the axisymmetric global model 80-81

Figures 29 to 41:

The results of the pseudo 3-D global model without abductor force 82-90

Figures 42 to 46:

The results of the pseudo 3-D global model with abductor force 91-94

Figure 47: Microradiograph showing bone ingrowth into a 24-week smooth-surfaced specimen 104

Figure 48: Back-scattered electron image of 12-week bone ingrowth into two rough-surfaced Ti channels and one HA-lined channel 105

Figure 49: Three implants were used by Carlsson et al (1986): screw, double cylinder and T-plate 106

Figure 50: Direct contact between bone and Titanium (Ti) on all sides of the screw threads 107

Figure 51 A histologic section demonstrated a relatively high degree of bone growth into almost 10% of the available pore volume 108

Figure 52: Schematic drawing showing cortical thickening two years postoperatively 109

Figure 53: Anteroposterior radiographs made soon postoperatively and one year postoperatively 110

Figure 54: (a) Clinical radiograph made immediately after *in vivo* implantation of the prosthesis shows bone of excellent quality 111

(b) The final radiograph made before the patient's death demonstrates resorptive remodeling of the lateral and medial cortices 111

Figure 55: Anteroposterior radiograph made 16 months postoperatively shows cortical thickening on lateral side clearly 112

1. INTRODUCTION

The total hip replacement is the most commonly performed joint replacement. It is estimated that about 300,000 are done annually in this country and 600,000 worldwide. Although the technology of artificial total joint replacement has progressively evolved in the last thirty years the problem of long term (10 years plus) stability has not been solved. Loosening of total hip arthroplasty (THA) has been observed in both cemented (PMMA) and cementless prostheses. The femur, the implant and various bone-implant interfaces are illustrated in Figure 1. The stability of the implant is progressively lost as the interface bond between the implant and the bone (or the cement and the bone) deteriorates.

The overall objective of this dissertation is to evaluate the influence of local bone remodeling at the bone-implant interface on the long term global stability of the implant. The effect of the interactive time evolution of bone remodeling on all surfaces, the bone-implant interface as well as the periosteum and portions of the endosteum that do not contact the implant, on the long term stability of the implant, is computationally studied in order to achieve this goal.

A review of the studies on the total hip implant, including modeling of the bone-implant interface, computational stability studies and surface bone remodeling theories, is given in Chapter 2. The approach employed in this dissertation consists of three parts: local models, global models and the local-global feedback mechanism. In this dissertation the words global and local are used to distinguish between events associated

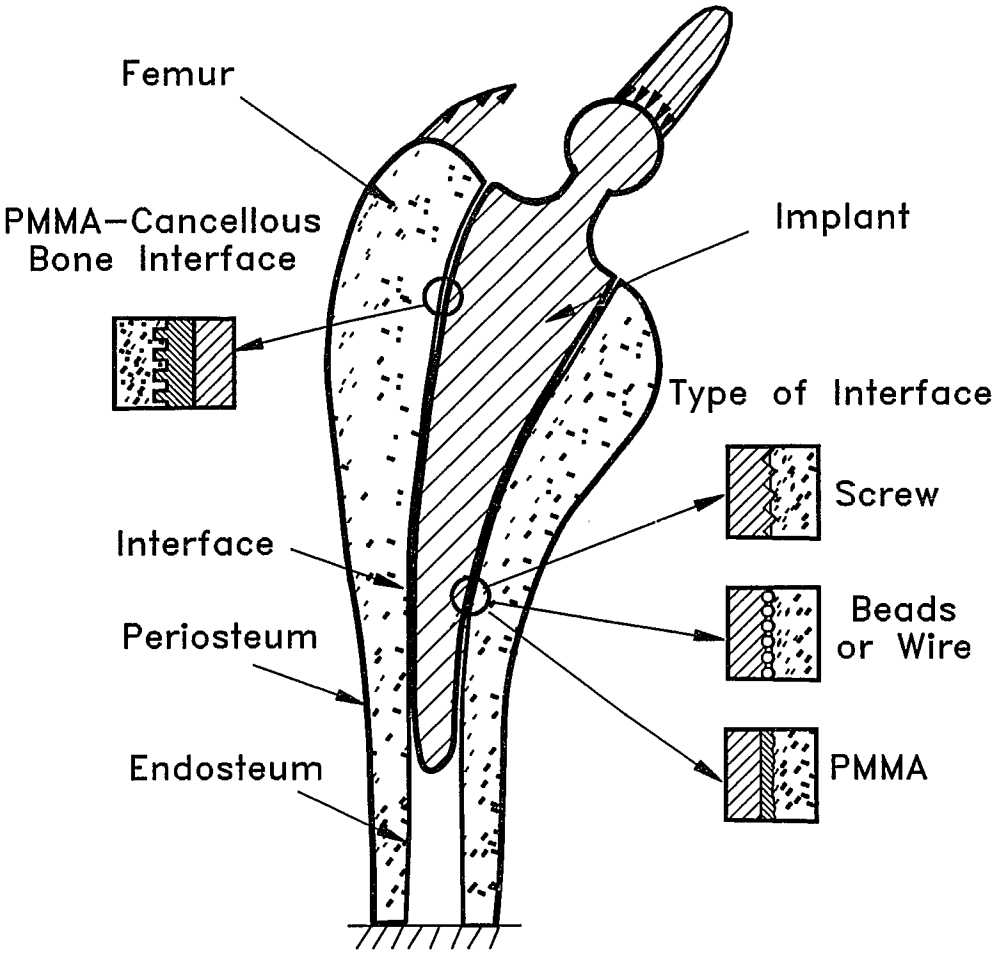

Figure 1. Cross-section of a hip arthroplasty. The femur, the implant and various interfaces are illustrated. The domain of the entire figure is referred to as the global model. The local models are represented by the various inserts illustrating models of various types of interfaces.

with the entire bone-implant system, Figure 1, and those events associated with small regions of the implant interface illustrated by inserts in Figure 1. The details of the method employed in this dissertation are discussed in Chapters 3, 4 and 5. A set of interchangeable local computational models of contact surface structures that permit the modeling of different interfaces has been constructed. Global computational models which permit the interactive time evolution of bone remodeling on all remodeling surfaces have been developed. The models have been employed to determine the long term stability and load carrying capacity of the implant. The detailed results of the dissertation are presented in Chapter 6. Comparisons of the numerical results with animal experiments and clinical observations are presented in Chapter 7, followed by a discussion.

1.1 Interference, initial ingrowth and micromotion

An implant is generally placed in bone with an initially tight fit. In this work this tight fit is called the initial interference where interference is a quantitative measure of tightness. The *interference* is a length equal to the excess of the cross-sectional dimension of the implant (or implant plus cement in a cemented hip prosthesis) over the cross-sectional dimension of the bone cavity in which the implant is currently residing, both cross-sectional dimensional lengths being measured in the same direction. Interference can vary with anatomical site due to the shape mismatch of the prosthesis with the bone cavity into which it is placed. There are two major reasons that the

loosening might occur. First, there is the possibility of too small an initial interference (Ling, 1986). Second, if significant initial interference exists, the amount of the interference may diminish in time due to bone loss at the interface. In cementless implants nonuniform bone-implant surface contact at the initial stage of placement occurs frequently because it is almost impossible to accomplish uniform contact in the placement surgery. This initial nonuniform bone-implant surface contact leads to localized areas of low and high stresses, bone resorption, and thus instability and loosening.

A second concept that is employed in this dissertation and which might be confused with interference is initial ingrowth. To describe the initial state of the implant on certain bone interfaces it is assumed there is some initial bone ingrowth into the implant cavities such as screw threads or pores on a porous surface before any external load is applied. This initial bone ingrowth is called *initial ingrowth* and is not the same as interference. The lack of interference, initial or evolved, and initial ingrowth leads to excessive *micromotion* (relative displacement between bone and implant surfaces) which can stop the formation of bone tissue and create a structurally insubstantial fibrous tissue in its place.

1.2 Methods for total hip implant studies

Traditionally, animal experiments have been employed to explore solutions and an understanding of loosening problems. Animal experiments are very expensive and

are therefore only maintained for a few years' duration at best (Maniatopoulos *et al.* 1986; Engh *et al.* 1987; and Haddad *et al.* 1990). While animal experiments can provide a reliable prediction for the overall clinical performance of new implants, they are prohibitively expensive for addressing the question of the long term (10 year plus) stability of implants. Computer modeling, on the other hand, is a reliable, inexpensive, and fast technique to predict the long term stability of implants. Many investigators have employed computer modeling to find stress, strain, and other mechanical aspects of bone and implants (Huiskes and Chao 1983; Fitzgerald 1988; Weinans 1991; Keaveny and Bartel 1991; and others).

Both internal and external bone remodeling theories have been used in computational stability studies. Internal bone remodeling means the change of bone porosity or bulk density and microstructural anisotropy, which are two of the most important parameters characterizing the internal morphology. External or surface bone remodeling refers to net bone growth or resorption, which redefines the external geometry of the structure. The studies of internal bone remodeling theories can be divided into two groups. All models assume that bone is a linear elastic material. The first group of the internal bone remodeling theories considers only bone porosity or density change. The bone density change is determined by the mechanical stimulation, e.g. strain (Cowin *et al.* 1976, Cowin 1981) or strain energy density (SED) (Fyhrie *et al.* 1986; Huiskes *et al.* 1987; Huiskes 1988 and Weinans 1991). For models in the first group, bone is often assumed to be an isotropic material. The second group of internal bone remodeling theories allows both bone density and microstructural anisotropy to

change due to the mechanical stimulation, e.g. strain state (Cowin *et al.* 1992). The microstructural anisotropy is modeled by a fabric tensor. Definitions of the fabric tensor for various porous materials are described by (Cowin 1985a; Cowin *et al.* 1991; Luo *et al.* 1991; and Sadegh *et al.* 1991). Although internal bone remodeling theories are employed by many researchers, there are problems associated with their use. One of the problems is the large minimum length scale over which the stress must be averaged in order to achieve a continuum. Harrigan *et al.* (1988) suggest that, if the results of a stress analysis "...vary by more than 20-30% over a distance spanning three to five trabeculae, the results are suspect." This restriction requires a minimum length scale of 5 mm, which is quite large. The price paid by a complete remodeling theory that incorporates an internal remodeling rate equation is not only the penalty of a large minimum length scale below which the theory is inapplicable (Cowin, 1989), but the potentially more serious penalty that inhomogeneous elasticity theory must be employed. In the case of inhomogeneous elasticity theory, one is not assured of the uniqueness, and probably the existence, of the solution. It has been the practice in computational bone stress adaptation studies to employ the standard finite element techniques based on linear elasticity. When these methods are applied to non-linear adaptive elasticity problems for materially inhomogeneous objects, there is as yet no assurance that there is a solution, or if there is a solution, that there are not many solutions. In a revealing and stimulating study Weinans *et al.* (1992d) computationally investigated the stability of a particular remodeling rate equation in which the stimulus was the strain energy. They showed that the instability is characterized by a process that

causes regions controlled by sensing elements to be either cortical bone with a density ρ = 1.74 g/cm3 or fragile trabecular bone with a density ρ = 0.01 g/cm3. In two geometrically simple situations, Harrigan and Hamilton (1992) did produce two evolutionary, inhomogeneous density solutions for the model of Weinans *et al.* (1990b, 92d); however Harrigan and Hamilton show that the solutions obtained are unstable, results that echo the analysis of Weinans *et al.* (1990b, 92d). In the special case of remodeling in a homogeneous stress field, Cowin *et al.* (1993) show that the discrete-time computational algorithm of that stress adaptation model has a well-known chaos mechanism for stress values of practical interest. This chaos mechanism is only present in the discrete-time computational algorithm. It is shown that the corresponding differential equation form of the one-density stress adaptation model is smooth, monotonic and non-chaotic. Cowin *et al.* (1993) also note the existence of an overshooting calculational step in the discrete-time computational algorithm which, when coupled with the input from an inhomogeneous stress field, could deflect the algorithm from the path prescribed by the bone-density stress adaptation model. This is a very complicated situation and the conclusions to be made are not clear. In the external or surface bone remodeling models, the bone surfaces are moved according to surface bone remodeling theories that assume the surface bone remodeling speed at a point depends on the surface bone remodeling stimulus, e.g. the strain state (Cowin 1985b; Hart *et al.* 1984) or strain energy density (Huiskes *et al.* 1987) or the strain rate (Luo *et al.* 1994b) at or near the remodeling surface. Since all bone remodeling occurs by deposition or resorption from surfaces, surface bone remodeling rate equations have

the potential advantage of mimicking the actual behavior of bone. A second advantage is that surface bone remodeling rate equations require a minimum length scale of only 50 μm in the associated elastic continuum model while internal remodeling rate equations require a minimum length scale of 5 mm. Another important advantage of a complete remodeling theory that incorporates a surface bone remodeling rate equation is that homogeneous elasticity theory can be employed and thus one is assured of the uniqueness of solution and probably the existence of the solution. A disadvantage of surface bone remodeling rate equations is easily visualized if one imagines the calculation of the surface bone remodeling on all the trabecular bone surfaces in the proximal end of a large animal or human femur. The surface area of the trabecular bone is large and irregular, and it is a major effort to document numerically this large internal surface structure. The remodeling will potentially move each surface point and thus requires an unacceptably large computational memory and usage time demands (CPU time).

In computational studies of the internal or surface bone remodeling, it is necessary to determine the stress, strain distribution and displacement distribution which is used to find micromotion. Previous global numerical analysis (FEM) of porous coated implants have treated the interfacial zone as either a bonded or contact surface or a layer of soft tissue. However in these previous models there is no detail of the local interface structure (Huiskes *et al.* 1983; Vanderby *et al.* 1985; Rohlmann *et al.* 1988; Weinans *et al.* 1988). Recent localized models have analyzed the structure of the interfacial zone and quantified local analysis, but these models have not related the local

analysis to the global analysis (Wolfarth *et al.* 1990; Vaillancourt and Johnson 1990). The difficulty of connecting the local to the global analysis of a whole implant stems from the following fact. It is very difficult to create an FEM model including the whole global implant with the details of local structures, because the dimension of a typical local structure, as illustrated by inserts in Figure 1, is less than 1 mm, and the size of a typical global implant for THA, as illustrated in Figure 1, is about 200 mm long and 30 mm in diameter. If one meshes a global implant that retains the details of all local structures, one has to assemble an unacceptably large structure matrix and spend a very large amount of CPU time to solve the corresponding system of equations. When non-linearity and the duration of the bone remodeling are taken into account, a super computer would be required.

1.3 A new approach for total hip implant stability

There are two methods used to solve the problem of global calculation with much detailed local structure. One method is called homogenization theory (Kohn *et al.* 1992), and may be used if the local geometry is periodic. In this method the global or macro stress and strain tensors are obtained by volume averaging (homogenization) of the micro stress and strain tensors. Localization is the inverse of homogenization. In localization, the micro strain tensor is obtained from the macro strain tensor using a mapping function. If local material structures have a periodic geometry, the method is effective for finding stress and strain distributions at both global and local levels. In the

study of the long term stability, non-linearity must be included if it is assumed the bone implant interface is not perfectly bonded. The non-linearity makes the mapping function (localization) and effective (homogenized) material properties very complicated. On the other hand, if surface bone remodeling theory is used to study the long term stability, it requires only the strain distribution near the remodeling surface, while homogenization theory provides the strain distribution over the whole field. The superfluous information is costly in CPU time and memory storage. Another problem is that the change of bone geometry in the surface bone remodeling theory makes it very difficult to get the mapping function and the effective material properties. This method is not appropriate for the long term stability study of the total hip implant. In this dissertation, a method based on the local-global interaction model, described in Chapter 3, was used.

The topic addressed in this dissertation is the influence of local bone remodeling at the bone-implant interface on the long term global stability of the implant. The influence of remodeling has been evaluated at the bone-implant interface and on the bone surfaces not contacting the implant, the periosteum and endosteum, over time and under specified load conditions. This was accomplished using a combination of a global model and local models. The local models are used to determine the ingrowth and effective friction coefficient at the interface employed in the global model. The results of the local analysis are used as input in the global model which is used to determine the surface bone remodeling on the periosteum and endosteum. Since the overall bone remodeling, in turn, influences the local interface conditions, it is necessary to make the

models interactive, the output of one being the input for the other. Therefore a computational model has been developed for the interaction between the time dependent global bone-implant structure and the time dependent local interface conditions.

One feature of this computational model is a variety of bone-implant interface structures that permit the modeling of different bone-implant interfaces, including screw and sintered bead. Another feature of this study is the creation of a database for the remodeling ingrowth or resorption at each interface segment along the interface. Thus, rather than computing the local remodeling ingrowth or resorption along the interface at each iteration of the computational program at each local site from the basic equations, the appropriate result is taken from a previously created database. This database is different for each type of interface. The global model contains variable parameters including the mechanical loading, the initial interference in the fit between the implant and the bone cavity in which it is placed, and the significant characteristics of the bone-implant interface. These characteristics include the roughness and degree of initial compatibility or match of the two surfaces of the interface, the bone-implant surface friction and the materials of the interface. The local bone-implant surface friction can be varied to reflect different implant surface coatings such as a form of the mineral hydroxyapatite, one of the two basic constituents of bone tissue which has been found to enhance bone tissue attachment and growth, (Spivak *et al.* 1990 and Ducheyne *et al.* 1991).

2. BACKGROUND TOPICS

2.1 Historical notes on modeling the bone-implant interface

The implant fixation and the mechanical state of the bone-implant interface have been reviewed by Albrektsson and Albrektsson (1988), Lewis (1988) and Oh (1988). It has long been recognized that the mechanism of load transfer from implant to bone is directly related to the bone-implant interface condition. In computational studies the actual bone-implant interface conditions are idealized as mathematical boundary conditions. These boundary conditions represent the type of bonding, the type of coating and/or the presence of fibrous tissue. Some of the different computational model interface conditions that have been employed are illustrated in Figure 2. These include the rigidly bonded interface (Figure 2a), the interface incapable of supporting tension (Figure 2b), and the interface which includes a tissue layer and which is incapable of supporting tension (Figure 2c). The two interfaces which are incapable of supporting tension each contain three special cases with regard to the assumption made concerning the transmission of shear across the interface. The pads shown in Figures 2b and 2c imply either finite Coulomb friction or one of the two limiting cases, the case of no friction and the case of infinite friction.

Many computational finite element models have been employed to study the mechanism of load transfer from the implant to the bone in cemented and non-cemented implants. Huiskes and Schouten (1983) studied the interface loosening of the stem of

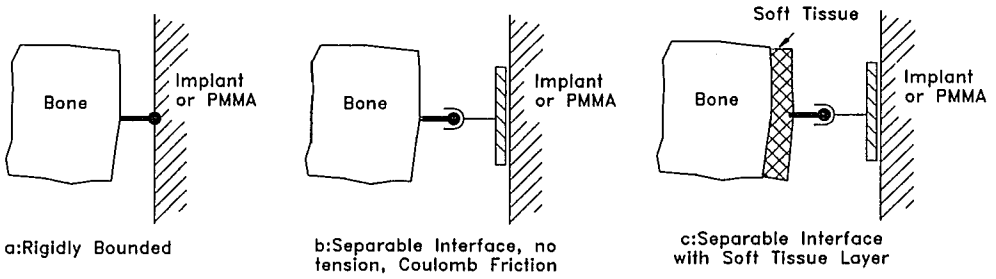

Figure 2. Schematic illustration of various idealized boundary conditions at the bone-implant interface.

a hip implant with a model that idealized the geometry of the diaphysis as being circular. They employed the interface condition illustrated in Figure 2b with zero friction. Huiskes *et al.* (1989) used a similar model to study the evolution of the cementless hip prosthesis-induced bone loss in the proximal femur. Bone loss in the proximal femur due to hip prosthesis placement is called *stress shielding*. Rohlmann *et al.* (1988) used a geometrically simplified three-dimensional finite element model to investigate load transfer between a porous coated hip implant and a femur. Two types of interface conditions were employed in that study, the rigid bond of Figure 2a simulating fully developed bone ingrowth and the tensionless bond of Figure 2b with zero friction simulating a smooth bone and implant contact. Their calculations indicate that, for implants with the same elastic modules as cortical bone, the relative motion (micromotion) at the bone implant interface was greater proximally than the relative motion predicted by calculations that assumed more rigid implants. It is an undesirable effect because the micromotion prevents the structural integration of the bone and the implant.

When different interface conditions are employed, they predict different bone remodeling patterns because the stress distributions are highly dependent on the interface conditions. A three-dimensional finite element model that included the bone, cement and a hip implant was employed by Mann *et al.* (1990, 1991) and Mann (1991) to study the stresses in the cement and at the cement-bone interface. They assumed the interface condition illustrated in Figure 2b with finite Coulomb friction between the bone and the cement. They found that the inclusion of Coulomb friction in the interface condition substantially changes the stress distributions in the cement.

The effect of friction and the mechanism of load transfer in cementless hips were studied by Keaveny (1991) whose three-dimensional finite element model was of two concentric cylinders representing the distal region of the implant and bone subjected to a bending moment. In this study the immediate post operative situation was modeled first using the interface condition illustrated in Figure 2b with finite or infinite Coulomb friction to represent the porous coated implant interface. Keaveny (1991) studied the mechanism of load transfer by employing a non-linear strain hardening stress-strain relation for a thin layer (0.5 mm) representing fibrous tissue. The fibrous tissue layer was assumed to have zero tensile and shear strength , but it could carry compressive load, similar to the interface condition illustrated in Figure 2c with zero Coulomb friction. Keaveny found that the fibrous layer allowed separation at the interface over approximately half of the interface. For the entire model, combined porous coated and fibrous layers, Keaveny found that the bending load transfer was relatively insensitive to the shear strength of the no-tension bond at the interface. Keaveny employed the

final interface conditions of the immediately post operative situation described above as the initial conditions for a long term post operative computational study of the load transfer mechanism. The model of Keaveny does not, however, address the question of the deposition and resorption of bone tissue at the local level and its influence on the temporal evolution of the interface condition and, consequently, on the long-term load transfer mechanism.

It is thought that the lack of initial interference of the implant or excessive micromotion (micromotion in the range of 100-150 microns or larger) (Pilliar *et al.*, 1986) leads to the development of a fibrous tissue at the bone implant interface. Hori and Lewis (1982) studied the mechanical properties of harvested interfacial fibrous tissue at the bone-cement interface. They found the tissue to be a very compliant and deformable material with a mat-like structure composed of collagen fibers distributed at random in sheets. Ling (1986) also suggested that the fibrous layer has very low shear and tensile strength and that its initial compressive stiffness is very low. The effect of this fibrous tissue on bonding and interface conditions was studied by Vanderby *et al.* (1985), Weinans *et al.* (1988) and Weinans *et al.* (1990a). Weinans *et al.* (1990a) employed a two-dimensional simulation of the axisymmetric femoral prosthesis to study the effect of this fibrous tissue. They assumed the existence of a 1 mm interface region of fibrous tissue around the bone. They examined four different boundary conditions at the interface and found that the fibrous tissue causes excessive stress concentration in the bone and cement and high relative displacements between these materials.

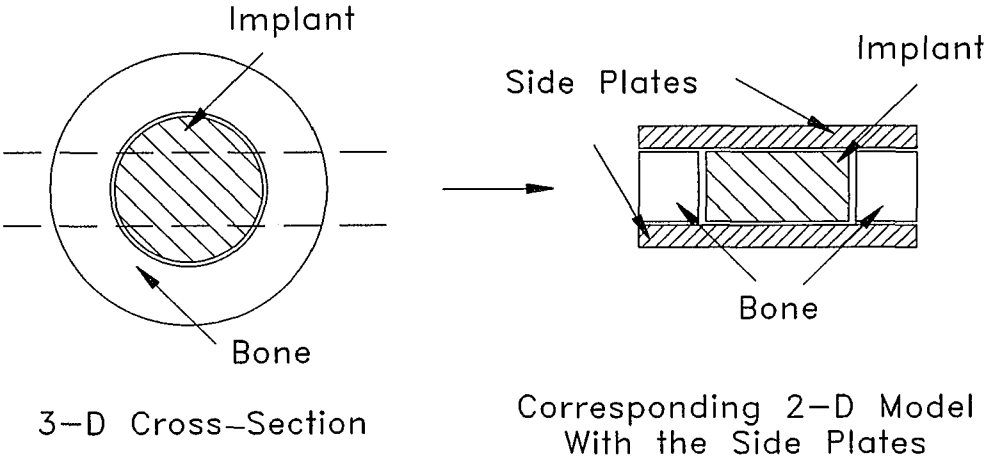

Figure 3. The simulation of the 3-D cylindrical geometry by a 2-D model. This simulation employs side plates to account for the hoop stress. The cross-sectional area moment of inertia of the 2-D side plate simulation is set equal to the cross-sectional area moment of inertia of the 3-D cylindrical shape.

2.2 Historical notes on computational stability studies

A computational modeling approach to the prediction of the bone loss in the proximal femur due to the interface boundary conditions was reported by Huiskes *et al.* (1987), Huiskes (1988) and Weinans (1991). Huiskes *et al.* (1987) and Huiskes (1988) employed a strain energy density criterion for adaptive bone remodeling and studied the problem of stress shielding and cortical bone remodeling on the periosteum and the endosteum around intramedullary prostheses, but did not allow bone remodeling at the implant interface. In later work, Weinans *et al.* (1993) discussed below, a form of

surface bone remodeling was allowed. These authors developed a two-dimensional finite element model that simulates an axisymmetric straight bone and axisymmetric stem. This simulation is achieved by using non-adaptive side-plates on the two-dimensional model to represent the effect of the three-dimensional topology and the hoop stresses. A similar method to simulate three-dimensional topology with a two-dimensional finite element model was employed in this dissertation, and the simulation is illustrated in Figure 3. The side-plate characteristics are selected so that the moment of inertia of the stem and the bone in the axisymmetric model are the same as in the two-dimensional model. Huiskes *et al.* (1987) and Huiskes (1988) assumed the interface condition illustrated in Figure 2b with zero Coulomb friction. They found that the calcar is resorbed and that the bone remodeling around the implant is highly dependent on the interface condition. Their finding is in agreement with the animal experimental results of Turner *et al.* (1987). Weinans *et al.* (1992a), using an approach similar to that of Huiskes *et al.* (1987), studied a three-dimensional model of a dog hip prosthesis and compared their remodeled bone predictions with the two year animal study reported by Summer *et al.* (1990). Weinans *et al.* (1992b) also conducted a computational parametric study of the influence of the material properties of the hip implant and interface conditions on periosteal bone remodeling. A two-dimensional model with the interface condition illustrated in Figure 2a was employed, and the periosteal bone loss for different types of implant materials and cementless and/or cemented interfaces was determined. They reaffirmed the well established result that bone resorption increases as the implant rigidity increases, the greatest bone resorption increase occurring

proximally. They also found that a high localized interface stress occurs when the implant stiffness is close to the stiffness of bone. Weinans *et al.* (1992c) also employed the two-dimensional simulation of the axisymmetric femoral prosthesis, described above, to study the effect of interface bonding on the bone remodeling. In this study they compared bone resorption of the proximal femur for different coating conditions, fully coated, partly coated, press fit and over-reamed cavity (gap). They also compared relative motions and subsidence of smooth and partly coated implants. In their finite element model they used either the completely bonded interface condition illustrated in Figure 2a, and/or the separated (2 mm gap of over-reamed) interface condition illustrated by the zero Coulomb friction case of Figure 2b. They observed that the fully or partly coated stem may induce severe proximal bone loss.

Weinans *et al.* (1993) also studied bone resorption at the implant interface and fibrous tissue formation due to the relative motion between the implant and bone in a cementless implant. In their study a thin layer of very soft material was assumed to represent the interface layer in their two-dimensional finite element model. The strength criterion of Stone *et al.* (1983) was employed to predict the initiation of bone loss. The authors studied screw fixation, a femoral head, and a simple model of a cemented stem in the femoral medullary canal. They found a reasonable, qualitative agreement between the predicted resorption patterns and animal experiments.

The computational procedure known as the boundary element method (BEM) was employed for the local surface bone remodeling in this dissertation. The surface bone remodeling problems studied concern the prediction of the movement of the

remodeling bone surfaces. The BEM is generally superior to other numerical methods in problems involving moving and evolving boundaries (Sadegh *et al.* 1993). The bone remodeling near or at the implant interface was extensively studied by the authors as presented in Chapter 3.

It is important to note that the model is the first to permit local, evolutionary (remodeling) adaptation of the interface conditions to the prevailing stress environment; previous models have, at best, only permitted global adaptation of the interface conditions. The local models also permit us to detail the local stress situation around a screw thread or a cavity of sintered beads, for example. Thus any of the interface conditions described in the previous paragraph may occur in the model and the interface conditions may be changed from one type to another in the remodeling process, in the sense that the effective Coulomb coefficient of friction along the bone-implant interface may vary from zero to infinity. It is also appropriate to note that in the model the effective friction is a combination of the traditional planar Coulomb friction and the effect of the irregular boundary (similar to the concept of a friction coefficient as it is employed in the local mechanics of particulate materials).

It is clear from the literature that implant interface conditions can determine the long term stability and load carrying capacity of implants. Interface disruption due to bone remodeling at the interface and changes in the integrity of the cement and/or micromotion can be the cause of loosening and reduction of the load carrying capacity of the implant. No study has yet addressed the question of local bone remodeling at the implant interface and its influence on the overall long-term stability of the implant.

2.3 Surface bone remodeling theory

Surface bone remodeling theory was employed in the calculation of bone remodeling shape changes in both the local and global models. Surface bone remodeling is due to the deposition and resorption of the surface layer of bone. Actually, all bone remodeling occurs by deposition or resorption from surfaces; surface bone remodeling means external surface bone remodeling. In all the cases of bone ingrowth into the cavities formed between beads, screw threads and slots considered here, the free surface of bone may move into or retract from a cavity by different combinations of deposition and resorption, with deposition and resorption sometimes occurring on the same free surface at different times.

In the surface bone remodeling theories the bone is assumed to be a linear elastic solid with an additional constitutive equation that specifies the velocity of movement of the exterior bone surfaces. The remodeling rate equation is the equation that governs the velocity U(**X**, t) of the free surface movement as a function of the tensorial remodeling stimulus S_{ij}(**X**, t) at the surface point **X** at the time t on the remodeling time scale. The equation that governs the velocity U of the free bone surface is written as a function of tensorial stimulus S_{ij}(**X**, t) at the bone surface,

$$U(\boldsymbol{X}, t) = C_{ij}\left(S_{ij}(\boldsymbol{X}, t) - S_{ij}^{o}(\boldsymbol{X})\right), \qquad (1)$$

where C_{ij} is a constant second rank tensor and S_{ij}^{o} is a reference value of the second rank tensor stimulus S_{ij}(**X**, t). There are two time scales in the theories of the

remodeling process, time scales that differ by many orders of magnitude. Let T_r denote the time that the biological processes take to complete most of the remodeling associated with a major change in mechanical bone loading, such as the placement of an implant, and let T_l denote the characteristic period of mechanical loading of a bone. Rough estimates of these numbers are six months and one second, respectively; thus T_l/T_r is a small number, of the order 10^{-8}. In order to keep these time scales separate we let τ denote time on the loading time scale and t denote time on the remodeling time scale. The surface bone remodeling equation (1) is formulated on the remodeling time scale t.

The particular aspect of the strain history of living bone tissue that is employed by the tissue to sense its mechanical load environment and signal for the deposition or resorption of tissue is called the *stimulus*. The stimulus, although much discussed, is unknown. In the past the mechanical stimuli employed included strain (Cowin *et al.* 1985b) and strain energy density (Huiskes *et al.* 1987). A recent study (Weinbaum *et al.* 1991, 93) of mechanical osteolytic stimulation by bone fluid shear stresses suggests that bone adaptation could depend upon strain rate. The model for strain generated potentials (SGPs) of Salzstein *et al.* (1987), extended by Harrigan and Hamilton (1993) to cell-to-cell signaling, depends upon the same fluid motion as the model of Weinbaum *et al.* (1991, 93); the difference in the models is only in the mechanism for cellular stimulus, not in the motive force for the cellular stimulus, which is in both cases the fluid movement. The fluid motion common to these cell signaling models is driven by the differential straining of the bone due to the combined axial and bending loads

applied to a whole bone. Poroelasticity or Biot theory is the theoretical mechanism that relates the applied mechanical load to the fluid motion. The fluid motion resulting from the differential straining of the bone depends upon the rate of strain of the bone. In particular, if the rate of strain is zero, there is no fluid motion and the strain rate stimulus is zero, independent of the magnitude of the strains.

Based on experimental observations, Lanyon (1984) suggested strain rate as a stimulus a number of years ago. Animal experiments by Rubin and Lanyon (1987) showed that constant, non time varying strain was not a stimulus for bone deposition; rather it caused bone resorption. Recent experimental studies by McLeod *et al.* (1993) suggest a frequency dependence of the bone remodeling stimulus, an effect that would easily be understood if strain rate were the stimulus, or a stimulus. These data suggest that if a certain periodic strain amplitude stimulates bone remodeling at one Hz, a periodic strain amplitude of one tenth that magnitude will stimulate bone remodeling at twenty to thirty Hz, the frequencies associated with muscle firing.

Bone is mechanically strained on the loading time scale τ and therefore, in this model, the strain depends on both time scales. Let $\varepsilon_{ij}(\mathbf{X}, \tau, t)$ denote the matrix of strain tensor components at the point $\mathbf{X}$ at the time τ on the loading time scale and t on the bone remodeling time scale and thus,

$$\varepsilon_{ij}(\boldsymbol{X}, \tau, t) = \kappa_{ij}(\boldsymbol{X}, t) + \alpha_{ij}(\boldsymbol{X}, t) f(\omega\tau), \quad f(\omega\tau) = f(\omega\tau + 2\pi), \quad |f\omega\tau)| \le 1,$$

where

$$\kappa_{ij}(\boldsymbol{X}, t) = \frac{1}{2}\left(Max(\varepsilon_{ij}(\boldsymbol{X}, \tau, t)) + Min(\varepsilon_{ij}(\boldsymbol{X}, \tau, t))\right) \text{ and} \qquad (2)$$

$$\alpha_{ij}(\boldsymbol{X}, t) = \frac{1}{2}\left(Max(\varepsilon_{ij}(\boldsymbol{X}, \tau, t)) - Min(\varepsilon_{ij}(\boldsymbol{X}, \tau, t))\right).$$

In equation (2), $f(\omega\tau)$ is a periodic function of maximum absolute magnitude one with a period equal to $2\pi/\omega$. The steady component $\kappa_{ij}(\mathbf{X}, t)$ on the time scale τ and the periodic component $\alpha_{ij}(\mathbf{X}, t)$ on the time scale τ are expressed in terms of the total strain history $\varepsilon_{ij}(\mathbf{X}, \tau, t)$ as the mean and one-half the non-negative difference of the maximum value and the minimum value, respectively, of the total strain history over the period $2\pi/\omega$. It follows that the magnitudes of the periodic component $\alpha_{ij}(\mathbf{X}, t)$ are non-negative numbers. The strain rate on the loading time scale τ of the periodic strain of equation (2) is given by

$$\dot{\varepsilon}_{ij}(\boldsymbol{X}, \tau, t) = \omega \alpha_{ij}(\boldsymbol{X}, t)\, \dot{f}(\omega\tau), \quad \dot{f}(\omega\tau) = \dot{f}(\omega\tau + 2\pi), \tag{3}$$

where the superposed dot indicates the time derivative on the loading time scale τ.

In the present work a strain rate stimulus is employed. The strain rate stimulus $S_{ij}(\mathbf{X}, t)$ on the remodeling time scale t is assumed to be

$$S_{ij}(\boldsymbol{X}, t) = 2\alpha_{ij}(\boldsymbol{X}, t)\, \frac{\omega F[\dot{f}(\omega\tau)]}{\omega_{ref.} F[\dot{f}(\omega_{ref.}\tau)_{ref.}]} \tag{4}$$

where the factor of two occurs because the stimulus is based on the minimum to maximum peak values. Recall that the periodic component $\alpha_{ij}(\mathbf{X}, t)$ on the time scale was defined as one-half the non-negative difference of the maximum and the minimum of the total strain history $\varepsilon_{ij}(\mathbf{X}, \tau, t)$ over the period $2\pi/\omega$. In the transition from the excitation strain rate given by (3) to the stimulus given by (4) the loading frequency and the shape of the loading function have been normalized to the typical or a normal reference loading experienced by the tissue in question. Thus $\omega/\omega_{ref.}$ appears in (4) whereas only ω appeared in (3). The functional F[ ] is the load shape functional and it

varies with the shape of the loading cycle. It will be different for square waves, for half sine pulses, triangular pulses, etc. It is normalized by the shape load functional of the reference loading.

The surface bone remodeling constitutive equation (1) is valid for an anisotropic elastic model of the bone tissue. If, contrary to reality but in the interest of model simplification, isotropy is assumed, then $C_{ij} = K\delta_{ij}$, where δ_{ij} is the Kronecker delta and K is a constant and the surface bone remodeling equation (1) is written for a range of remodeling equilibrium stimuli as

$$U=\begin{cases} K_1 (S - S_{0-}), & if\ S < S_{0-}, \\ 0, & if\ S_{0-} < S < S_{0+}, \\ K_2 (S - S_{0+}), & if\ S_{0+} < S. \end{cases} \qquad (5)$$

where S_{o+} is the value of the stimulus above which deposition occurs, and S_{o-} is the value of the stimulus below which resorption occurs. The stimulus domain, $S_{o-} < S < S_{o+}$, is the remodeling equilibrium domain. A graphical representation of (5) is shown in Figure 4. In this analysis the remodeling rate constant $K_1 = K_2 = K$ is equal to 1 mm per unit of time where the unit of time is unspecified. The value of K only affects the rate at which the final remodeled equilibrium shape is attained, not its form; Sadegh *et al.* (1993). In the calculations reported, bone was assumed to be an isotropic linear elastic solid with Young's modulus E (18 GPa), shear modulus G (7031 MPa) and Poisson's ratio ν (0.28). In the computational procedure, the stimulus is not evaluated at surface points but at points near the surface for accurate strain values, as explained in Sadegh *et al.* (1993).

Our implementation of the model (5) when strain rate is the stimulus, equation

(4), is accomplished here for the simple case of constant load frequency. The constant load frequency is assumed to be that of normal activity such as walking, say one to two Hz, and the shape of the applied load cycle is assumed to be the normal or reference shape; thus the surface bone remodeling strain rate stimulus is twice the trace of the periodic component $\alpha_{ij}(\mathbf{X},t)$.

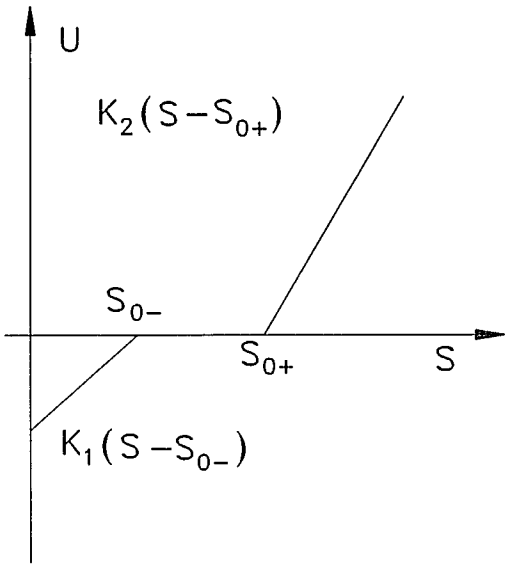

Figure 4. A plot of equation (5), which is employed to determine the velocity of the free bone surface movement as a function of the stimulus.

Based on the work of Lanyon (1984) and Rubin and Lanyon (1984, 1987), who could only measure peak value of one tangential strain, the tangential axial strain in a long bone, say ε_t, it is found that bone resorption will occur at strains ε_t greater than about -0.001, and that bone deposition will occur for strains ε_t less than -0.003. Since the stimulus defined by formula (4) for surface bone remodeling is in terms of the sum $2(\alpha_t + \alpha_s + \alpha_n)$, while the Rubin and Lanyon data are in terms of ε_t only, there is an adjustment that must be made in determination of the numerical value of the limits S_{0-} and S_{0+}. Assuming the uniaxial loading condition in the Rubin and Lanyon experiments, the other two normal strain components ε_s and ε_n are equal to each other and also to $-\nu\varepsilon_t$. Thus these data should be adjusted by multiplying the Rubin and Lanyon measured ε_t by $(1 - 2\nu)$, where Poisson's ratio ν is 0.28; thus $S_{0-} = 0.00044$ and

S_{0+} = 0.00132. Bone is in remodeling equilibrium between those two strain rate stimulus limits.

3. STUDY OF LOCAL MODELS

3.1 Local models

The local models were used to study the surface bone remodeling at the local level as represented by the inserts in Figure 1. The surface bone remodeling theory employed is based on a strain rate stimulus. Three typical local models are the screw thread model, as shown in Figure 5, the slot model, as shown in Figure 6 and the bead or wire model, as shown in Figure 7. These three 2-D models were used to simulate the surface treatment of an implant with screw threads, slots and beads or wire mesh. These models can be used to determine how bone grows into or resorbs from screw threads, slots or the space between beads under given loading and boundary conditions.

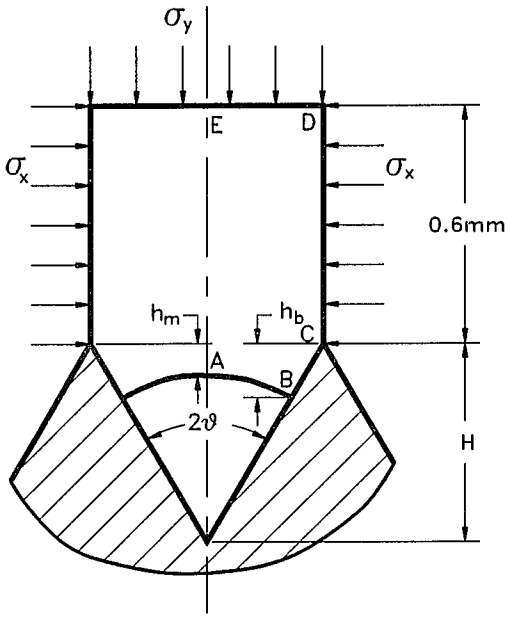

Figure 5. The screw thread model, a local model.

The boundary element method (BEM) (Banerjee 1981; Brebbia 1984) was used for these local models. In BEM, only the boundary values of the arguments, such as tractions and displacements, are determined. It is not necessary to consider the values of the arguments inside the boundary if these values are not used in the analysis. In contrast to BEM, in the finite element method (FEM) all the values of arguments, both

on and inside the boundary, must be calculated whether they are used or not, while the surface bone remodeling theory needs only the strain distribution near the bone remodeling surface. For surface bone remodeling problems, the geometry of the bone is changing all the time. In the BEM only the boundary needs to be meshed and it is easy to remesh the boundary. In the FEM a change of the boundary results in the remeshing of the whole domain instead of just the boundary. For surface bone remodeling problems, the BEM is more appropriate than the FEM.

In these local models, there are a number of factors that may change the course of bone ingrowth into, or resorption from, screw threads, slots or a cavity of beads. To understand the behavior of these local models, the following factors are studied: (a) the

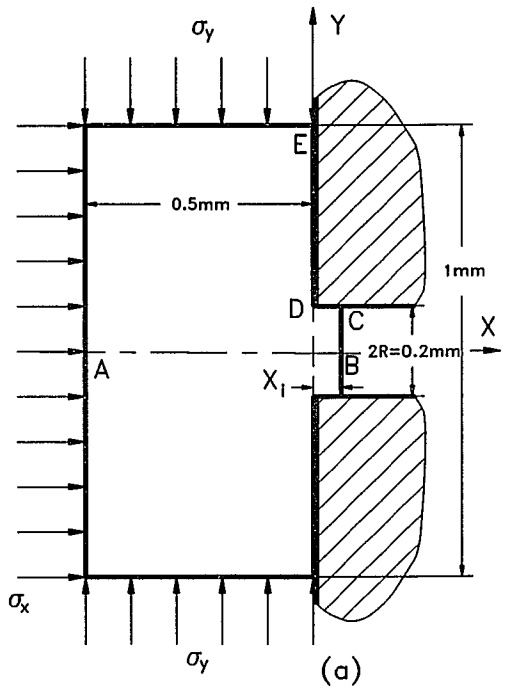

Figure 6. The slot model, a local model.

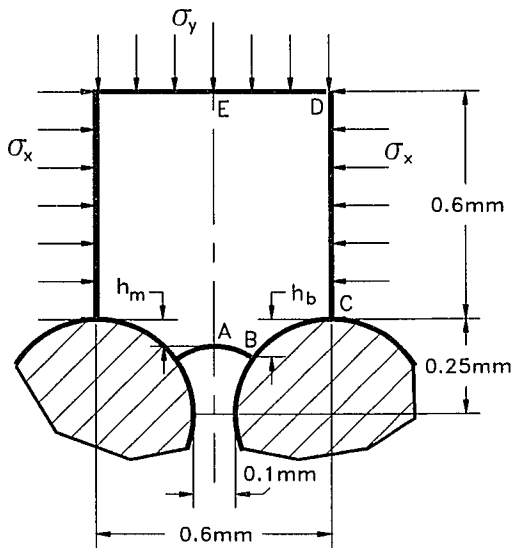

Figure 7. The bead or wire model, a local model.

boundary conditions and initial ingrowth, (b) stress concentration near a sharp corner, (c) the effect of loading on final ingrowth.

3.2 Boundary conditions and initial ingrowth

For a smooth implant surface the interface cannot sustain any shear stress, but for a rough implant surface with hydroxyapatite, perfect bonding may result. Perfect bonding allows no relative displacement between bone surface and implant surface. It is also possible that the roughness of an implant surface results in a bonding condition intermediate to a no-shear-stress condition and a no-relative-displacement condition. The surface condition is an important factor in surface bone remodeling. Another factor that may also affect the remodeling is initial ingrowth. Since bone remodeling processes are loading path dependent, different initial ingrowth may result in different final ingrowth. It is necessary to understand how the initial ingrowth changes the final result.

A slot local model shown in Figure 6 was used to study the effect of the interface bonding condition on ingrowth. In this study, it is assumed there is a non-zero initial ingrowth, denoted by X_i. The initial ingrowth considered is very small, from 0.01 to 0.1 mm. A two-dimensional boundary element model of the bone with initial ingrowth into the slot is used. Twenty-six quadratic boundary elements and 52 nodes are used for half of the symmetric model shown in Figure 6. While the initial ingrowth may affect the final remodeling equilibrium, the roughness of the surface of the slot plays an important role in the shape of the remodeling equilibrium. Different surface

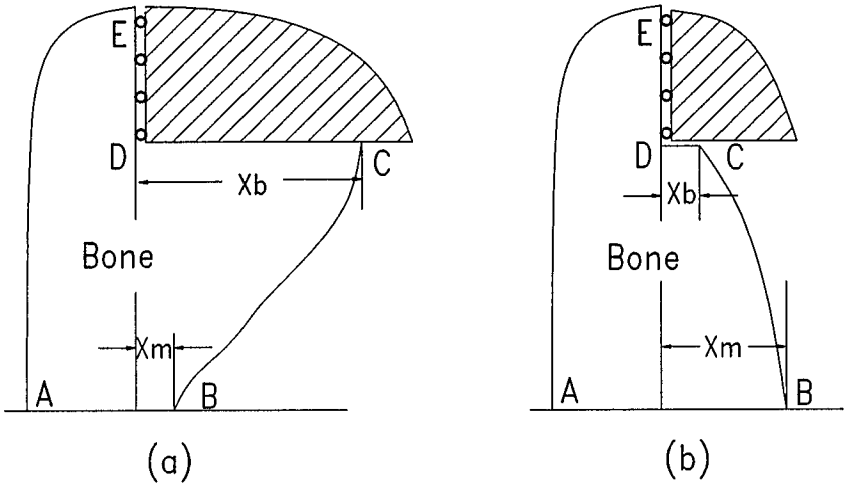

Figure 8. (a) An illustration of the fixed boundary condition corresponding to zero relative displacement in the plane of the bone-implant interface. (b) An illustration of the free boundary condition corresponding to zero shear stress in the plane of the bone-implant interface.

treatments of portions of an implant's surfaces can create different degrees of bonding between the bone tissue and the implant. These different degrees of bonding are modeled here by different boundary conditions on the bone-implant interface. For example, smooth surfaces associated with polished titanium or stainless steel were modeled as free surfaces when they were initially placed (it is possible that subsequent tissue deposition on such smooth surfaces could make them rough). Total bone-implant bonding of the type achieved with a hydroxyapatite surface treatment is modeled as a surface with zero relative displacement, or a fixed boundary condition, in the plane of the bone-implant interface. Two bone-implant interface boundary conditions considered are shown in Figure 8. Figure 8a illustrates the boundary condition corresponding to zero relative displacement in the plane of the bone-implant interface and a typical

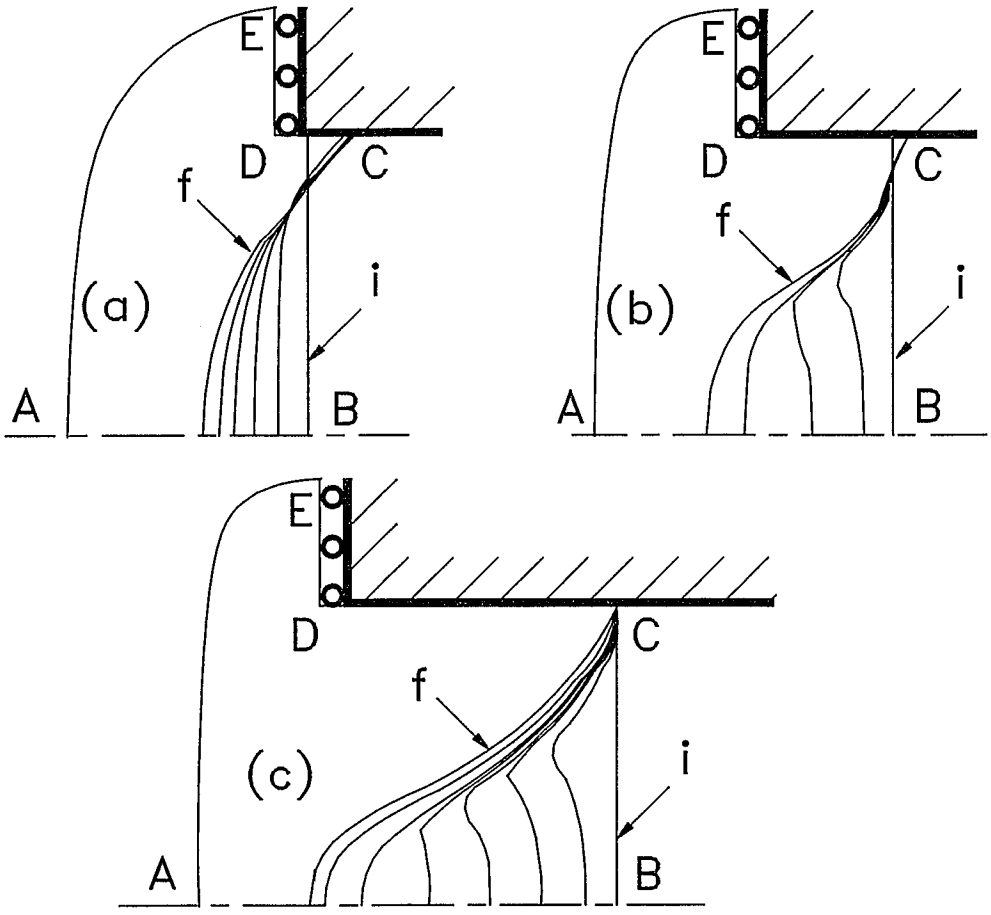

Figure 9. Illustrations of the bone remodeling in the slot for the fixed boundary condition at the wall with initial ingrowth of (a) 0.01 mm, (b) 0.05 mm and (c) 0.1 mm.

ingrowth surface. Figure 8b illustrates the free boundary condition associated with a smooth bone-implant interface. In the final shape, the ingrowth of the bone measured on the boundary is denoted by X_b and the ingrowth in the middle is denoted by X_m

Three initial ingrowth depths, denoted by X_i, were considered: 0.01, 0.05 and 0.1 mm. The bone was subjected to a compressive biaxial stress state, $\sigma_x = \sigma_y = -20$ MPa. When the fixed boundary condition, illustrated in Figure 8a, was applied on the

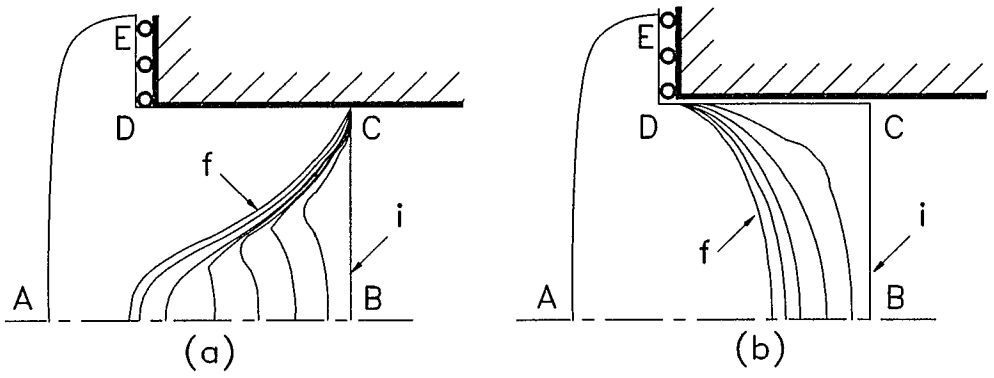

Figure 10. Illustrations of bone remodeling in a slot with initial ingrowth of 0.1 mm. (a) fixed and (b) free boundary condition.

portion CD of the boundary element model, the predicted patterns of bone ingrowth associated with the initial ingrowth depths 0.01, 0.05 and 0.1 mm are shown in Figures 9a, 9b and 9c, respectively. In Figure 9 the curves labeled "i" represent the initial shape, those labeled "f" represent the final shape and those other than initial and final are transition curves representing intermediate stages between the initial and the final.

With the free boundary condition as illustrated in Figure 8b, the bone is again subjected to a compressive biaxial stress state of -20 MPa. The pattern of bone ingrowth associated with the initial ingrowth depth of 0.1 mm for the free boundary condition is totally different from that for the fixed boundary condition shown in Figure 9. A comparison of the result with fixed boundary condition as illustrated in Figure 8a and the result with free boundary condition as illustrated in Figure 8b is shown in Figure 10.

Some of these data combined with data on rounded versus sharp corners, to be discussed later, are incorporated in Table 1. Table 1 presents data on the final ingrowth

of the bone at the middle, X_m, and at the boundary, X_b, as shown in Figure 8, of the slot for fixed and free boundary conditions. The rows that are applicable here are those containing data on fixed and free boundary conditions.

X_i	Boundary Condition	X_m	X_b
0.01mm	fixed	-0.0249mm	+0.0247mm
0.05mm	fixed	-0.0148mm	+0.0548mm
	sharp corner (with cavity)	**-0.0080mm**	**+0.0571mm**
	rounded corner (with cavity)	**-0.0074mm**	**+0.0576mm**
0.1mm	fixed	-0.0003mm	+0.1000mm
	free	+0.0553mm	+0.0000mm
	sharp corner (with cavity)	**-0.0071mm**	**+0.1000mm**
	rounded corner (with cavity)	**-0.0090mm**	**+0.1000mm**

Table 1. The values of the final ingrowth distance of bone at the center X_m and at the wall X_b for various boundary conditions and initial ingrowth depths considered. These data all apply to the various corner treatments.

In the calculation described, a mesh with 26 elements and 52 nodes is employed. To verify the accuracy of the calculation, a second mesh with 48 elements and 96 nodes was employed, and the bone ingrowth associated with the 0.05 mm initial ingrowth depth and fixed boundary condition was recalculated. The maximum difference in the predicted final ingrowth between the calculations with the different meshes is of the order of 1μm. Both the coarser (52 node) meshes and the finer (92 node) meshes predicted similar results. These results suggest the convergence of the computational procedure employed.

The effect of boundary conditions on boundary segment DE in Figure 6 on the

bone ingrowth was also studied. In this study the influence of surface coating of an implant on microstructural bone ingrowth into a slot of an implant is analyzed by varying the frictional boundary conditions. Four cases of biaxial loadings of the bone near the slot were considered. For each loading case three boundary conditions, roller, finite friction, and perfect bonding, were examined. Two major conclusions were made: (a) the final bone ingrowth into the slot is reduced when the perfect bonding condition at the bone-implant interface is employed and (b) the final bone ingrowth is increased when external loadings in both directions are increased. The detailed results are presented in Luo *et al.* (1994a).

3.3 Stress concentration near a sharp corner

A sharp corner on an implant surface may result in stress concentration in the bone that contacts the corner. How bone remodeling reacts to the stress concentration is important. In the problems concerned with remodeling around slots described above there are right angle external corners of the implant abutting right angle internal corners of bone tissue, e.g. point D in Figure 6. In a traditional elasticity problem such an internal corner would be associated with high concentrations of stress and strain in the bone tissue. Here the question addressed is how the theory under consideration predicts the remodeling behavior of the bone tissue near and at such corners (Luo *et al.* 1994a). It will be shown that the bone tissue remodels in a way that reduces the stress concentrations. It will also be shown how the remodeling in the vicinity of the corner

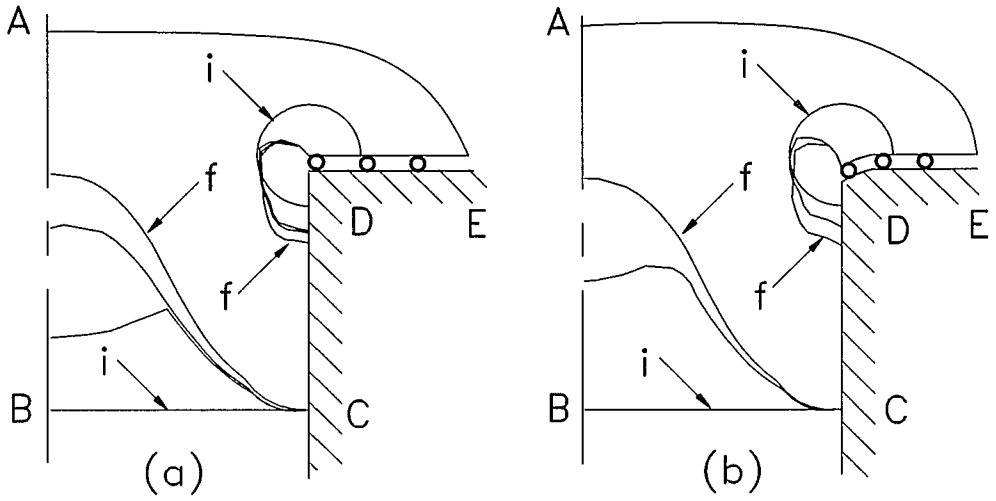

Figure 11. An illustration of the models used to study the effect of stress concentration at (a) a perfectly sharp right angle external corner and (b) a rounded right angle external corner. The idealization of the slot problem with the indentation depth of the bone into the slot, shown in Figure 6, is modified by removing a circular arc of material (bone tissue) centered at the point D and allowing the surface of the circular arc to remodel. The labels "i" represent initial shape, "f" represent the final shape.

at point D in Figure 6 influences the shape and depth of final ingrowth along the face BC. To develop these results in the BEM model shown in Figure 6, the idealization of the slot problem with the initial ingrowth depth of the bone into the slot, is modified by removing a circular arc of material (bone tissue) centered at point D, and the surface of the circular arc is allowed to remodel. The reason why this model was chosen is that it appears reasonable to assume that high stress levels will kill the bone cells, causing local resorption and mitigation of the stress concentration. Hence an approach of the tissue to the right angle corner from the surface, that has the initial form of a circular

arc, is modeled instead of modeling the relaxation of the bone contact with the right angle corner. The modification of the corners in Figure 6 is shown in Figure 11a.

The BEM problem considered is identical to the slot problem with the initial ingrowth depth shown in Figure 6, except for addition of the remodeling surface that has the initial form of a circular arc. The surface BC, which indicates the initial depth of ingrowth (0.05mm and 0.1 mm), is a remodeling surface as is the three-quarter circular arc around D (a radius of 0.02 mm). On the boundary CD the fixed boundary condition is applied and the boundary DE is assumed to have a roller contact between the tissue and the implant.

The result of the BEM remodeling calculation with initial depth of ingrowth 0.1 mm is illustrated in Figure 11a and the corresponding data with initial depth of ingrowth 0.05 mm and 0.1 mm are given in Table 1. It is shown that the three-quarter circular arc around the perfectly sharp corner D remodels into an ear-shaped cavity. The stress in the vicinity of the ear is still about four times higher than the stress far away from the ear, but much less than it would be in the case of a stress concentration arising from the right angle internal bone corner shown in Figure 6.

The corners that have just been considered are, of course, unrealistically sharp. The corners of implants will not be perfectly sharp, but will have some degree of roundness. In the case of a sintered surface, one would expect edges that are spherical surface arcs rather than sharp edged corners. Similarly, any ridged surface on an implant would have well rounded corners rather than sharp edges. These considerations lead us to model the approach of the tissue to the rounded right angle corner from the

surface that has the initial form of a circular arc. The modification of Figure 11a is shown in Figure 11b. The radius of the rounded corner is 0.005 mm. This makes the right angle internal corners of bone tissue a fillet and the right angle external corners of the implant a round, in the terminology of mechanical design.

The result of the rounded corner BEM remodeling calculation with initial depth of ingrowth 0.1 mm is illustrated in Figure 11b, and the corresponding data with initial depth of ingrowth 0.05 mm and 0.1 mm are given in Table 1. It is seen that the three-quarter circular arc around the rounded corner D still remodels into an ear-shaped cavity. The stress in the vicinity of the ear is still about twice as high as the stress far away from the ear. The final shape of the remodeling boundary BC is almost exactly the same as that on the perfectly sharp corner, suggesting that the precise shape of the corner does not influence the final ingrowth depth. The final results for the corner problems considered still show that final strains at the corner are higher than the strains far away from the corner because rounding the corner did not remove all the boundary discontinuities in the problems. There still exists the discontinuity associated with the transition of boundary conditions from roller to fixed at the corner. The results strongly suggest that, if the real situation could be modeled more accurately, the right angle internal corners in actively remodeling bone tissue would be shown not to be the cause of strain concentrations. This is because the strain concentration in the present calculation is due to the transition of boundary conditions at the corner, an artifact induced by the model of the corner.

3.4 The effect of loading on final ingrowth

To understand the influence of the applied load on the final ingrowth, a two-dimensional model, as shown in Figure 5, of a typical region of the bone around a screw thread was used. In this model the tooth angle of the screw is denoted by 2ϑ, the total height of the screw tooth is H, the pitch of the screw is $2H\tan\vartheta$, and the stress applied by the surrounding bone tissue is denoted by σ_x and σ_y. The initial penetration depth of the screw into the bone is denoted by h_i, the depth in the middle by h(t) and the final depth in the middle by h_f. The final penetration depth h_f is called the *final ingrowth*. The surface of the bone tissue represented by the linear domain BC is initially in contact with the implant. Due to the symmetry with respect to line AE, only half of the model needs to be studied. The meshes employed for this study are the same as those employed for the creation of the database of the screw interface in the next chapter. Plane strain is assumed in the calculation. The bone boundary represented by the domain AB is a free moving boundary, and it may move into the triangular region below AB as determined by the remodeling process governed by surface bone remodeling theory. As the ingrowth continues, the moving face AB of the bone becomes smaller and closer to the vertex between the teeth, and the domain of bone-implant contact, BC, increases. The velocity of the moving surface AB is inhomogeneous since it depends on the local strain state which is inhomogeneous along AB. The region of the moving surface AB close to the implant contacting faces BC is moving with slightly higher velocity than the central domain near point A. The cause

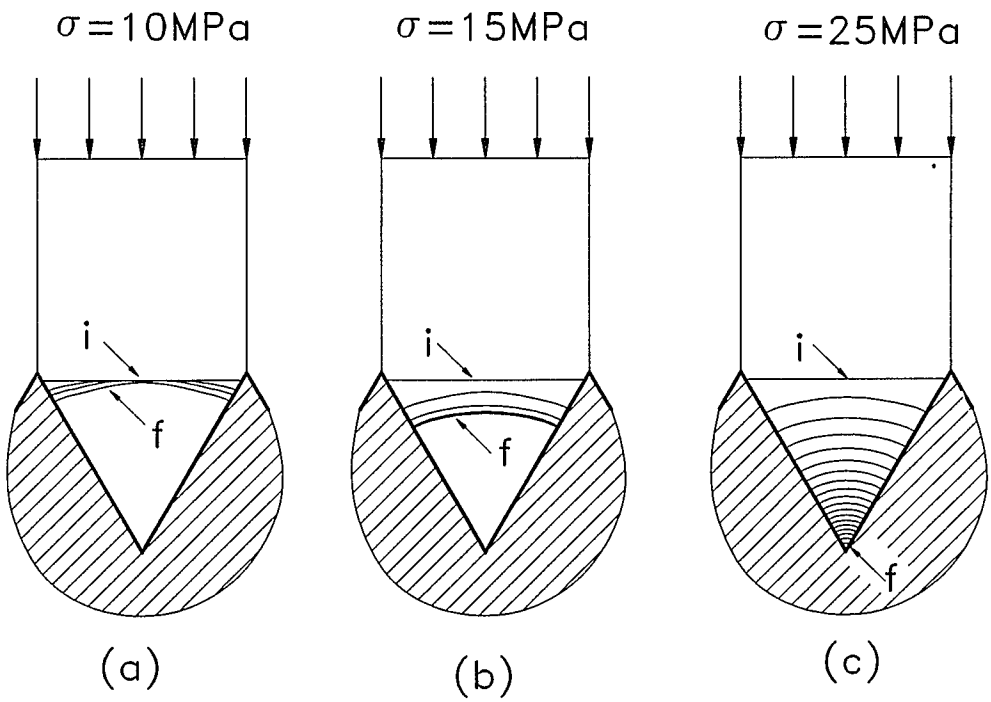

Figure 12 Illustration of the depth of bony ingrowth between the screw threads of an implant for three levels of applied stress. Marks "i" and "f" stand for initial and final.

of this more rapid movement at the edges closer to the screw thread surface is a greater compressive strain at the more rapidly moving locations. The difference in velocity of the moving surface creates an arched shape in the moving ingrowth bone surface AB, but the difference decreases as the moving face AB approaches the vertex.

The depth of the bone final ingrowth is a function of the applied compressive stress $\sigma_x = 0$ and $\sigma_y = \sigma$ as suggested by the three panels of Figure 12. The curves illustrating the progressive ingrowth of bone into the thread tooth in Figure 12 have significance only with regard to the method of calculation.

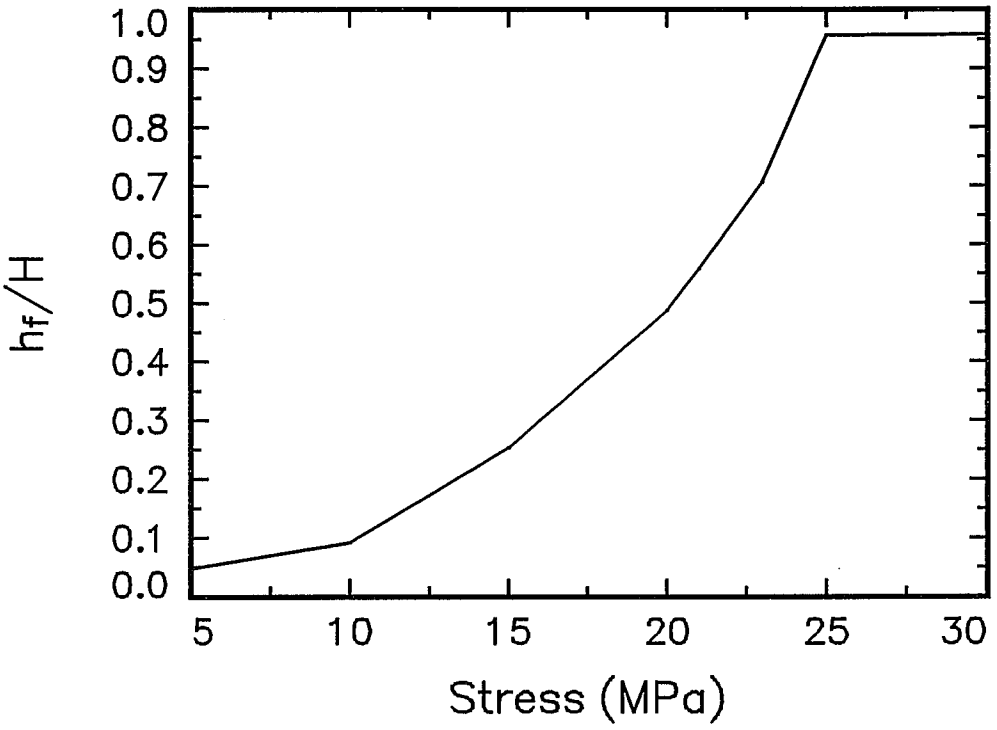

Figure 13. Plots of the curves representing the non-dimensionalized final ingrowth between the screw threads, h_f/H, as a function of the applied stress σ for the 60° thread angle considered.

The variation of the normalized final ingrowth depth, h_f/H, as a function of the load for thread angles of $2\vartheta = 60°$ is shown in Figure 13. This curve shows that the final ingrowth is almost complete if the compressive stress is greater than 23 MPa, while stresses less than 10 MPa produce incomplete final ingrowth.

4. LOCAL-GLOBAL FEEDBACK MODEL

4.1 General introduction to the model

The surface bone remodeling theory described in Chapter 2 is employed in this study of the long term stability of the total hip implant. In particular, the influence of the local surface bone remodeling on global implant stability is studied. The primary information required for implementation of surface bone remodeling theory is the strain distribution on all remodeling bone surfaces. As mentioned in Chapter 1, it is not feasible to construct a mesh for the whole total hip implant while keeping all the local structural details. The strategy to circumvent this restriction is to divide the problem into three parts. The first part is local models that are used to study the surface bone remodeling under given loading conditions for certain local structures, i.e. screw thread or bead models. The second part is global models that are used to find strain and displacement distribution near the bone surface of the global models without keeping local details. The local remodeling is reflected on the global model by changing the bone-implant interface condition and bone geometry. The last part is the interaction between the local model and the global model, i.e. the passage from the global level strain and displacement distribution to the local level and the reciprocal influence of the remodeling at the local level on the global level response. In the following sections, the database of local models, global models and the interaction between the local level and global level, that is called local-global feedback mechanism, will be introduced.

Range of $h_b(t)$ (mm)	Number of quadratic elements	Number of nodes	Number of nodes on a line				
			AB	BC	CD	DE	EA
0.02 - 0.15	20	40	9	5	13	5	13
0.15 - 0.35	25	50	7	13	13	5	17
0.35 - 0.48	26	52	3	17	13	5	19

Table 2. The different boundary element meshes with the three different ranges of $h_b(t)$ for the screw thread model. Note that the number of nodes on a line includes the nodes at both ends of the line.

4.2 Local models and databases

In this dissertation, two local models are used: the screw thread model as shown in Figure 5 and the bead model as shown in Figure 7. These local models are used to find the amount of ingrowth under given loading and boundary conditions in a given time interval. Rather than computing the local remodeling ingrowth or resorption at each iteration at each local site along the interface from the surface bone remodeling equation, a feature of this model is the creation of a database for remodeling ingrowth or resorption for each local model.

(a) The database for the screw interface

The database for the screw interface in the dissertation was based on the surface bone remodeling theory using strain rate as the stimulus. In the dissertation a range of

biaxial load values -30 to 30 MPa is prepared for the database. A two-dimensional local model of a typical region of the bone around a screw thread is shown in Figure 5. The model is assumed to be symmetric about its vertical bisector. In this local model the tooth angle of the screw is denoted by 2ϑ, the total height of the screw tooth is H, the pitch of the screw is $2H\tan\vartheta$, and the stresses applied by the surrounding bone tissue are denoted by σ_x and σ_y. The initial ingrowth depth of the bone into the screw is denoted by h_i, the depth measured at point B at time t is denoted by $h_b(t)$ and at the middle is denoted by $h_m(t)$. In this dissertation h_b is taken as the ingrowth distance. In the following studies, H = 0.5 mm and $2\vartheta = 60°$. It is assumed that the bone has been resorbed if $h_b(t) < 0.02$ mm = (0.04)H and that the bone has reached the maximum ingrowth if $h_b(t) > 0.48$ mm = (0.96)H.

The boundary element method (BEM) is employed for the local stress analysis. In order to obtain accurate numerical results, different boundary element meshes are used for three different ranges of $h_b(t)$. The properties of these boundary elements meshes are detailed in Table 2. The BEM model is, of course, one-half of Figure 5, and the boundary AB is a free remodeling surface. On boundary BC, bone is in contact with the implant and a roller boundary condition is applied. On boundary CD a uniform normal stress σ_x is applied, and on boundary DE a uniform normal stress σ_y is applied. The roller boundary condition is applied on surface EA. Plane strain is assumed in the calculation. The material properties are a Young's modulus of 18 GPa and a Poisson's ratio of 0.28.

To develop the database for the screw problem, the quantities $h_b(t)$ and $h_m(t)$ are

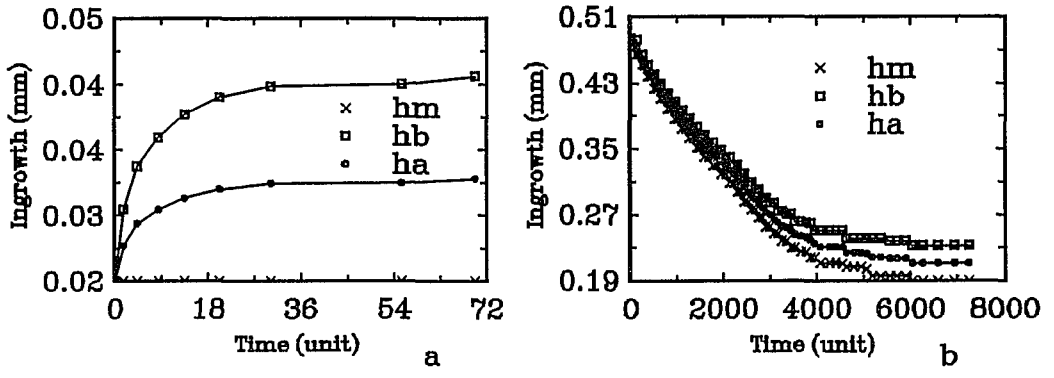

Figure 14. (a) A plot of bone ingrowth into a screw thread against time for an indentation of 0.02 mm. (b) A plot of bone resorption from a screw thread against time for an indentation of 0.48mm. Note that the definitions of h_b and h_m are illustrated in Figure 5.

calculated under the various combinations of σ_x and σ_y, as well as two different initial ingrowths, h_i = 0.02 mm and h_i = 0.48 mm. Typical results are shown in Figure 14a with h_i = 0.02 mm and in Figure 14b with h_i = 0.48 mm, under σ_x = - 10 MPa and σ_y = - 5 MPa. In the figure, h_a is defined as the average of h_b and h_m. A database for this model has been created. In the database, a set of integer values of loading ranging from -30 to 30 MPa are selected for both σ_x and σ_y. For the stresses which are not in the database, interpolation is used.

(b) The database for the sintered beads or wire mesh interface

In order to understand the mechanical interlocking of bone tissue with the porous surface formed with sintered beads, a database for the local bone ingrowth under various combined stress states in a range of -30 to 30 MPa was developed and

Range of $h_b(t)$ (mm)	Number of quadratic elements	Number of nodes	Number of nodes on a line				
			AB	BC	CD	DE	EA
0.005 - 0.02	20	40	9	5	13	5	13
0.02 - 0.1	21	42	7	9	13	5	13
0.1 - 0.25	23	46	5	13	13	5	15

Table 3. The different boundary element meshes with the three different ranges of $h_b(t)$ for the bead model. Note that the number of nodes on a line includes the nodes at both ends of the line.

employed in the dissertation. A two-dimensional model of a cavity between two sintered beads, as shown in Figure 7, is developed. In this model the bead's radius, or the cross-section of wire mesh radius, is r = 0.25 mm and the distance between the centers of the two circles is d = 0.6 mm. This model is subjected to a biaxial load with the same range of the loading as employed for the screw thread. The magnitude of bone ingrowth into the cavity between the two beads or the doughnut hole in the wire mesh is stored in the data base.

The two-dimensional local model of a typical region of the bone around a bead-coated implant is shown in Figure 7. The model is assumed to be symmetric about its vertical bisector. In this local model the stress applied by the surrounding bone tissue is denoted by σ_x and σ_y. The initial ingrowth depth of the bone into the cavities of beads is denoted by h_i, the depth measured at point B at time t is denoted by $h_b(t)$ and in the middle is denoted by $h_m(t)$. In this dissertation h_b is taken as the ingrowth distance. It is assumed that the bone has been resorbed if $h_b(t) < 0.005$ mm and that the

bone has reached the maximum ingrowth if $h_b(t) > 0.25$ mm.

In order to obtain accurate numerical results, different boundary element meshes were used for three different ranges of $h_b(t)$. The properties of these boundary element meshes are detailed in Table 3. The BEM model is one-half of Figure 7, and the boundary AB is a free remodeling surface. The remodeling process is based on the surface bone remodeling theory using strain rate stimulus. On boundary BC, bone is in contact with the implant and roller boundary conditions are applied. On boundary CD, a uniform normal stress σ_x is applied and on boundary DE, uniform normal stress σ_y is applied. The roller boundary condition is applied on surface EA. Plane strain is assumed in the calculation. The material properties are a Young's modulus of 18 GPa and a Poisson's ratio of 0.28.

To develop the database for the bead model, the quantities $h_b(t)$ and $h_m(t)$ are calculated under the various combinations of σ_x and σ_y, as well as two different initial ingrowths, $h_i = 0.005$ mm and $h_i = 0.25$ mm. A database for this model has been created. In the database, a set of integer values of σ_x and σ_y ranging from -30 to 30 MPa are selected for both σ_x and σ_y. For the stresses which are not in the database, interpolation is used.

4.3 Global models

The global models are used to find stresses near the bone remodeling surface and relative displacements at the interface between the bone and the implant as shown in

Figure 1. The finite element method is used for the analysis. The stresses and relative displacements found in the global model are used in local models as loading conditions and micromotions. Three global models, i.e. axisymmetric global model, pseudo 3-D global model without abductor force and pseudo 3-D global model with abductor force, are used for the dissertation. The details of these models will be discussed in the next chapter.

4.4 Conceptual framework of the local-global feedback mechanism

The conceptual framework underlying this dissertation is diagrammed in the Flow Chart 1 for the Local-Global Feedback model. In this section each of the process steps of the model represented on the flow chart is described by a block.

INITIAL AND BOUNDARY CONDITIONS: Here the first information required to start the calculation is described. The prescribed initial conditions are the following:

1. Initial interference associated with the force fitting

> The placement of an implant is one of those practical cases of connecting two objects where it is desirable to force fit one object into another. The external dimensions of the implant are usually greater by an amount δ than the dimensions of the bone cavity (medullary canal) into which the implant is to fit. Force fits are obtained by pressing the implant into the bone cavity. Once the implant is fitted into the bone, the bone and implant exert a compressive stress normal to the interface on one another. The

magnitude of this compressive stress is proportional to the interference δ, which is the difference between the external dimensions of the implant and the dimensions of the bone cavity into which the implant is to fit. The initial interference δ prevents the relative rigid body motion between the bone and the implant when an external load is applied. In the general case a distribution of initial interference δ can be specified along the bone-implant interface. Initial interference is a specified parameter of the model that can function as a variable in a parametric study, but the time evolution of the interference is determined by factors such as the changing loads and depth of initial ingrowth in the model.

2. Initial ingrowth

Assume there is some initial bone ingrowth into the implant's porous surface before any external load is applied. This initial bone ingrowth is not the same as interference.

3. Applied loading

The external load applied to the bone implant must be specified. This loading is specified as standard patterns, which vary periodically or quasi-periodically with time at a frequency of a few to twenty Hz. Loading with different patterns and frequencies other than the standard patterns will be transferred to equivalent standard patterns.

4. Initial distribution of the effective Coulomb friction coefficient along the interface.

In order to initiate the iteration process, the distribution of the initial effective Coulomb friction coefficient along the interface must be assumed.

GLOBAL ANALYSIS: The purpose of the global analysis performed by the ABAQUS

(Hibbitt *et al.* 1991) (FEM) program is to find the stress states and relative displacements along the bone-implant interface and the other bone remodeling surfaces given the applied loading, the present interference state and the slip potential. The non-implant contacting surfaces are assumed to be traction free and the surface bone remodeling theory is employed to predict their movement. The boundary condition illustrated in Figure 2b is employed in the FEM model of the bone-implant interface. The application of this non-linear boundary condition is an iterative process.

MECHANICAL EQUILIBRIUM CHECK: Mechanical and remodeling equilibrium checks are made at each iteration loop. If mechanical equilibrium is satisfied, the iteration loop is continued. If mechanical equilibrium is not satisfied, the system has failed, the iteration loop is exited and the calculation finishes.

REMODELING EQUILIBRIUM CHECK: For the remodeling equilibrium check each local site on all remodeling surfaces is tested to determine if the stimulus on the free surface of the current ingrowth has reached remodeling equilibrium. If it has, remodeling equilibrium has been reached for this local site, and the process stops locally. It also stops locally if the bone remodeling surface contacts a non-bone surface such as the implant or PMMA. If all the local site remodeling processes stop, the program stops. Otherwise, the iteration loop is continued.

LOCAL ANALYSIS: In the global analysis described above, the stress states near the

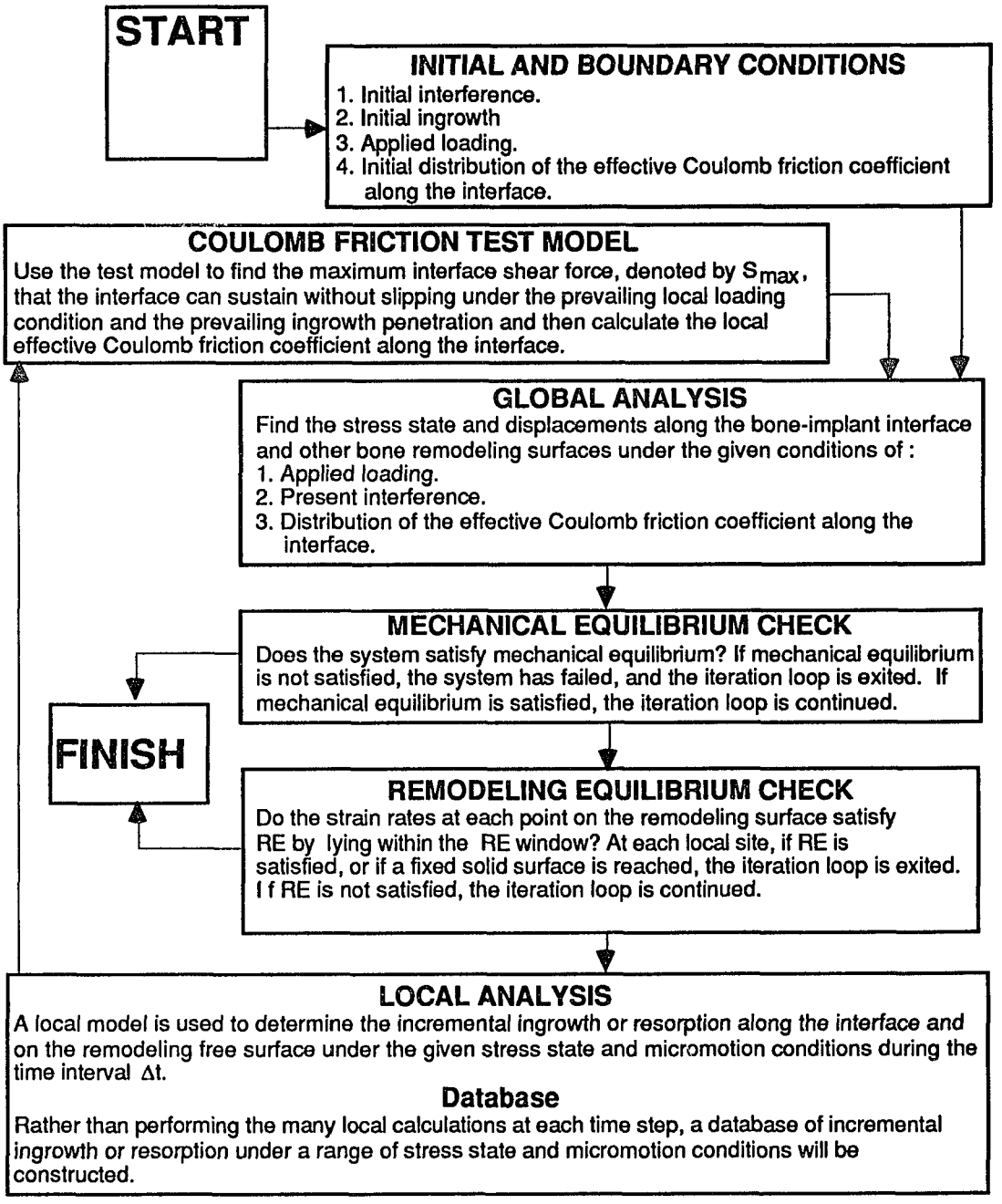

Flow Chart 1. The Local-Global Feedback Model

remodeling endosteal and periosteal free surfaces, and at the remodeling bone-implant interface are determined. In the local analysis performed with the boundary element method (BEM), the ingrowth during the time interval Δt at each node of the bone-implant interface under given stress states is calculated using the surface bone remodeling theory. Rather than performing the many local calculations at each time iteration, a database of incremental ingrowth or resorption under a range of stress state and micromotion conditions is constructed.

Micromotion, that is to say relative displacement per loading cycle between the bone and the implant, hinders the process of bone formation and causes bone resorption. Let M denote the magnitude of the micromotion in units of length per loading cycle. Although understanding of the effect of micromotion is limited, it is generally agreed that it has the effect of reducing surface bone deposition when $0 < M < Mc$ and stopping bone deposition when $M > Mc$ where Mc denotes the critical value of the micromotion. The value of Mc is estimated to be 100μm per cycle (Pilliar *et al.*, 1986). For surface bone remodeling, the modeling speed U at a surface point is determined from the surface bone remodeling theory that depends upon the strain rate at the surface point. If there is no micromotion ($M = 0$), the surface movement is determined from $\Delta x = U\,\Delta t$ where Δt is the time interval of an iteration. If there is micromotion, a modification will be adopted by the following formula that replaces the remodeling speed U by an effective remodeling speed U_{eff}:

$$U_{eff} = \begin{cases} U * f(M) & \text{if } U \geq 0, \\ U & \text{if } U < 0, \end{cases}$$

$$\text{where } f(M) = \begin{cases} \left(1 - \frac{M}{M_c}\right), & \text{if } 0 \leq M \leq M_c, \\ 0, & \text{if } M \geq M_c. \end{cases} \qquad (6)$$

The reason that the factor f(M) in (6) is assumed to be proportional to (1 - M/Mc) is that there are no data to better describe the transition from an effective value of f(M) = 1 at M = 0 to f(M) = 0 at M = Mc, so linearity is assumed for simplicity.

COULOMB FRICTION TEST MODEL:

The test model for the slip condition is used to find the maximum interface shear force, denoted by S_{max}, that the interface can sustain without slipping under the prevailing local loading conditions and the prevailing ingrowth penetration.

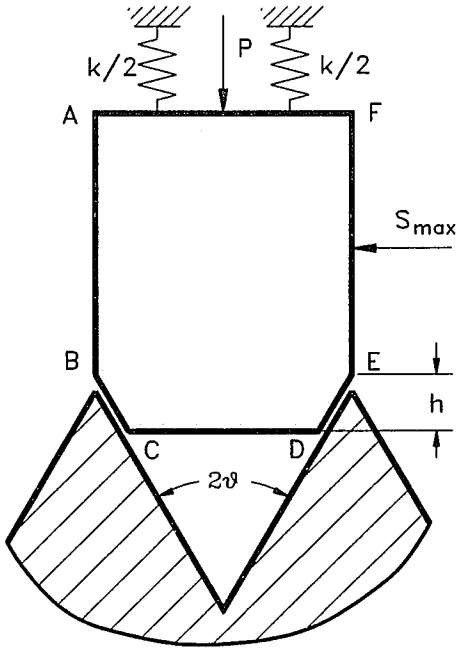

Figure 15. The maximum shear force test model.

The bone test block (isolated as a free body diagram) for the calculation of S_{max} is shown in Figure 15. It consists of a small piece of bone cut (conceptually) from near the implant surface. The determination of S_{max} requires the following information: the geometry of BC and DE, the ingrowth, the pre-stress force P, the stiffness k and the coefficient of friction f. In the determination of S_{max}, the following assumptions are made:

a. The effect of the outside bone on the bone test block isolated for the free body diagram can be reflected as a radially directed pre-stress force P and a spring with stiffness k acting on side AF.

b. The deformation of the bone test block is so small that it can be neglected, i.e. the

block can be assumed to be a rigid body.

c. There is no rotation of the block.

d. There is Coulomb friction on the interfaces BC and DE with the coefficient of friction f.

Based on the above assumptions, the maximum shear force S_{max} can be found as a function of the geometry of BC and DE, the ingrowth distance h, the pre-stress force P , the stiffness k and the coefficient of friction f, thus

$$S_{max} = \frac{(P + kh)(\cos\theta + f\sin\theta)}{\sin\theta - f\cos\theta}, \qquad (7)$$

where the effective coefficient of friction is defined by

$$f_{eff} = \begin{cases} \dfrac{S_{max}}{P} & for\ P \geq 1\ MPa, \\ \dfrac{S_{max}}{1\ MPa} & for\ P \leq 1\ MPa, \\ 0 & for\ P \leq 0. \end{cases} \qquad (8)$$

It is important to keep in mind that the curves BC and DE do not have to be straight lines, but can be portions of circular arcs or similar curves that preserve the symmetry of the bone block isolated for the free body diagram in Figure 15. Of course, the formula (7) will be modified to reflect the particular curve employed.

4.5 Computational implementation of the local-global feedback mechanism

The programming of the conceptual framework described in the previous section is diagrammed in Flow Chart 2, Feedback Process Programming. The flow chart illustrates the interaction between the sub-programs and the data files. Descriptions are

given for each sub-program or process step and data file represented on the chart, and their interaction with the other sub-programs or process steps and data files. The sequential steps in the program are illustrated by the thicker lines with arrowheads, and the data exchanges at each step are indicated by thinner lines with arrowheads.

FILES: Before the start of the computing process, two files that contain both local and global information are required; these files are:

1. Remodeling Data: This is the initial DATA FILE, which is updated in the feedback process. For local remodeling this includes the remodeling node number, the location, the initial ingrowth, the initial normal of the remodeling surface and the type of local model at each node. For the linking of the local and global analyses this includes the test block with remodeling surface, Coulomb friction coefficient (different from effective Coulomb friction coefficient) associated with the surface.

2. Input file: This is the input file for global FEM analysis. A commercial FEM program, ABAQUS, is employed. This file includes meshes, material properties, boundary conditions, loads and interface conditions between bone and implant.

ABAQUS PROGRAM (FEM analysis): The program reads the Input file, then solves the FEM problem. Since no tension and Coulomb friction are introduced on the interface, the analysis is nonlinear. When the analysis is complete, an output file

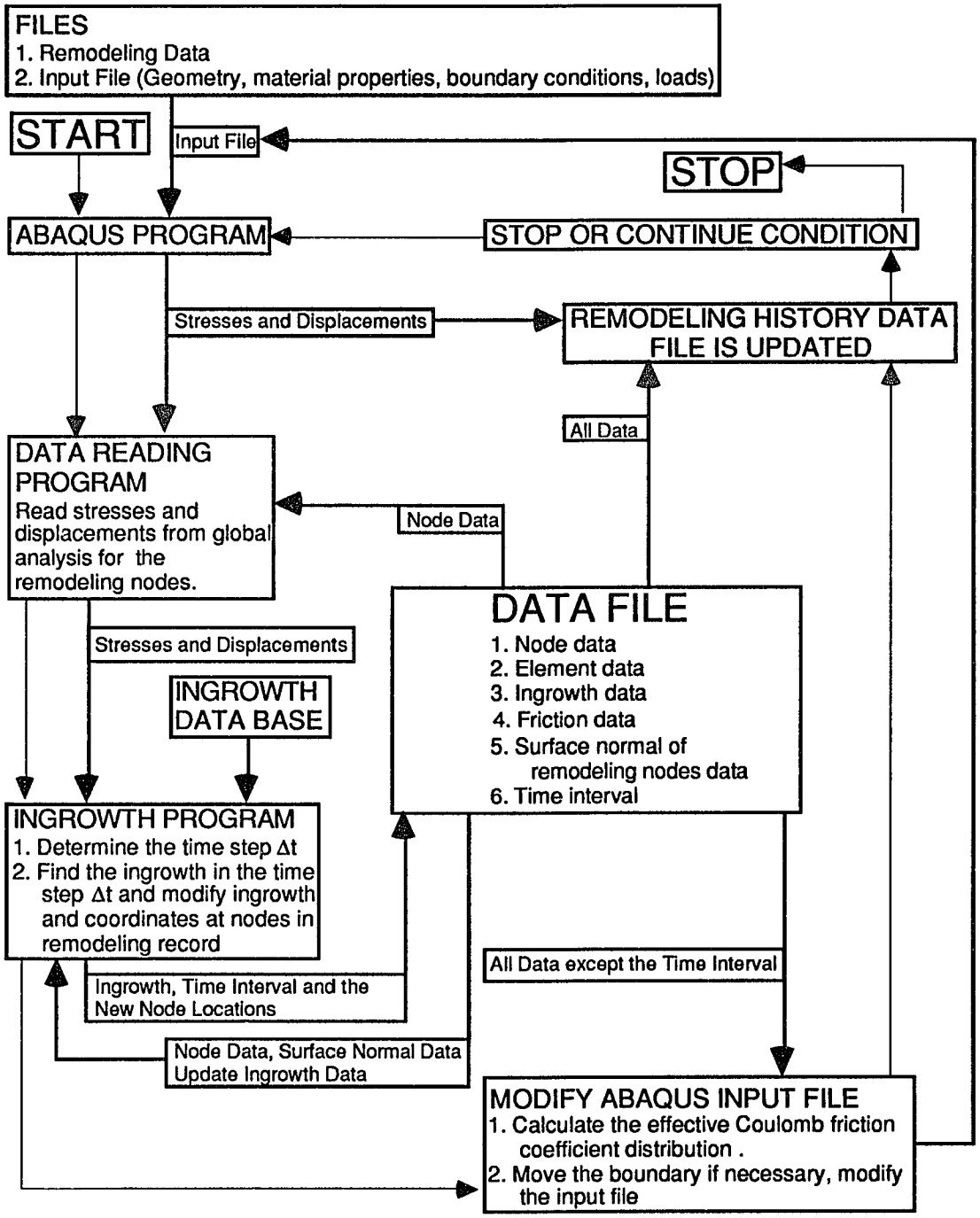

Flow Chart 2. Feedback Process Programming

containing stresses and displacements is created. This file will be used in the local remodeling process.

DATA READING PROGRAM: From the output file created by the ABAQUS PROGRAM, the data reading program reads stresses and displacements of these remodeling nodes specified in the DATA FILE. The stresses and displacements of these remodeling nodes are passed to the next step, the INGROWTH PROGRAM.

INGROWTH PROGRAM: There are two tasks to be accomplished by this program:

1. Determine the time interval: In a remodeling process, the time interval of an iteration is a very important parameter. Too small a time interval will result in convergence so slow that the process will take an extremely long time. On the other hand, too large a time interval will result in non-smooth convergence or no convergence (even chaos). In this program, the time interval is chosen in such away that the maximum increase of the ingrowth and free surface movement due to remodeling on all active remodeling surfaces will not exceed a specified value in one iteration. Different specified values were used in different situations, e.g. local models, free surface. This value will be reduced as the process converges.

2. Find ingrowth and free surface bone remodeling in the time interval: To find the amount of ingrowth, a database that contains ingrowth versus the time period under

different stress states is used. The specific database employed depends upon the particular interface being modeled. The effect of the micromotion is considered in the way described by formula (6). For free surface bone remodeling, the surface bone remodeling theory is adopted. The node locations, ingrowth and surface normals of the remodeling nodes of the last iteration are read from the DATA FILE. After finding the new ingrowth and new node locations, the data, as well as the time interval, in DATA FILE are updated.

MODIFY ABAQUS INPUT FILE: There are also two tasks performed here:

1. All the necessary information is read from the DATA FILE. The effective Coulomb friction coefficient for each interface element between the bone and the implant is evaluated by using the method described in the previous section.

2. The Input File is modified in this sub-program. The effective Coulomb friction coefficient in the Input File is replaced by the new one evaluated in the task 1, above. If any surface bone remodeling is found in this iteration, the node locations are also updated.

REMODELING HISTORY DATA FILE IS UPDATED: This sub-program creates a history record file. For the first iteration it records the Remodeling Data, which is the initial DATA FILE. For each subsequent iteration it records the stresses and the

displacements of the remodeling surface and all the data in the DATA FILE.

STOP OR CONTINUE EQUILIBRIA CONDITIONS: There are two conditions which are used to determine whether to stop the process or to let it continue. The first one is the mechanical equilibrium check. If mechanical equilibrium is not satisfied, stop the process. If mechanical equilibrium is satisfied, then go to the next step, the remodeling equilibrium check. For the remodeling equilibrium check each local site on all remodeling surfaces is tested to determine if the stimulus on the free surface of the current ingrowth has reached remodeling equilibrium. If it has, remodeling equilibrium has been reached for this local site, and the process stops locally. It also stops locally if the bone remodeling surface contacts a non-bone surface such as the implant or PMMA. If all the local site remodeling processes stop, the program stops. Otherwise, the iteration looping is continued. For final equilibrium it is not required that the surface change in the final remodeling steps be zero, only that it be small in the sense of asymptotic convergence to a fixed limit.

5. GLOBAL MODELS EMPLOYED IN THE DISSERTATION

Global models are used to find the stress and displacement distribution which are employed in the bone remodeling process. Three global models are used: axisymmetric global model, pseudo 3-D global model without abductor force and pseudo 3-D global model with abductor force. The details of these models will be described in the following sections.

In these global models, the size of the implant is slightly bigger than the size of the bone cavity where the implant is placed. The interference δ causes the pressure between the bone and the implant. The interference δ is small in the

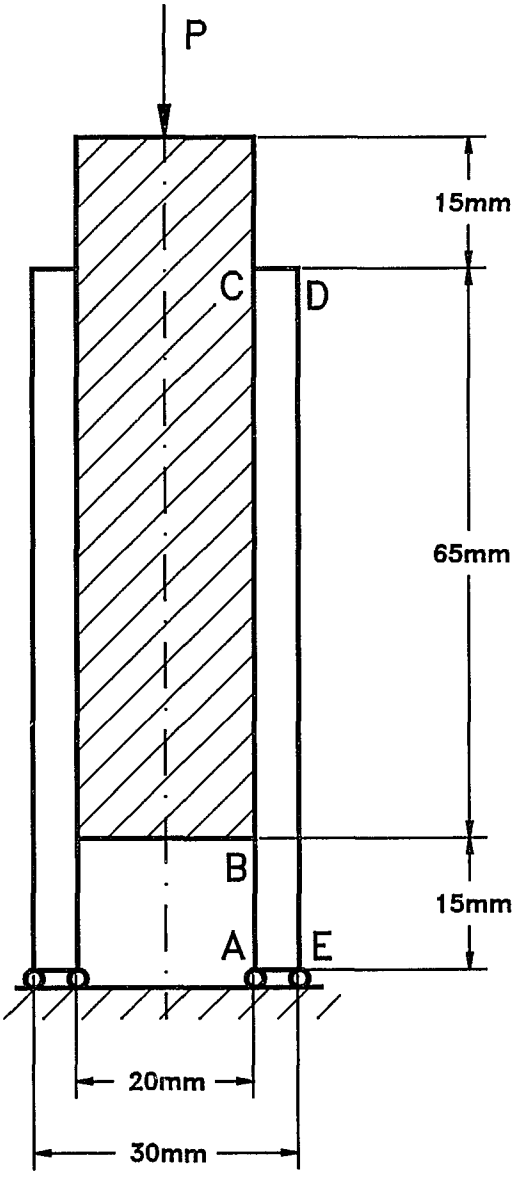

Figure 16. The axisymmetric global model including illustration of the loading and boundary conditions.

studies described here. The pressure on the interface is necessary in order to prevent rigid body motion between bone and implant.

The material properties employed for the dissertation are: for the bone, a Young's modulus of 18 GPa and a Poisson's ratio of 0.28; for the steel implant, a Young's modulus of 200 GPa, a Poisson's ratio of 0.29; for titanium, a Young's modulus of 110 GPa and a Poisson's ratio of 0.29 and a k of 600 MPa/mm.

The interface conditions between bone and implant are no tension and Coulomb friction. The initial effective Coulomb friction coefficient is assumed uniform at 1.0 along the interface, but the evolutionary value of the effective Coulomb friction coefficient, which

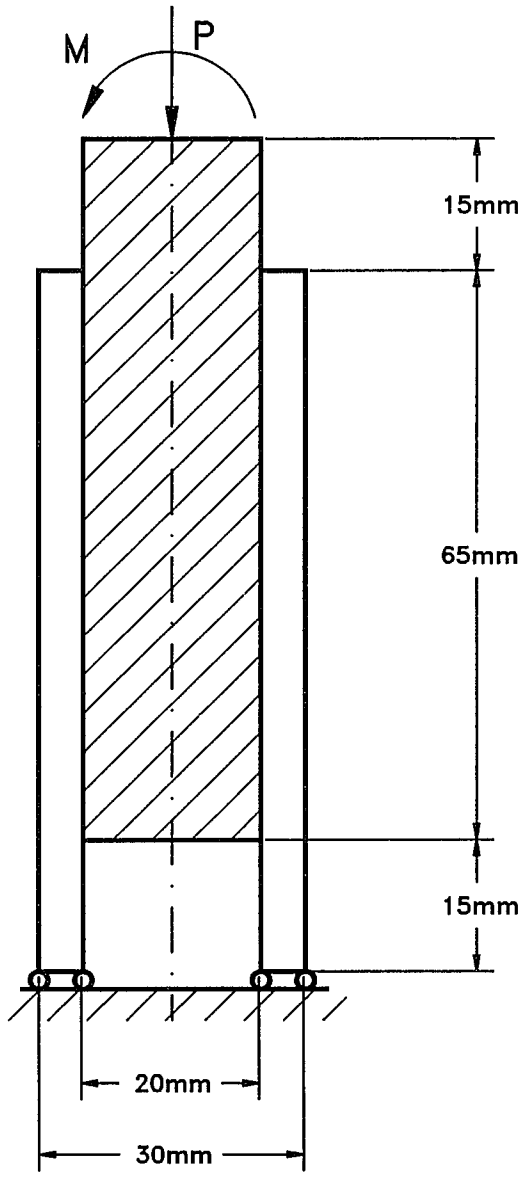

Figure 17 Pseudo 3-D global model without abductor force. The loading and boundary conditions are also presented.

is a function of the ingrowth at each location, was evaluated in the way described in the section on the conceptual framework of the local-global feedback mechanism in the previous Chapter.

5.1 Axisymmetric global model

In this global model an axisymmetric straight bone with an axisymmetric straight implant was used to simulate a THA. The dimensions of the bone and the implant are shown in Figure 16, as are the boundary conditions. The height of both the bone and the implant is 80 mm and the implant is placed 15 mm higher than the bone. The outer radius of the bone is 15 mm, the inner radius is 10 mm. The outer radius of the implant is 10 mm + δ which is slightly larger than the inner

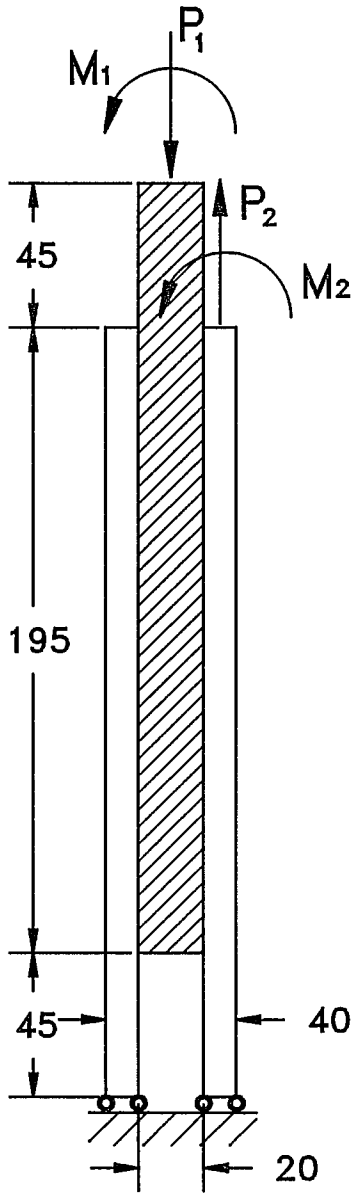

Figure 18. Pseudo 3-D global model with an abductor force. The loading and boundary conditions are also presented. The length units are mm's.

radius of the bone. Eight-node quadratic finite elements were used for both bone and implant. There were 80 elements for the bone, 30 elements for the implant and 20 slide-line elements for the interface.

In this axisymmetric global model, only an axial load P = 10,000 N was applied on the top of the implant. In reality the load applied at the top of the implant is a combined axial load and couple. The magnitude of the couple is significant and dominates the total loading. In this model the amount of the axial load P was selected so that it created stress levels similar to those created by the real combined axial load and couple.

5.2 Pseudo 3-D global model without abductor force

In the model a 2-D bone with side plates and a 2-D straight implant were used to simulate a THA. The height and width of the bone and the implant are shown in Figure 17, as are the boundary conditions. The thickness of the bone, side plates and the implant, as shown in Figure 19, were calculated in the section 5.4. The width of the implant is l0 mm + δ which is slightly bigger than the inner width of the bone. Eight-node quadratic finite elements were used for both bone and implant. There were 128 elements for the bone, 256 elements for the side plates, 64 elements for the implant and 64 slide-line elements for the interface.

In this pseudo 3-D global model, the load applied on the top of the implant is forcea combined axial load and couple. The magnitude of the couple is significant and

dominates the total loading. The bending moment M was 80 Nm and the axial load P was zero or 100 N.

Hx	1492 N
Hy	915 N
Hz	-2925 N
Ax	-1342 N
Ay	-832 N
Az	2055 N

Table 4. The head and abductor forces employed by Keaveny (1991).
Unit = Newton, Bodyweight = 750 N.

X - Medial to Lateral,
Y - Anterior to posterior,
Z - Distal to proximal.
H - Head, A - Abductor.

5.3 Pseudo 3-D global model with abductor

In this global model, a 2-D bone with side plates and a 2-D straight implant were used to simulate a THA. The height and width of the bone and the implant are shown in Figure 18, as are the boundary conditions. The thickness of the bone, side plates and the implant were calculated in section 5.4. The width of the implant is 10 mm + δ which is slightly bigger than the inner width of the bone. Eight-node quadratic finite elements were used for both bone and implant. There were 128 elements for the bone, 256 elements for side plates, 64 elements for the implant and 64 slide-line elements for the interface. The dimensions of this global model are based on measurement from a radiograph of a femur with implant supplied by the Hospital for Joint Diseases in New York City

The load applied on this model is similar to that employed by Keaveny (1991). The x, y, z components of the forces applied on the femur head (H) and abductor (A) are listed in Table 4. A strenuous loading case on the hip represents the load in the

early post-operative period. In this study, a loading case similar to the strenuous case is used.

In this pseudo 3-D global model, the load applied on the top of the implant is a combination of an axial load P_1 and a couple M_1. A combination of an axial load P_2 and a couple M_2 applied on the greater trochanter simulates the abductor muscle. The magnitude of the couples is significant and dominates the total loading. In this model the amount of the bending moment M_1 was 180 Nm, the axial load P_1 was 3150 N and M_2 was 0 or 15 Nm, the axial load P_2 was 2100 N.

5.4 Dimensions in pseudo 3-D global models

Here the dimensions of the pseudo 3-D global model are determined, based on the assumption that the moment of inertia of the pseudo 3-D model equals that of the 3-D model. First we determine the dimensions of an implant by assuming that the moment of inertia of the implant in the pseudo 3-D model equals that in the 3-D model. The moment of inertia of the circular cross-section of a 3-D implant is

$$I_i = \frac{\pi r^4}{4} \qquad (9)$$

and the moment of inertia of the rectangular cross-section of the pseudo 3-D implant is

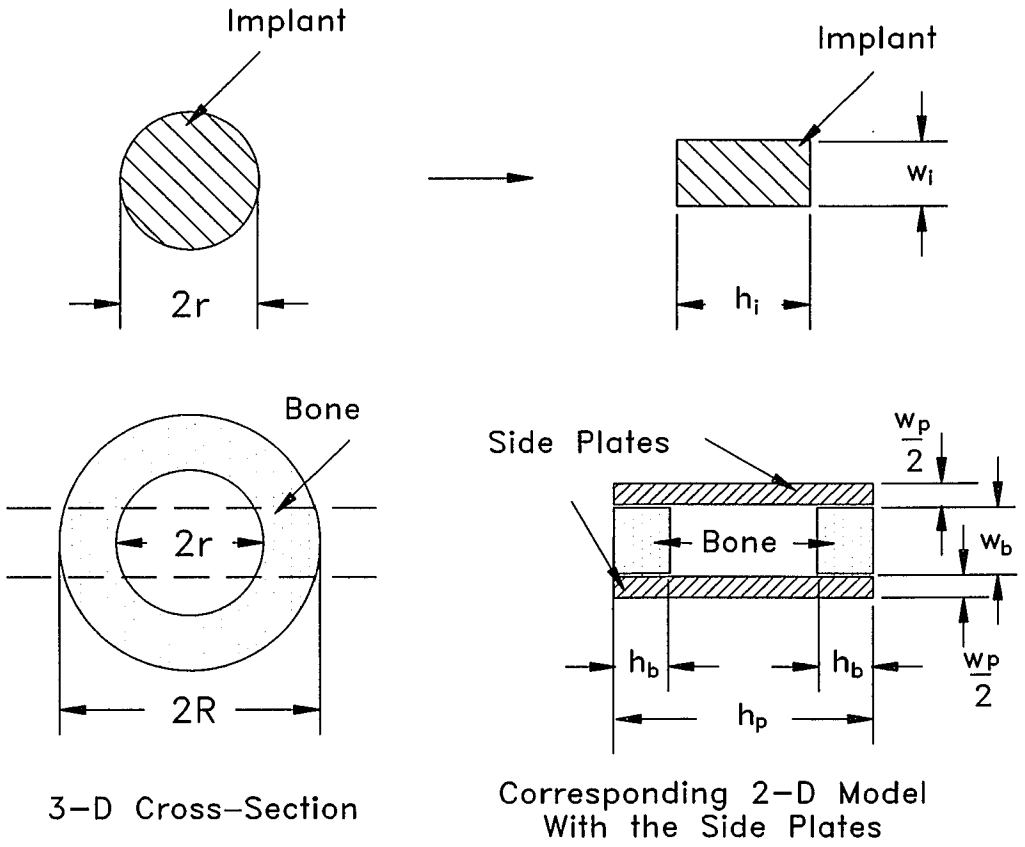

Figure 19. The cross-sections of a real 3-D model (left) and a pseudo 3-D model (right). The implant is on the top and the bone is on the bottom.

$$\overline{I_i} = \frac{w_i h_i^3}{12}. \tag{10}$$

Let the moments of inertia of the cross-sections of the 3-D implant and the pseudo 3-D implant equal

$$I_i = \overline{I_i}, \ i.e. \ \frac{\pi r^4}{4} = \frac{w_i h_i^3}{12} \tag{11}$$

and assume $h_i = 2r_i$; then we can find w_i from the above equation,

$$w_i = \frac{3\pi r_i}{8}. \tag{12}$$

Secondly, we determine the dimensions of the bone and side plates by assuming that the moment of inertia of the bone and side plates in the pseudo 3-D model equals that of the bone in the 3-D model, and the derivative of the moment of inertia with respect to wall thickness h_b in the pseudo 3-D model equals the derivative of the moment of inertia with respect to wall thickness (R-r) in the 3-D model. The above two assumptions mean that both the pseudo 3-D cross-section and the 3-D cross-section have the same moment of inertia as well as the same variation of the moment of inertia with respect to given bone thickness change due to remodeling.

The moment of inertia of the ring cross-section of 3-D bone is

$$I_b = \frac{\pi (R^4 - r^4)}{4}, \tag{13}$$

and the moment of inertia of the cross-section of pseudo 3-D bone and side plates is

$$\overline{I_b} = 2\frac{w_b h_b^3}{12} + 2w_b h_b\left(\frac{h_i + h_b}{2}\right)^2 + \frac{w_p h_p^3}{12}. \tag{14}$$

The derivative of the moment of inertia of the ring cross-section of 3-D bone with respect to the thickness of the cylinder wall (R-r) is

$$\frac{dI_b}{d(R-r)} = \frac{\pi}{4}(R + r)(R^2 + r^2), \tag{15}$$

and the derivative of the moment of inertia of the cross-section of pseudo 3-D bone and side plates with respect to the thickness h_b is

$$\frac{d\overline{I_b}}{dh_b} = 2w_b h_b^2 + \frac{1}{2}w_b h_i^2 + 2w_b h_i h_b. \qquad (16)$$

Let the moments of inertia of the cross-sections of 3-D bone and pseudo 3-D bone equal

$$I_b = \overline{I_b},\ i.e.\ \frac{\pi(R^4-r^4)}{4} = 2\frac{w_b h_b^3}{12} + 2w_b h_b\left(\frac{h_i+h_b}{2}\right)^2 + \frac{w_p h_p^3}{12} \qquad (17)$$

and assume the derivative of the moment of inertia of the ring cross-section of 3-D bone with respect to wall thickness (R-r) is equal to the derivative of the moment of inertia of the cross-section of pseudo 3-D bone and side plates with respect to the thickness h_b,

$$\frac{dI_b}{d(R-r)} = \frac{d\overline{I_b}}{dh_b},\ i.e.$$
$$\frac{\pi}{4}(R+r)(R^2+r^2) = 2w_b h_b^2 + \frac{1}{2}w_b h_i^2 + 2w_b h_i h_b. \qquad (18)$$

Solving equation (18), we can find the value of w_b,

$$W_b = \frac{-\left(\frac{1}{4}\pi R^3 + \frac{1}{4}\pi R^2 r + \frac{1}{4}\pi R r^2 + \frac{1}{4}\pi r^3\right)}{\left(-2h_b^2 - \frac{1}{2}h_i^2 - 2h_i h_b\right)}, \qquad (19)$$

and solving equation (17) , we can find the value of w_p,

$$w_p = 12\frac{\left(\frac{1}{4}\pi R^4 - \frac{1}{4}\pi r^4 - \frac{2}{3}w_b h_b^3 - \frac{1}{2}w_b h_b h_i^2 - w_b h_b^2 h_i\right)}{h_p^3}. \qquad (20)$$

Thus, if R and r are given, w_p and w_b can be calculated.

For the pseudo 3-D model without and with abductor force, the dimensions are

	R	r	h_i	w_i	h_b	w_b	h_p	w_p
Model A	15	10	20	11.78	5	14.18	30	4.202
Model B	20	10	20	11.78	10	14.73	40	9.204

Table 5. The dimensions of pseudo 3-D global models. The length unit is one mm.
Model A: Pseudo 3-D global model without abductor force.
Model B: Pseudo 3-D global model with abductor force.

listed in Table 5.

5.5 Meshes of global models

In global analysis, a commercial FEM software (ABAQUS) is used. It is important to find an appropriate mesh that can maintain a desirable accuracy while including less elements. Here two different meshes were studied and compared, so that an appropriate mesh could be employed.

The global model studied here is a pseudo 3-D model. The two different FEM meshes are shown in Figures 20 and 21. The eight-node quadrilateral plane strain element (ABAQUS classification CPE8) was used in all calculations. In the coarse mesh, there are 32 elements for the bone and 32 elements for the implant (Figure 20a) and 96 elements for the side plates (Figure 20b). In the finer mesh, there are 64 elements for the bone and 128 elements for the implant (Figure 21a) and 192 elements for the side plates (Figure 21b).

For the two meshes, the same loading, boundary and connection conditions were

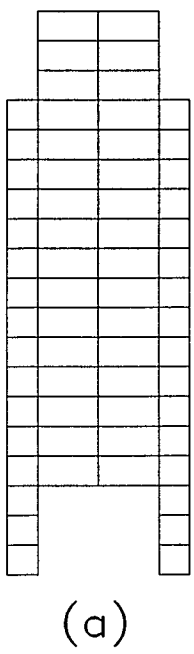

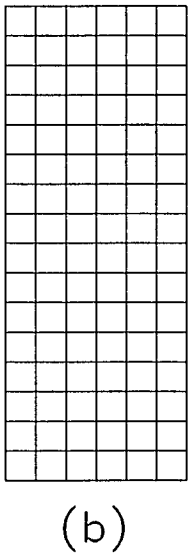

Figure 20. A coarse global mesh. (a) the mesh of bone and implant, (b) the mesh of side plates.

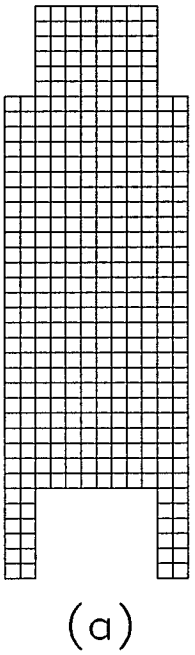

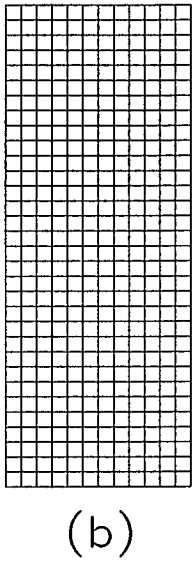

Figure 21. A finer global mesh. (a) the mesh of bone and implant, (b) the mesh of side plates.

employed. According to Keaveny (1991), an axial compressive load of 750 N and a bending moment of 80 Nm are applied at the top of an implant. Thus in this study, a concentrated downward force (750 N) is applied at the middle point of the top side of the implant to simulate the axial load; a concentrated downward force (4,000 N) is applied at the left corner of the top side of the implant and a concentrated upward force (4,000 N) is applied at the right corner of the top side of the implant to simulate the bending moment. The roller boundary conditions are applied to the whole bottom side of the bone and the side plates, i.e. no vertical displacement of all the nodes on the bottom line. To restrict rigid body motion in the horizontal direction, the middle node of the bottom side of the side plates is fixed. All nodes of the bone mesh and the

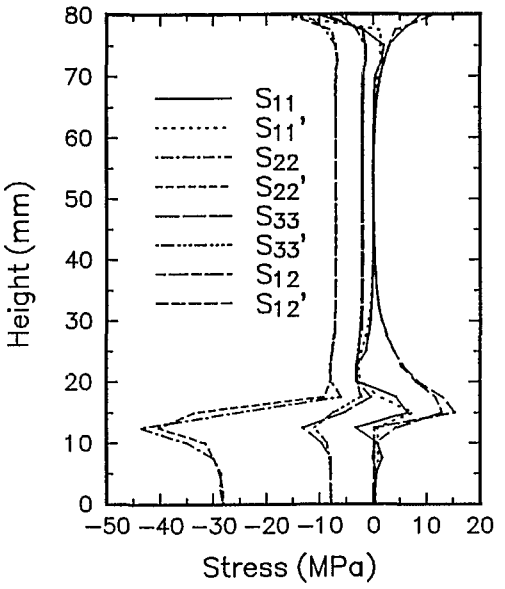

Figure 22. Stress distribution along the medial interface. Curves without prime mark and curves with prime mark are corresponding to the coarse mesh and finer mesh respectively.

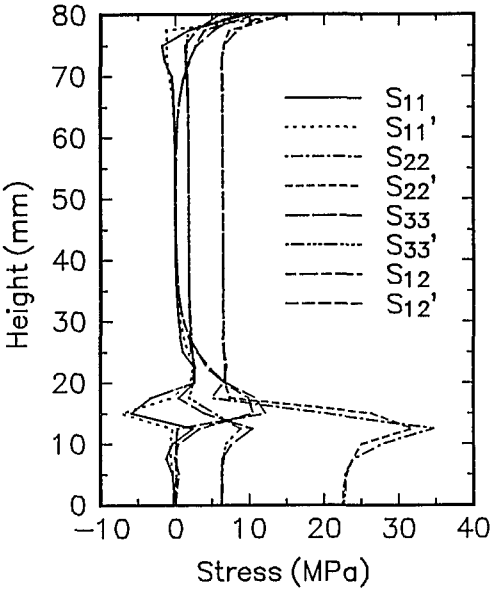

Figure 23. Stress distribution along the lateral interface. Curves without prime mark and curves with prime mark are corresponding to the coarse mesh and finer mesh respectively.

implant mesh on the bone-implant interface are directly connected to each other. All nodes of the side plates mesh that overlap the bone mesh are connected to the corresponding nodes on the bone mesh. There is no connection between the nodes on the side plates mesh and the implant mesh.

Since the purpose of the global analysis is to find the stress distribution in the bone mesh which is under remodeling, only the accuracy of stress in the bone mesh was studied. It is well known that the accuracy of displacement is always higher than that of stress for a given mesh. Thus although the distribution of displacement will be used in the local global feedback model when micromotion is taken into account, the accuracy of the distribution of displacement should not be a problem if a mesh can

ensure an accurate stress distribution. In FEM analysis, inaccuracy usually occurs at the place where there is a sudden change of geometry, material property, boundary condition or at the place where there is relatively higher shear stress. It is clear that inaccuracy may occur along the endosteal surface where the implant begins or where the bone ends.

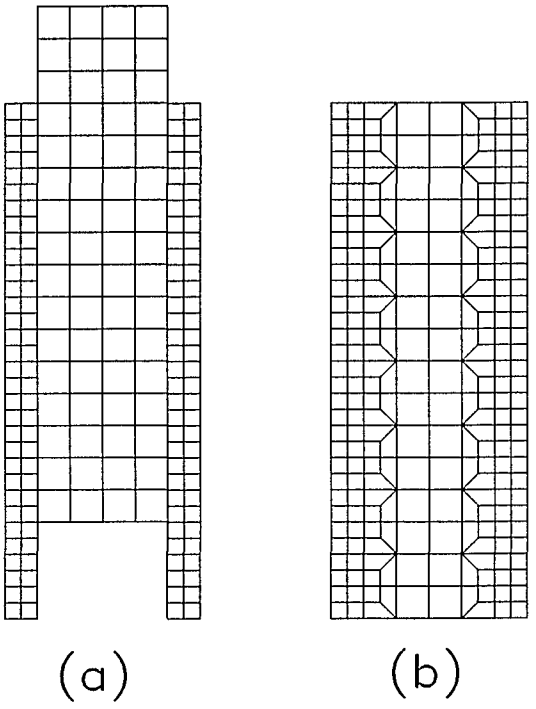

Figure 24. The global FEM mesh used in the dissertation. (a) mesh of bone and implant (b) mesh of side plate.

The stress distribution along the medial endosteal surface is plotted in Figure 22, where the stresses without prime mark and with prime mark correspond to the coarse mesh and finer mesh respectively. The stress distribution along the lateral endosteal surface is plotted in Figure 23, where the prime mark has the same significance.

Both the coarse and finer meshes result in the same stress distribution except the two connection discontinuities near the point at the top of the bone and the point at the bottom of the implant, as may been seen in Figures 22 and 23. The difference between the maximum stresses in these two meshes is less than 4 MPa. Both meshes appear to be appropriate for global analysis. To ensure an accurate global analysis, a mesh as in Figure 24 is used in this dissertation.

6. RESULTS

All numerical remodeling results of the three global models are presented in this chapter. The three models are the axisymmetric global model, the pseudo 3-D global model without abductor force and the pseudo 3-D global model with abductor force. The figures of these results are attached at the end of this chapter.

6.1 Results of the axisymmetric global model

The axisymmetric global model was used to study: a) the effect of different interfaces, i.e. bead or screw thread, b) initial interference along the bone implant interface, c) initial ingrowth. Three cases and figure numbers of the corresponding results are listed in Table 6. In these cases, it was assumed that the implant was made of steel and that the interface was fully covered with beads or screw threads.

The limitation of the axisymmetric model is that the model precludes the application of bending moments which violate the axisymmetry. In the absence of a bending moment, the dynamic strain along the bone implant interface is much lower than what exists under a combination of bending moment and axial load. The lower dynamic strain along the bone implant interface caused bone resorption and results in mechanical failure in most calculations before significant resorption occurred on the periosteal surface. This model fails more easily with a bead interface than with a screw thread interface.

Case	Figure No.	Initial interference	Initial ingrowth
1	26	0.01 mm	0.25 mm
2	27	0.02 mm	0.48 mm
3	28	0.01 mm	0.48 mm

Table 6. The three cases of screw thread interface for the axisymmetric global model; the numbers of the Figures illustrating the results are listed for each case.

6.2 Results of the pseudo 3-D global model without abductor force

The effect of varying the following parameters was studied using the model: a) different interfaces, i.e. bead or screw thread, b) initial interference along the bone implant interface, c) initial ingrowth, d) material properties of the implant, e) axial load, f) the size of the coated area of the implant, g) effect of the periosteal surface bone remodeling on the bone implant interface remodeling.

Thirteen cases and figure numbers of the corresponding results are listed in Table 7. The load applied at the top of the implant consisted of a moment 80 Nm and axial load 0 N or 100 N. In all the above cases, except for case 13, calcar resorption, bone resorption at the lateral upper corner, interface resorption on both the medial side and lateral side are predicted. In most cases, the development of humps on the medial and lateral sides is predicted. These humps are the result of bone deposition on the periosteal surface due to the high stress created by the distal end of the implant. A demonstration of these results is shown in Figure 25. In case 13, it was assumed there was no periosteal surface bone remodeling. This case did not simulate a real bone

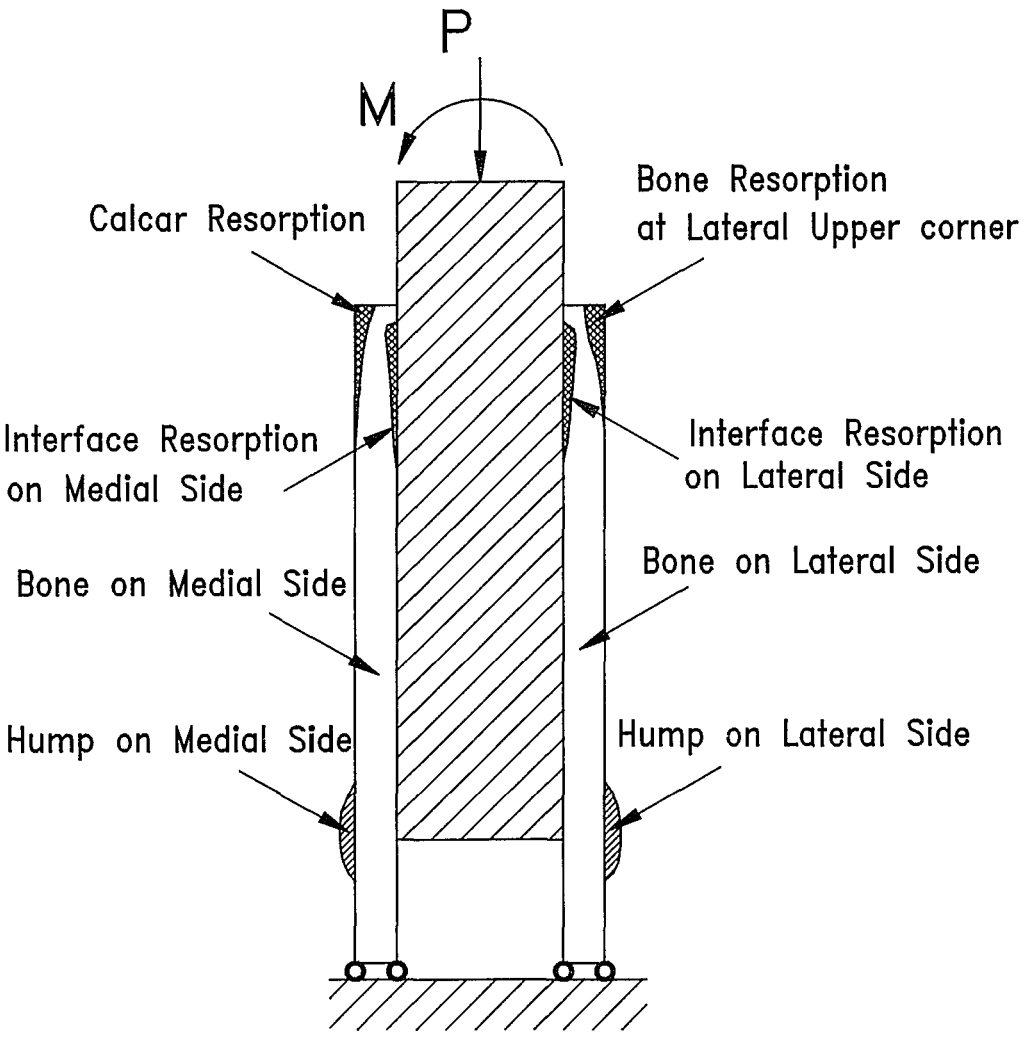

Figure 25 The Figure shows the terms used in the Results section.

remodeling process. However, it may help to understand the effect of periosteal surface bone remodeling on bone-implant interface remodeling.

Bone remodeling equilibrium was not reached in the above cases because the calcar resorption and the bone resorption at the lateral upper corner do not achieve equilibrium. Therefore the numerical process must be stopped to avoid mesh distortion.

Case	Figure No.	Interface	Initial inter-ference	Intial ingrowth	Implant	Coated interface
1	29	screw threads	0.01 mm	0.48 mm	titanium	100%
2	30	screw threads	0.01 mm	0.48 mm	titanium	38%
3	31	screw threads	0.01 mm	0.24 mm	titanium	38%
4	32	screw threads	0.02 mm	0.48 mm	titanium	100%
5	33	beads	0.01 mm	0.25 mm	steel	100%
6	34	beads	0.01 mm	0.25 mm	titanium	100%
7	35	beads	0.01 mm	0.25 mm	bone	100%
8	36	beads	0.01 mm	0.25 mm	titanium	38%
9	37	beads	0.01 mm	0.25 mm	titanium	100%
10	38	beads	0.02 mm	0.25 mm	titanium	38%
11	39	beads	0.01 mm	0.15 mm	titanium	38%
12	40	beads	0.02 mm	0.25 mm	titanium	100%
13	41	beads	0.01 mm	0.25 mm	titanium	38%

Table 7. A list of thirteen cases and figure numbers of their corresponding results with different values of parameters for the pseudo 3-D global model without abductor force. Axial load was zero except for case 9 that was 100 N.

In these figures, the word "initial" means the status before the remodeling process starts and the word "last" means the status of the last step of the remodeling process.

Based on the results of the pseudo 3-D global model, the following observations are made:

Case	Figure No.	Interface	Initial ingrowth	Initial interference	M_2 (Nm)	Coated interface
1	42	screw threads	0.48 mm	0.015 mm	22.5	100%
2	43	screw threads	0.48 mm	0.015 mm	0	100%
3	44	screw threads	0.48 mm	0.015 mm	22.5	38%
4	45	beads	0.25 mm	0.02 mm	22.5	100%
5	46	beads	0.25 mm	0.02 mm	22.5	38%

Table 8. A list of five cases and figure numbers of their corresponding results with different values of parameters for the pseudo 3-D global model with abductor force. Axial load P_2 was 2100 N.

a) Different interfaces, i.e. beads or screw threads, predict similar global remodeling. This can be seen by comparing cases 1 and 6, cases 2 and 8, cases 3 and 11 and cases 4 and 12.

b) The existence of initial interference is important for successful THA. However the difference between an interference of 0.01 mm and one of 0.02 mm on global remodeling is not significant except for the humps on the periosteal surface. This can be seen by comparing the results of cases 1 and 4, cases 6 and 12 and cases 8 and 10. Other values of the interference were not studied.

c) Initial ingrowth is also important for successful THA. When initial ingrowth was too small,

the numerical process failed at the first few steps. However the difference between 0.15

mm and 0.25 mm for the bead interface and 0.24 mm and 0.48 mm for the screw thread interface was not significant. This can be seen by comparing the results of cases 2 and 3 and cases 8 and 11.

d) The stiffness of the implant can change the global remodeling pattern. The higher the stiffness of an implant, the greater calcar resorption and the greater bone resorption at the lateral upper corner. Also, higher stiffness creates a larger hump on the periosteal surface; compare cases 5, 6 and 7, as the material varies from steel to titanium to bone.

e) The global remodeling process is dominated by the bending moment. An axial load varying from zero to 100 N does not change the remodeling process.

f) The global remodeling pattern associated with a fully coated implant is different from that associated with a partially coated implant. The model predicts more interface resorption on both the medial side and the lateral side for a fully coated implant than for a partially coated implant. However global remodeling patterns on a periosteal surface associated with both fully coated implants and partially coated implants are almost the same.

6.3 Results of the pseudo 3-D global model with abductor force

The effect of varying the following parameters was studied using this global model: a) different interfaces, i.e. bead or screw thread, b) initial interference along the bone implant interface, c) the load on the greater trochanter, d) the size of the coated area of an implant.

Five cases and figure numbers of the corresponding results are listed in Table 8. In these cases, it was assumed that the implant was made of titanium and the load applied at the top of the implant was P_1 = 3150 N, M_1 = 180 Nm.

Based on the results of this pseudo 3-D global model, the followings observations are made:

a) The maximum shear stress that an interface can sustain depends on the local interface model, i.e. bead or screw thread. However, as long as the bone-implant interface can sustain the external load, both interfaces predict similar resorption patterns.

b) The remodeling along the bone-implant interface develops friction. This developed friction is higher for the screw thread interface than for the bead interface.

c) The global remodeling associated with the fully coated implant is different from that associated with the partially coated implant. The models predict more interface resorption on both the medial side and the lateral side for fully coated implants than for partially coated implants. However the global remodeling patterns on the periosteal surface associated with both the fully coated implant and the partially coated implant are very similar. Here we use "coated" to indicate either a bead or a screw interface.

6.4 Comments on these global models

Three global models, the axisymmetric global model, the pseudo 3-D global model without abductor force and the pseudo 3-D global model with abductor force,

have been studied. By comparing the results obtained with these global models, the following conclusions may be drawn:

a) The axisymmetric global model is not an appropriate model for the local-global feedback process to study the long term stability of a hip implant. This is due to the fact that, in reality, the hip is mainly loaded by bending, and the axisymmetric global model precludes bending. This results in a lower dynamic stress amplitude and bone resorption along the bone-implant interface. Hence the model predicts an early failure of the implant.

b) The pseudo 3-D global model without abductor force predicts remodeling patterns that are consistent with clinical observation in the proximal end of the model (near the greater trochanter). This is because the model retains the basic features of the load applied to the hip implant.

c) The pseudo 3-D global model with abductor force predicts remodeling patterns that are consistent with clinical observations even in the greater trochanter area. This is because the model maintains the features of load applied on both the hip implant and the region of the greater trochanter.

d) The results obtained with these global models can be compared only qualitatively with clinical observations, due to the simplification of geometry, material properties and loadings.

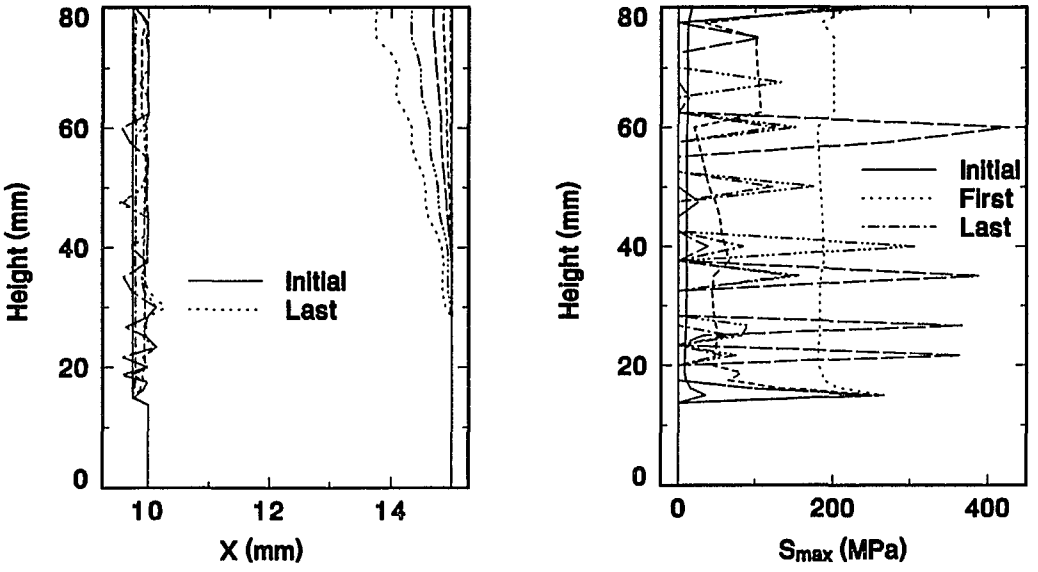

Figure 26. Remodeling predictions for a steel implant fully covered with screw threads. The initial ingrowth was 0.25 mm and initial interference was 0.01 mm. Bone outline (left), maximum shear stress can be sustained along the interface (right).

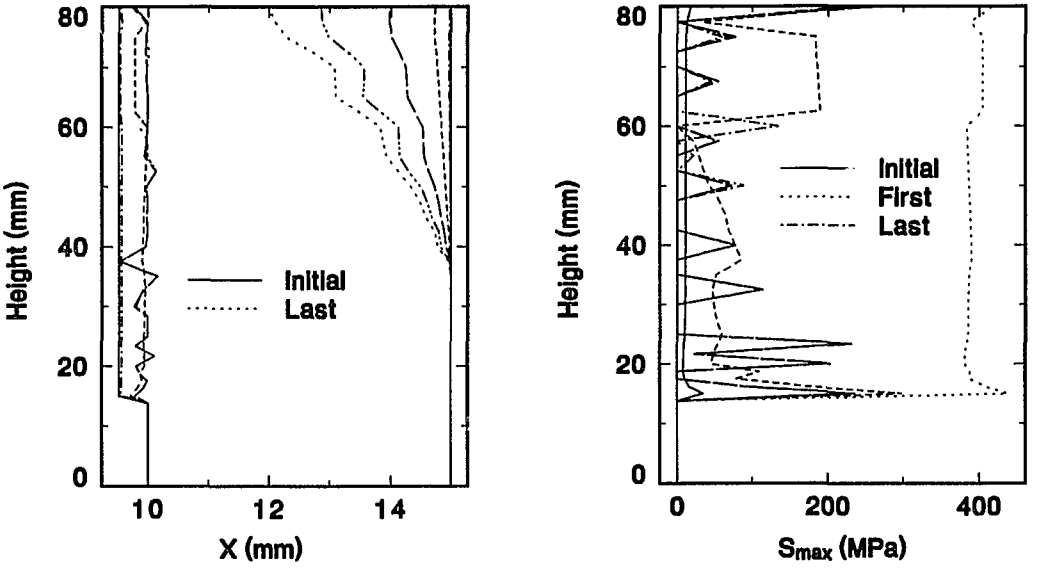

Figure 27. Remodeling predictions for a steel implant fully covered with screw threads. The initial ingrowth was 0.48 mm and initial interference was 0.02 mm. Bone outline (left), maximum shear stress can be sustained along the interface (right).

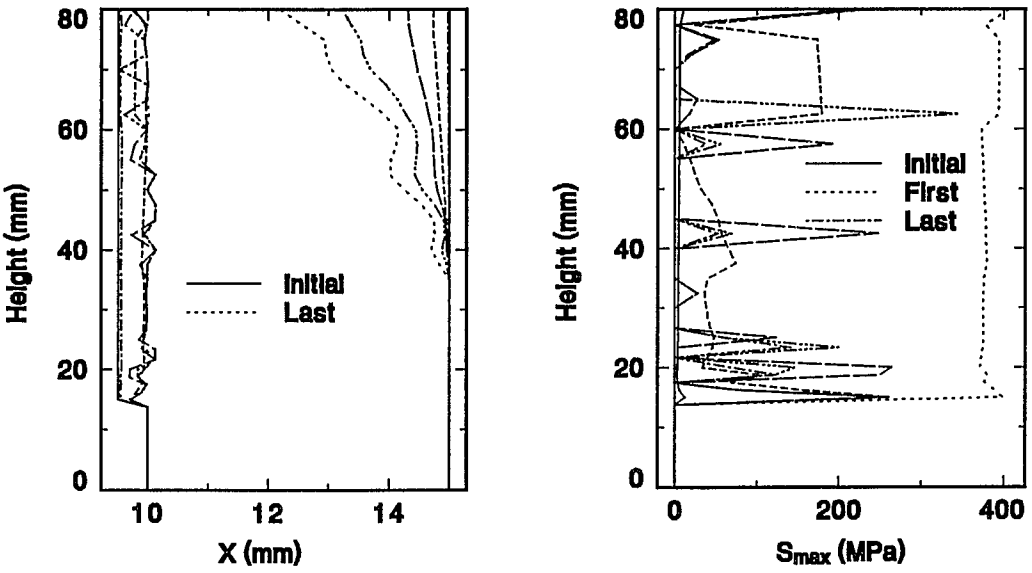

Figure 28. Remodeling predictions for a steel implant fully covered with screw threads. The initial ingrowth was 0.48 mm and initial interference was 0.01 mm. Bone outline (left), maximum shear stress along interface (right).

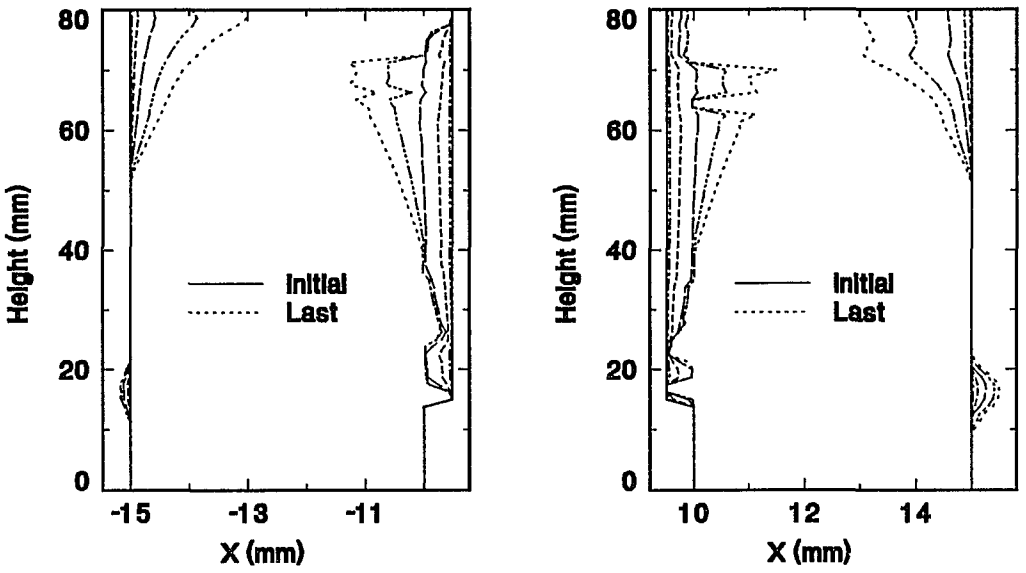

Figure 29. Remodeling predictions for a titanium implant fully covered with screw threads. The initial ingrowth was 0.48 mm and the initial interference was 0.01 mm. The bone remodels along the bone-implant interface as well as on the endosteal and periosteal surfaces on the medial side (left) and the lateral side (right).

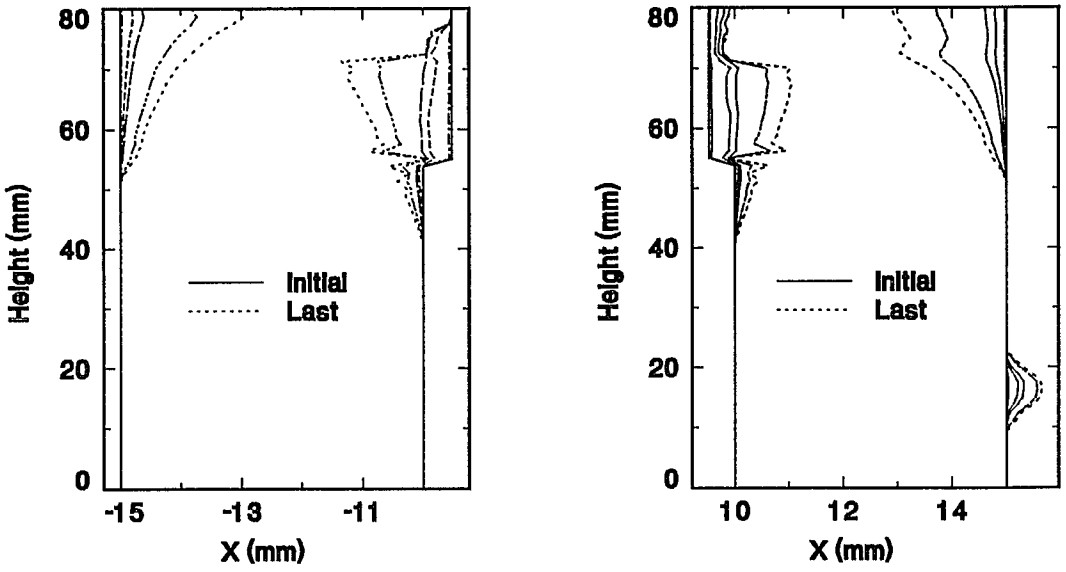

Figure 30a. Remodeling predictions for a titanium implant partially covered with screw threads. The initial ingrowth was 0.48 mm and the initial interference was 0.01 mm. The bone remodels along the bone-implant interface as well as on the endosteal and periosteal surfaces on the medial side (left) and the lateral side (right).

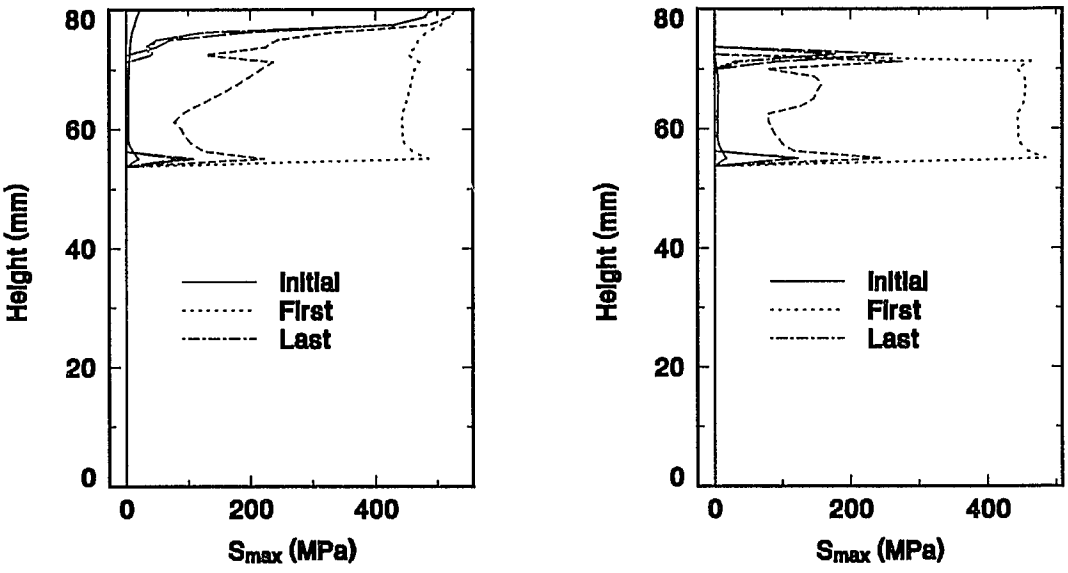

Figure 30b. The maximum shear stress can be sustained along the bone-implant interface on the medial side (left) and the lateral side (right) for a titanium implant partially covered with screw threads. The initial ingrowth was 0.48 mm and the initial interference was 0.01 mm.

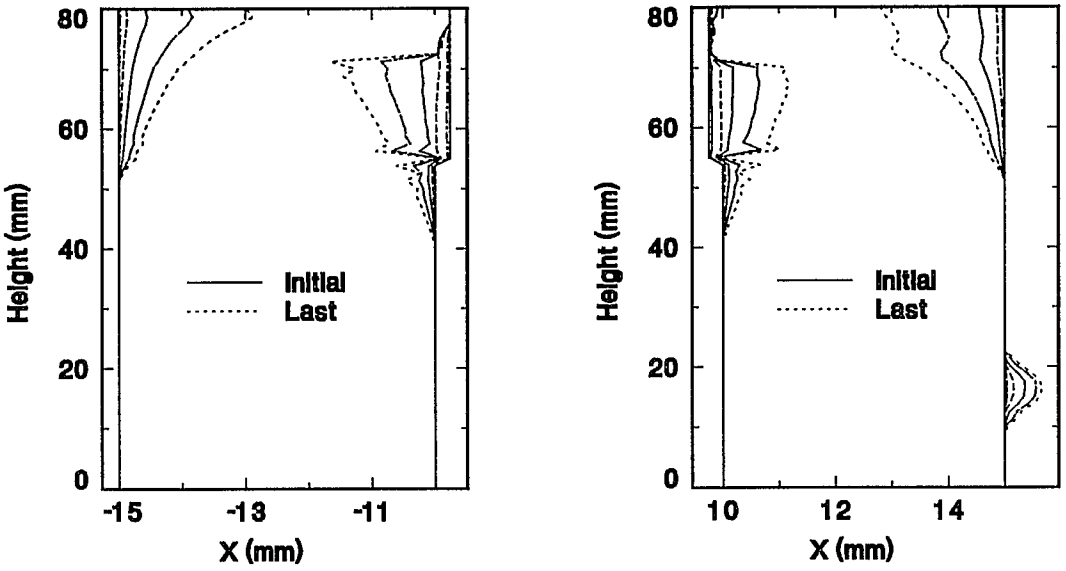

Figure 31. Remodeling predictions for a titanium implant partially covered with screw threads. The initial ingrowth was 0.24 mm and the initial interference was 0.01 mm. The bone remodels along the bone-implant interface as well as on the endosteal and periosteal surfaces on the medial side (left) and the lateral side (right).

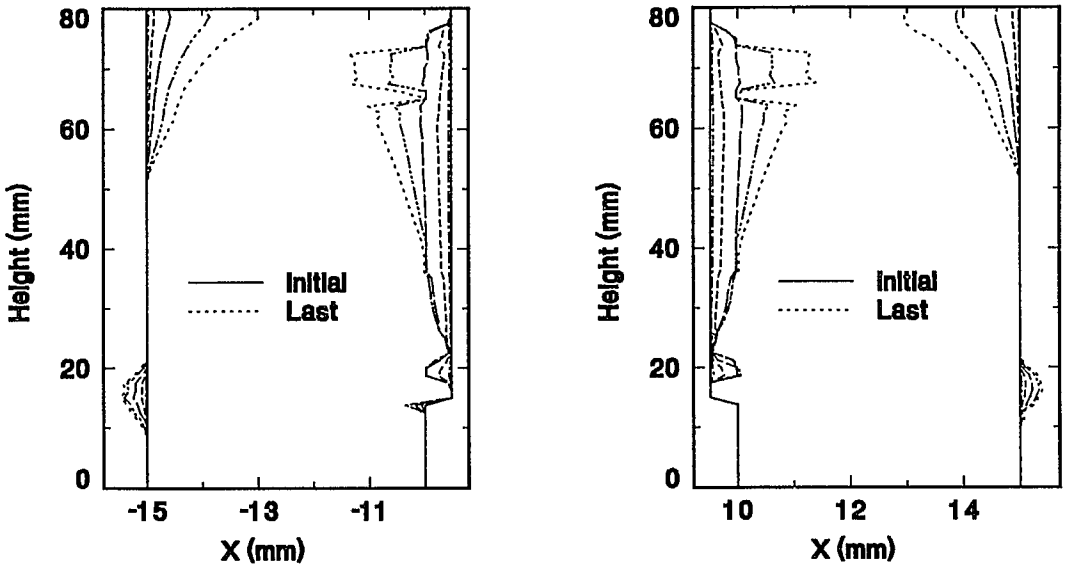

Figure 32. Remodeling predictions for a titanium implant fully covered with screw threads. The initial ingrowth was 0.48 mm and the initial interference was 0.02 mm. The bone remodels along the bone-implant interface as well as on the endosteal and periosteal surfaces on the medial side (left) and the lateral side (right).

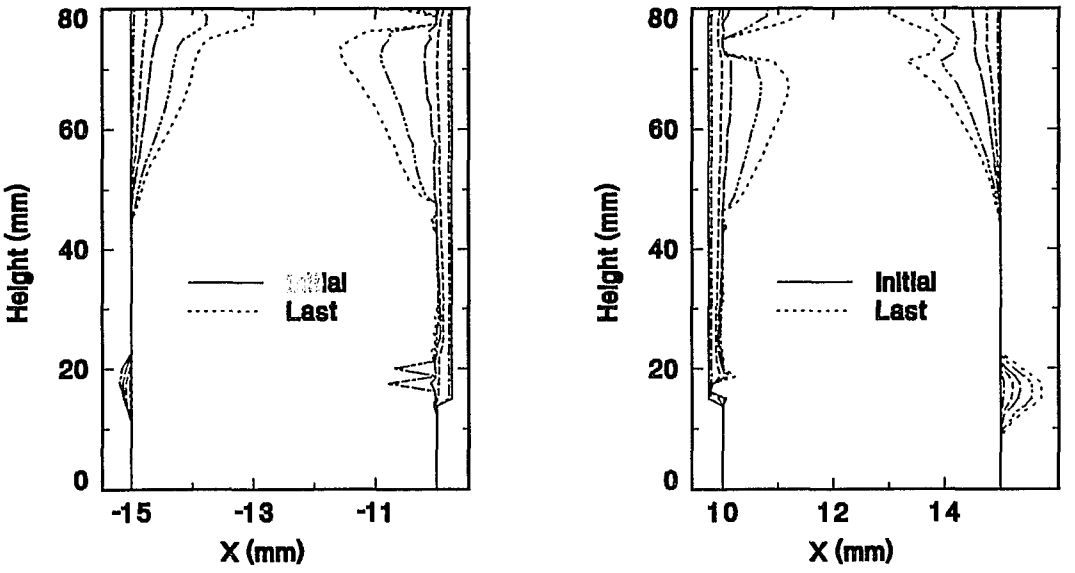

Figure 33. Remodeling predictions for a steel implant fully covered with beads. The initial ingrowth was 0.25 mm and the initial interference was 0.01 mm. The bone remodels along the bone-implant interface as well as on the endosteal and periosteal surfaces on the medial side (left) and the lateral side (right).

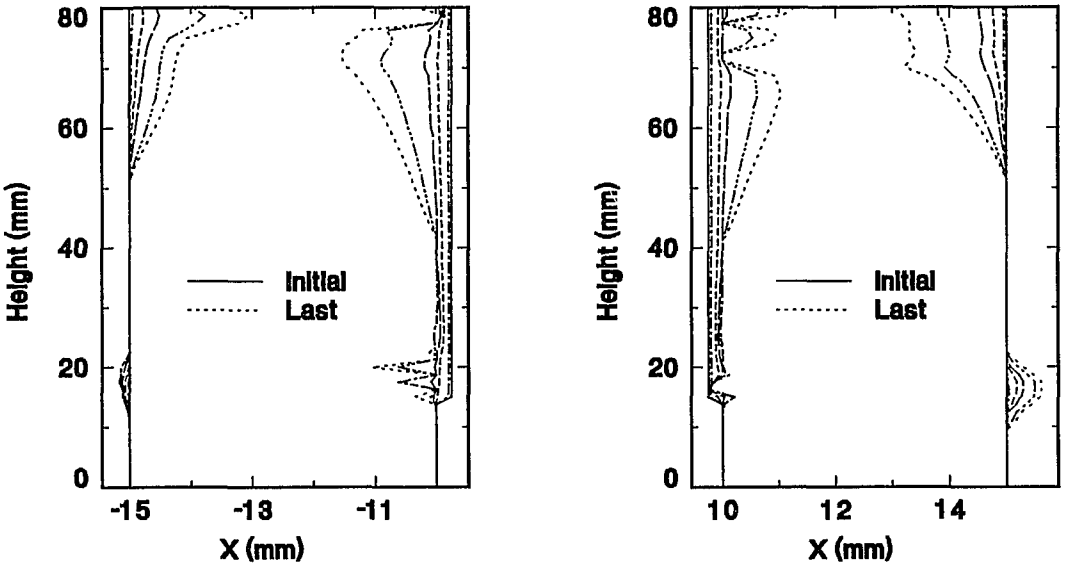

Figure 34. Remodeling predictions for a titanium implant fully covered with beads. The initial ingrowth was 0.25 mm and the initial interference was 0.01 mm. The bone remodels on the bone-implant interface as well as on the endosteal and periosteal surfaces on the medial side (left) and the lateral side (right).

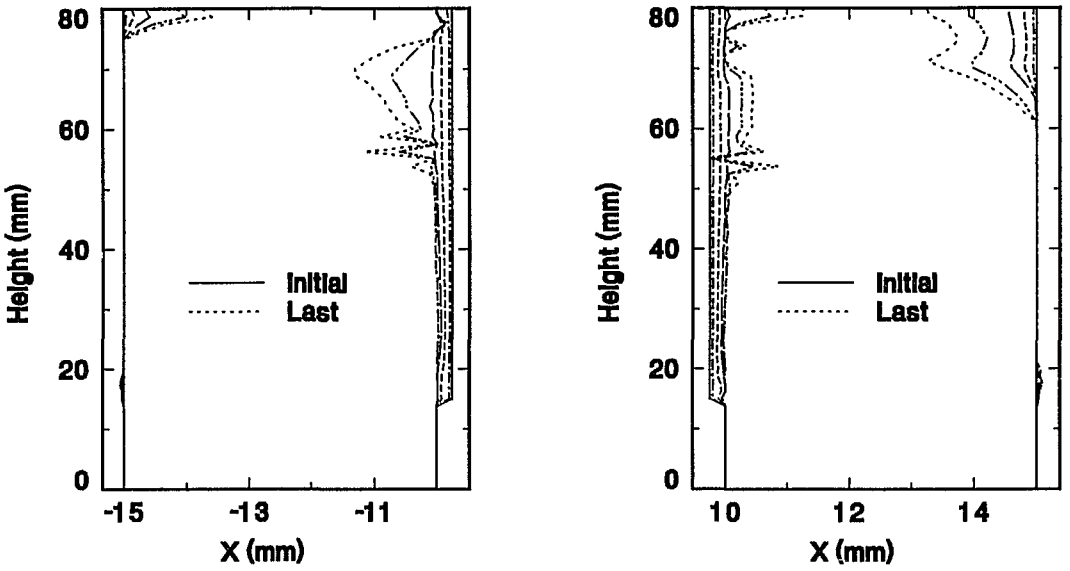

Figure 35. Remodeling predictions for a bone implant fully covered with beads. The initial ingrowth was 0.25 mm and the initial interference was 0.01 mm. The bone remodels along the bone-implant interface as well as on the endosteal and periosteal surfaces on the medial side (left) and the lateral side (right).

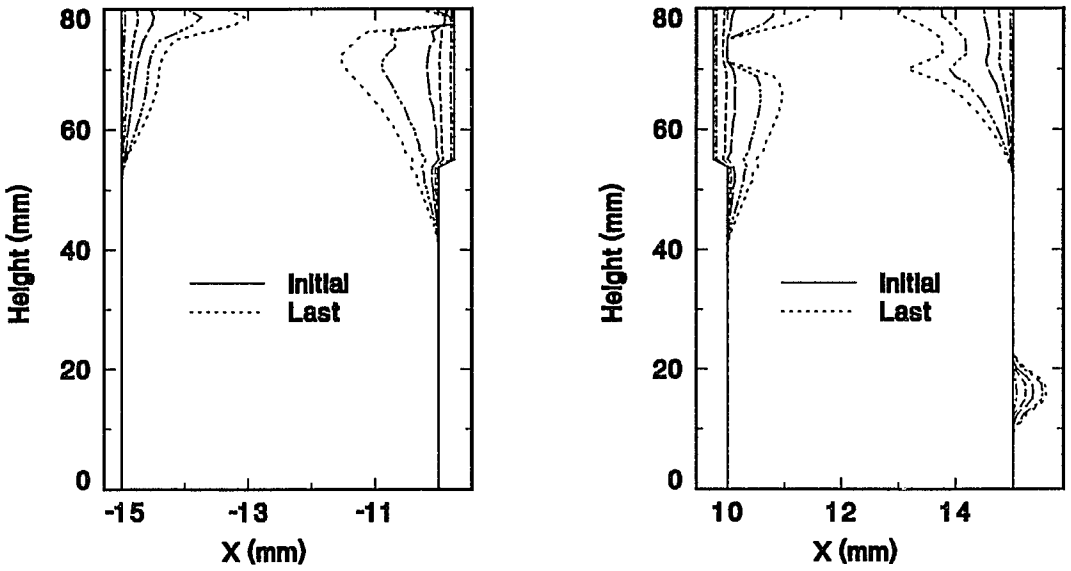

Figure 36a. Remodeling predictions for a titanium implant partially covered with beads. The initial ingrowth was 0.25 mm and the initial interference was 0.01 mm. The bone remodels along the bone-implant interface as well as on the endosteal and periosteal surfaces on the medial side (left) and the lateral side (right).

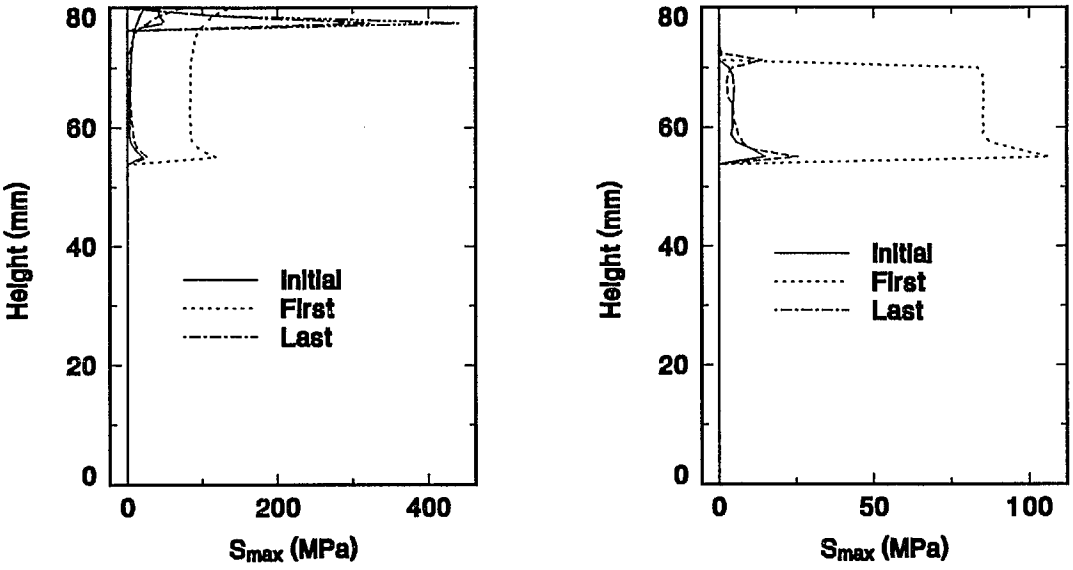

Figure 36b. The maximum shear stress can be sustained along the bone-implant interface on the medial side (left) and the lateral side (right) for a titanium implant partially covered with beads. The initial ingrowth was 0.25 mm and the initial interference was 0.01 mm.

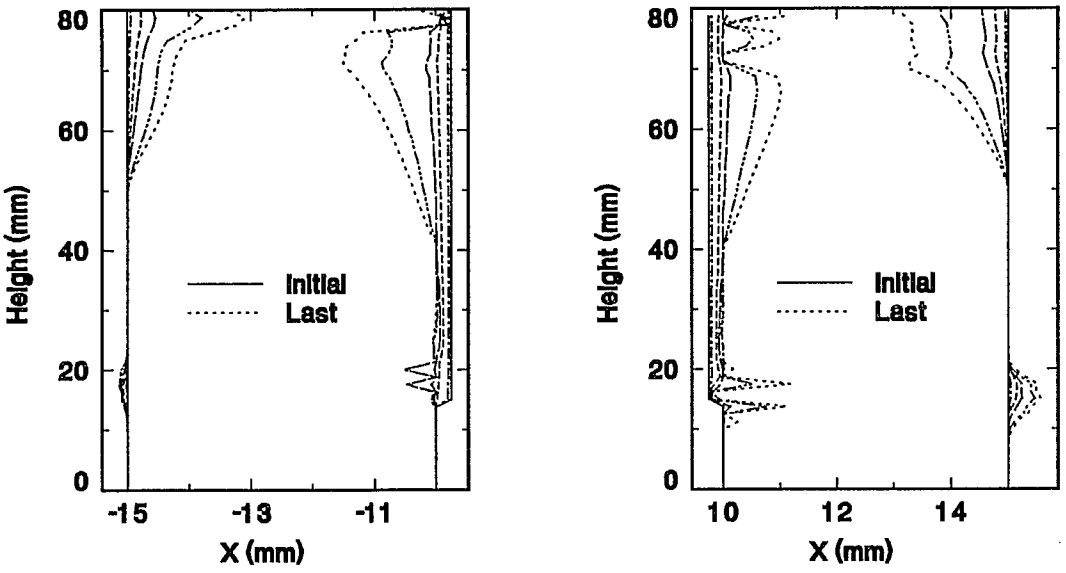

Figure 37. Remodeling predictions for a titanium implant fully covered with beads under bending and 100 N axial load. The initial ingrowth was 0.25 mm and the initial interference was 0.01 mm. The bone remodels along the bone-implant interface as well as on the endosteal and periosteal surfaces on the medial side (left) and the lateral side (right).

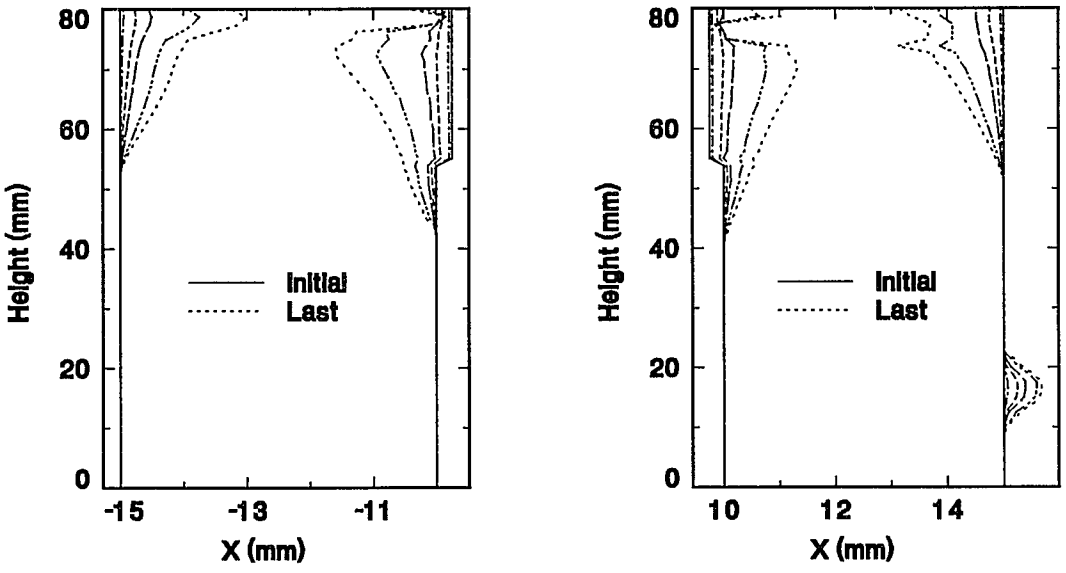

Figure 38. Remodeling predictions for a titanium implant partially covered with beads. The initial ingrowth was 0.25 mm and the initial interference was 0.02 mm. The bone remodels along the bone-implant interface as well as on the endosteal and periosteal surfaces on the medial side (left) and the lateral side (right).

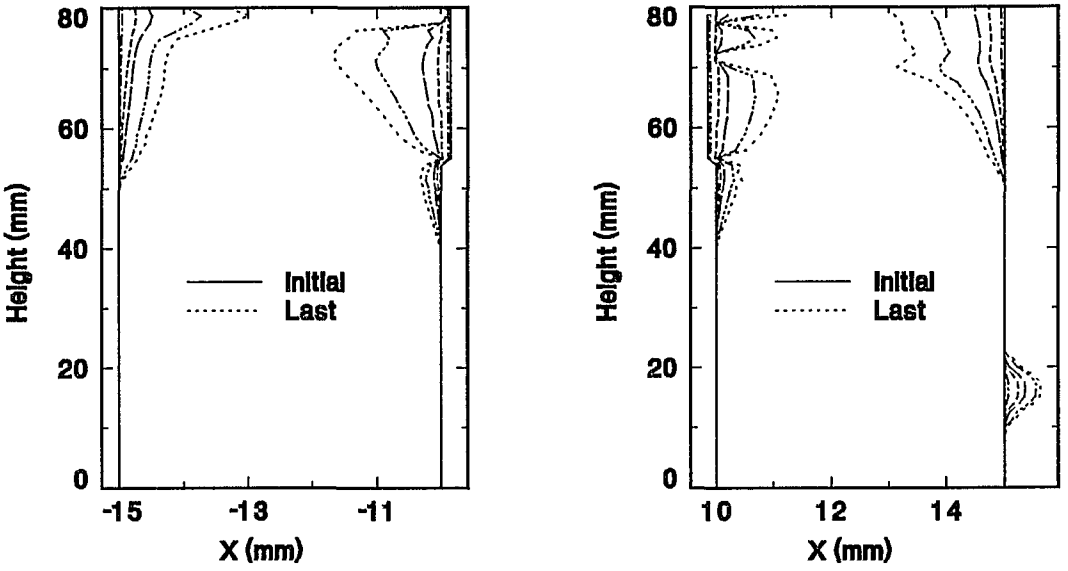

Figure 39. Remodeling predictions for a titanium implant partially covered with beads. The initial ingrowth was 0.15 mm and the initial interference was 0.01 mm. The bone remodels along the bone-implant interface as well as on the endosteal and periosteal surfaces on the medial side (left) and the lateral side (right).

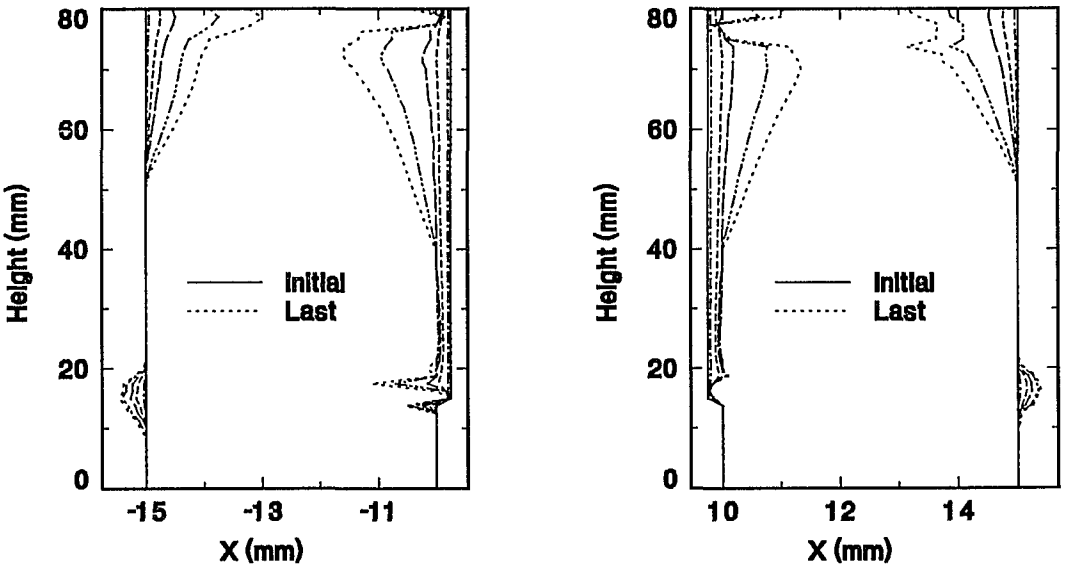

Figure 40. Remodeling predictions for a titanium implant partially covered with beads. The initial ingrowth was 0.25 mm and the initial interference was 0.02 mm. The bone remodels along the bone-implant interface as well as on the endosteal and periosteal surfaces on the medial side (left) and the lateral side (right).

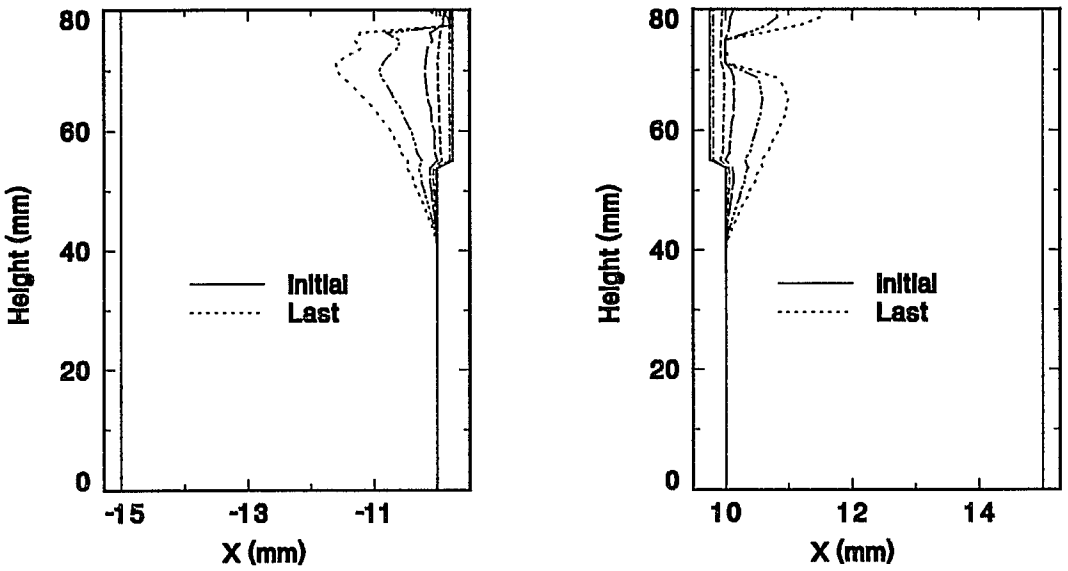

Figure 41a. Remodeling predictions for a titanium implant partially covered with beads. The initial ingrowth was 0.25 mm and the initial interference was 0.01 mm. The bone remodels along the bone-implant interface as well as on the endosteal only on the medial side (left) and lateral side (right).

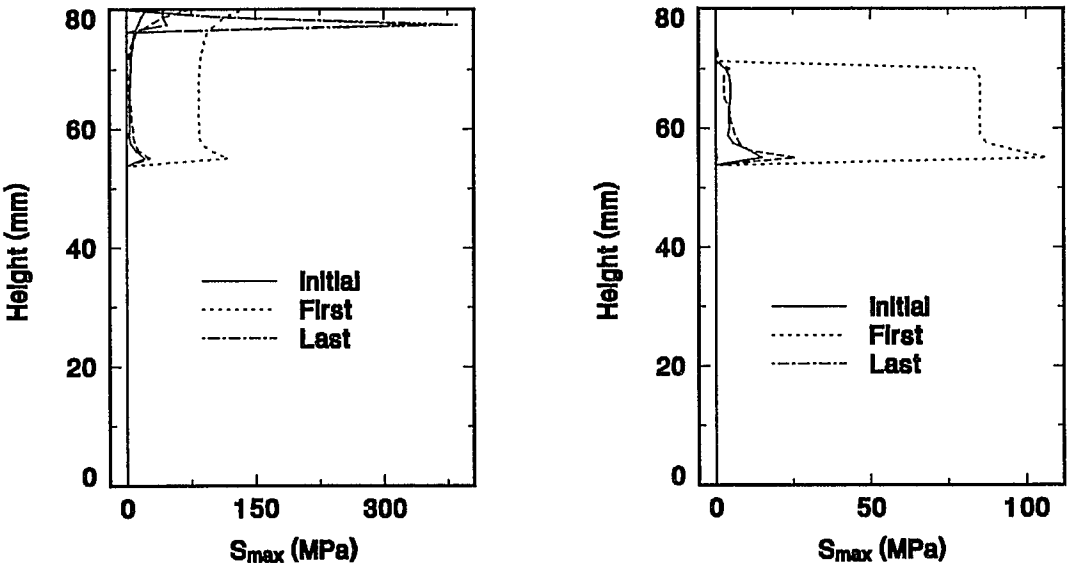

Figure 41b. The maximum shear stress can be sustained along the bone-implant interface on the medial side (left) and the lateral side (right) for a titanium implant partially covered with beads. The initial ingrowth was 0.25 mm and the initial interference was 0.01 mm.

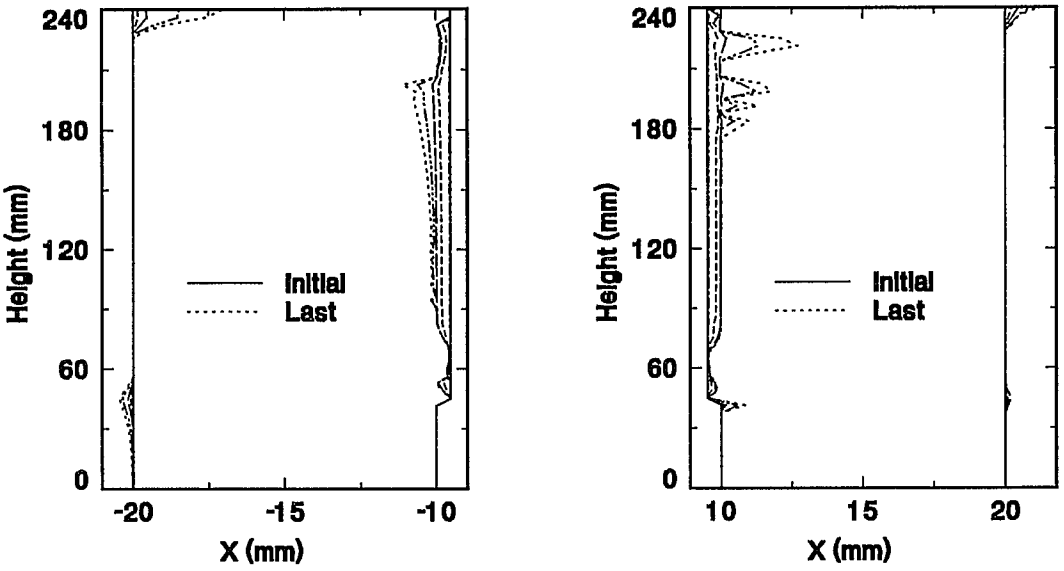

Figure 42. Remodeling predictions for a titanium implant fully covered with screw threads. The initial ingrowth was 0.48 mm and the initial interference was 0.015 mm. The bone remodels along the bone-implant interface as well as on both the endosteal and periosteal surfaces on the medial side (left) and the lateral side (right).

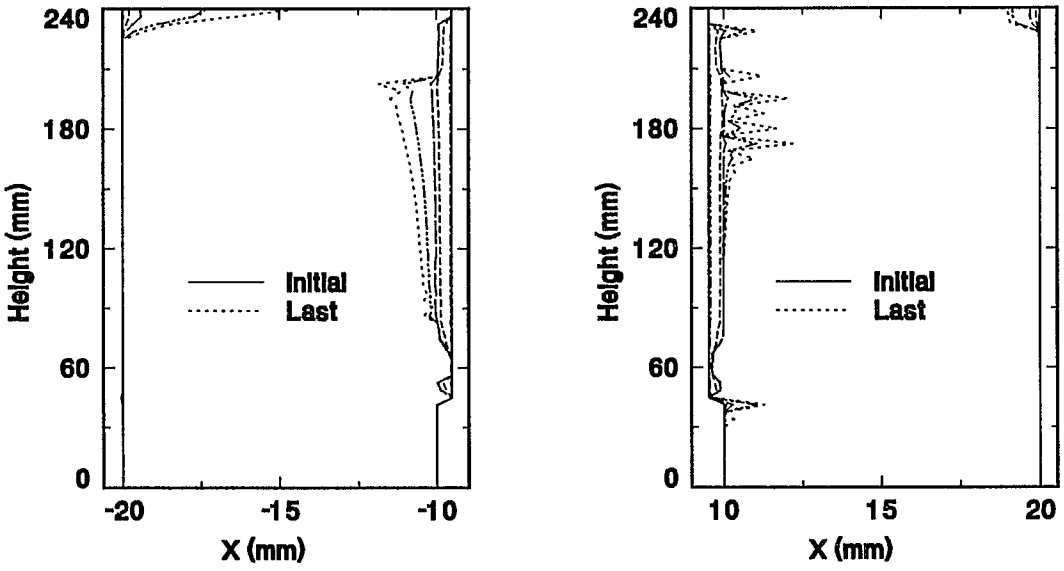

Figure 43. Remodeling predictions for a titanium implant fully covered with screw threads. The initial ingrowth was 0.48 mm and the initial interference was 0.015 mm. The bone remodels along the bone-implant interface as well as on both the endosteal and periosteal surfaces on the medial side (left) and the lateral side (right).

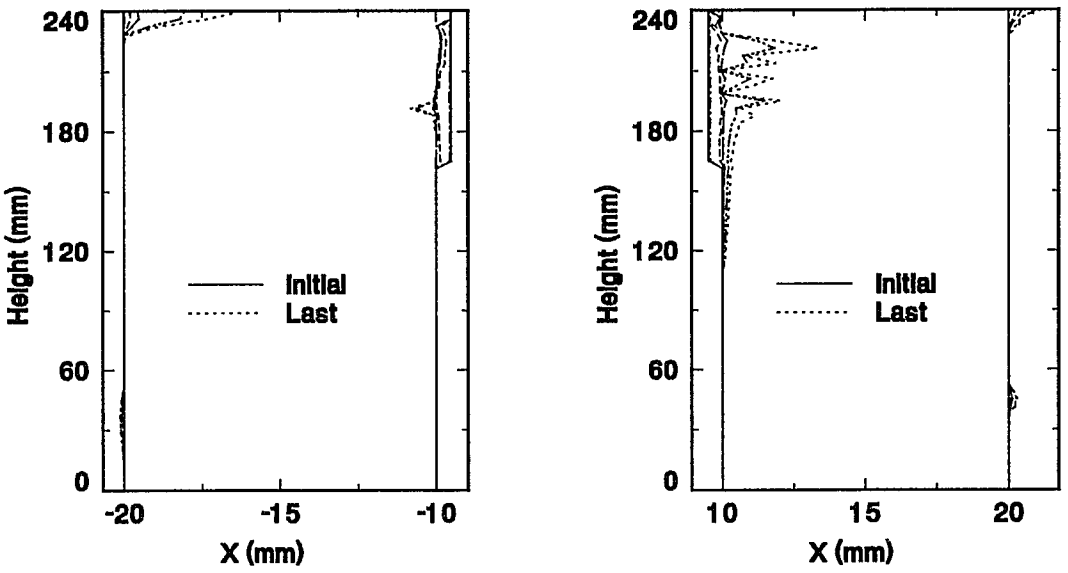

Figure 44a. Remodeling predictions for a titanium implant partially covered with screw threads. The initial ingrowth was 0.48 mm and the initial interference was 0.015 mm. The bone remodels along the bone-implant interface as well as on both the endosteal and periosteal surfaces on the medial side (left) and the lateral side (right).

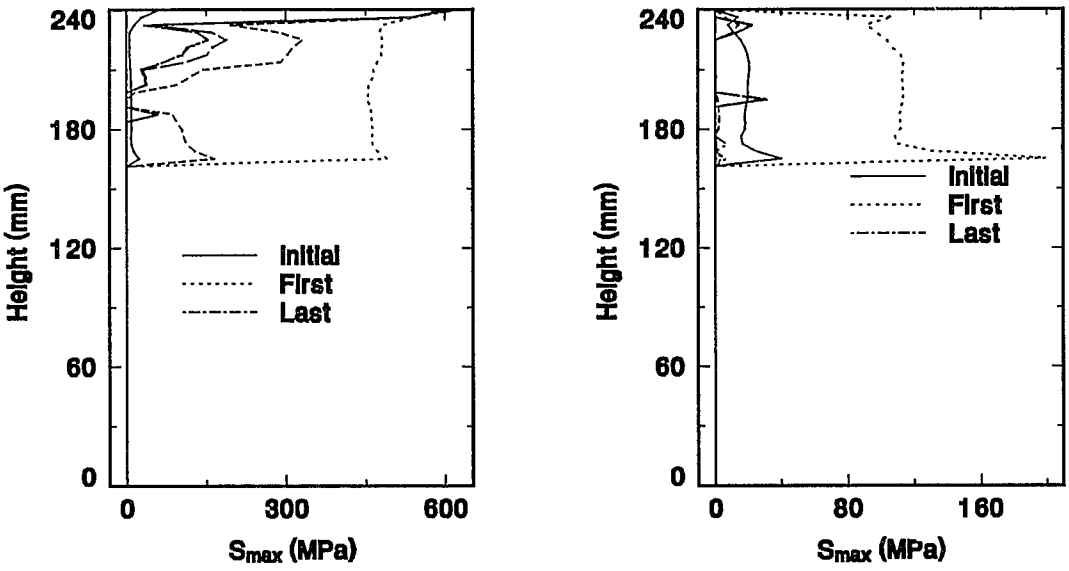

Figure 44b. The maximum shear stress can be sustained along the bone-implant interface on the medial side (left) and the lateral side (right) for a titanium implant fully covered with screw threads. The initial ingrowth was 0.48 mm and the initial interference was 0.015 mm.

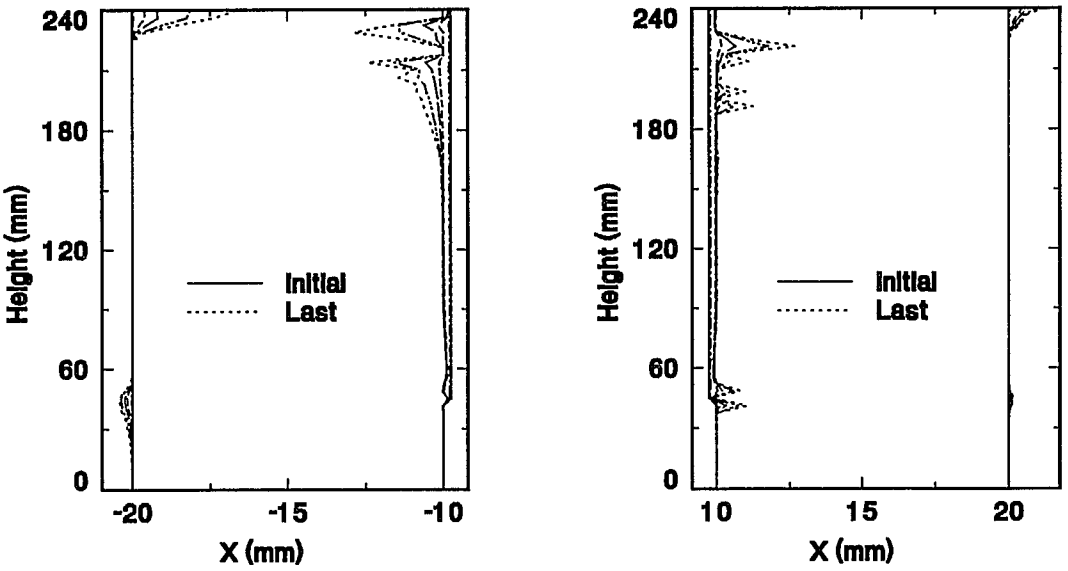

Figure 45. Remodeling predictions for a titanium implant fully covered with beads. The initial ingrowth was 0.25 mm and the initial interference was 0.02 mm. The bone remodels along the bone-implant interface as well as on both the endosteal and periosteal surfaces on the medial side (left) and the lateral side (right).

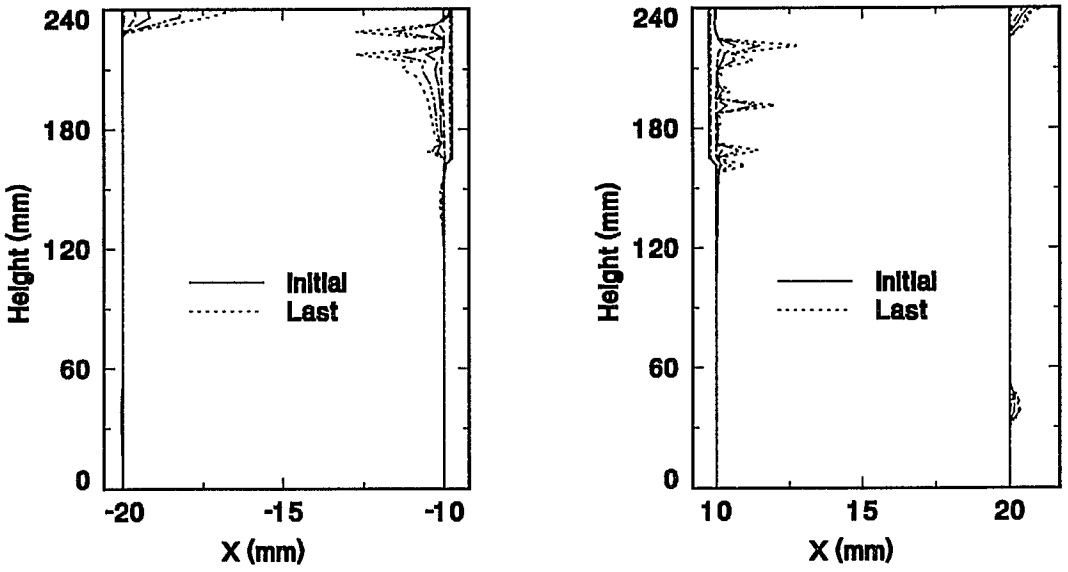

Figure 46a. Remodeling predictions for a titanium implant partially covered with beads. The initial ingrowth was 0.25 mm and the initial interference was 0.02 mm. The bone remodels along the bone-implant interface as well as on both the endosteal and periosteal surfaces on the medial side (left) and the lateral side (right).

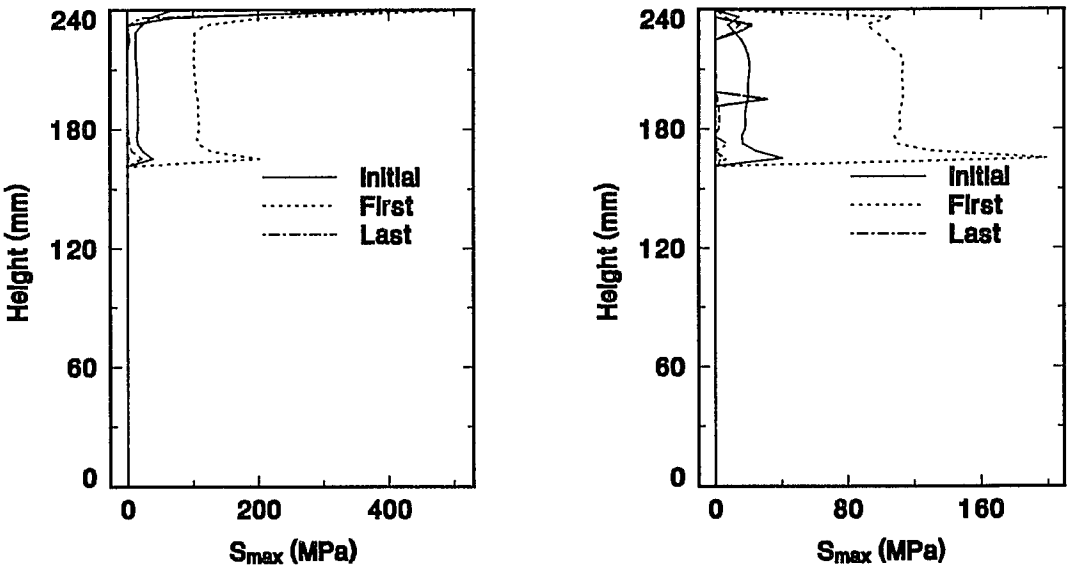

Figure 46b. The maximum shear stress can be sustained along the bone-implant interface on the medial side (left) and the lateral side (right) for a titanium implant fully covered with beads. The initial ingrowth was 0.25 mm and the initial interference was 0.02 mm.

7. COMPARISONS WITH ANIMAL EXPERIMENTS AND CLINICAL OBSERVATIONS

The results obtained in this dissertation are based on numerical models of surface bone remodeling theory with a strain rate stimulus. It is critical to verify whether the results we have obtained numerically are consistent with animal experiments and clinical observations. In the following two sections we compare our numerical results from both the local and the global models with animal experiments and clinical observations. All figures for this chapter are attached at the end of this chapter.

7.1 Comparisons of local models

(a) Slot model

In the slot local model, two different boundary conditions have been used. One is a fixed boundary condition which corresponds to perfect bonding. The other is a free boundary condition which corresponds to no bonding between bone and the smooth implant surface. For these two boundary conditions the numerical model predicts different remodeling outcomes. For the fixed boundary condition the model predicts bone ingrowth along the bone-implant interface and resorption in the middle of the slot. For the free boundary condition the model predicts bone ingrowth in the middle of the slot and bone resorption along the bone-implant interface.

Ricci *et al.* (1991) conducted an animal experiment study to determine the effect of surface chemistry and roughness on bone ingrowth into slots. In their experiment, rectangular implant chambers, measuring 8 mm wide by 25 mm long by 10 mm deep and containing a central open area 5 by 18 mm, were machined out of medical-grade UHMW polyethylene. Coupons of various materials and surfaces, each measuring 7 by 8 by 0.4 mm thick, were washed in an organic solvent and air-passivated. Twenty such test coupons were placed widthwise along slots cut into the top and bottom of the central space in the major surfaces lining the ten 1-by-5 mm ingrowth channels created. Sixteen skeletally mature mongrel dogs were used in this study and killed 2, 6, 12 and 24 weeks postoperatively. The rectangular implant chamber was placed in a longitudinal cortical window defect in the lateral metaphysis of the distal femur. After implantation, the ingrowth channels were oriented perpendicular to the long axis of the femur; the channel openings faced the endosteal surface of the intact anterior and posterior cortices. For smooth-surfaced coupons, their experiment shows that by 24 weeks, the bone in the channels appeared thickened and mature. The bone was of a dense lamellar structure (Figure 47). The same temporal pattern of bone ingrowth and remodeling was found in all sample groups. For HA coated coupons, their experiment shows that by 12 weeks, there is a complete bridge of bone within the HA coated channels in all cases and the interface between the bone and HA coating was observed to be completely mineralized (Figure 48).

From the present perspective, the difficulty in this local model comparison is that the loading history in their experiment is not recorded. That means the comparison of

numerical results with experimental results is based only on the given boundary conditions, i.e., the free boundary condition in the numerical model corresponds to smooth coupon surfaces and the fixed boundary condition corresponds to HA coated coupon surfaces and not the magnitude of the applied loads. However both our numerical results and their experimental results show that for smooth coupon surfaces, bone tends to resorb from these surfaces and for HA coated coupon surfaces, bone tends to not resorb from these surfaces but resorb in the middle of the channels.

In the comparison of the numerical results and the experimental results, we assume that bone is under a remodeling process instead of a healing process. The experimental results compared here are after twelve weeks postoperatively. Ricci *et al.* (1991) found that at twelve weeks the central connective tissue appeared as mature, well-oriented fibrous tissue, intimately associated with, and oriented to, the ingrown bone.

(b) Screw thread and bead models

Screw threads are widely used in orthopaedic and dental implants. Bone ingrowth into screw threads is widely observed and documented (Albrektsson *at al.* 1988; Carlsson *et al.* 1986). However, why some screws fail while others function well for years is not fully understood. How well a screw remains fixed to the bone may depend on the material properties of the screw, the surface treatment and loading conditions. In our numerical model, two boundary conditions, the free boundary

condition simulating a smooth surface and the fixed boundary condition simulating an HA coated surface, are used. The bone ingrowth into screw threads is determined numerically for a variety of loading conditions. The results show that for the given boundary condition, increasing loading results in more bone ingrowth into screw threads and reducing loading results in less bone ingrowth into screw threads. An interesting observation is that, for a given loading condition, the numerical model predicts less bone ingrowth into screw threads for HA coated surfaces than for smooth surfaces. It is important to note that the results predicted are based on a surface bone remodeling theory for mature bone instead of the results of the healing process and/or trauma reaction.

Carlsson *et al.* (1986) inserted sixty implants of three designs into the proximal tibial or distal femoral metaphysis of 6 dogs, Figure 49. A screw (12 mm long, 3.75 mm in diameter) was inserted in a pre-tapped hole (n = 48). A double cylinder with an irregular surface (length 24 mm, 8 mm in diameter) was inserted into a preformed defect (n = 6). A T plate was placed with the transverse part of the T (length 18 mm) on the bone surface, and the 8 mm long shaft was inserted into a preformed slit in the cortical bone (n = 6). Their results show that the titanium screws were well integrated into the bone. At the cortical passage, bone with haversian systems filled the threads of the implants entirely, Figure 50. There were no differences between the level of bone contact after three months and that after 14 months.

The comparison of our numerical prediction of bone ingrowth into screw threads and Carlsson's experimental results shows under certain conditions bone may fill the

screw threads. Due to the lack of loading history data on the screws and adjacent bone, only quantitative comparison is possible.

Beads are used to increase the stability of a total hip implant. Bone ingrowth into the cavities of a bead coated implant will increase the mechanical stability of the implant. Our numerical results show that under given boundary conditions, bone ingrowth into the cavities of beads depends highly on the load applied or the stress distribution near the beads. The higher load results in the more bone ingrowth and *vice versa*. Cook *et al.* (1988) conducted a histologic and radiographic analysis of 36 porous-coated total hip components (22 femoral and 14 acetabular) retrieved from 30 patients. They found bone ingrowth tended to occur where the implant made direct contact with the endosteal cortical surface. Figure 51 shows that a primary area of a bone ingrowth was at the distal lateral portion of the porous coating. Their study did not provide the loading history for the portion. However stress analysis shows that there exist high dynamical normal stresses near the endosteal surface at the distal lateral portion and there exist lower dynamical normal stresses near the endosteal surfaces if there is no direct contact of bone and implant surfaces. Our numerical bead model predicts significant bone ingrowth into the cavities of beads under high dynamic normal stresses and bone resorption from the cavities of beads under lower dynamic normal stresses. At this point, our numerical results are consistent with their clinical observations.

7.2 Comparisons of global models

In this dissertation, three global models are employed. Since a bending moment cannot be applied to the axisymmetric model, the dynamical stress along the bone-implant interface is very low. The model therefore predicts bone resorption from the interface and the instability of an implant. The above problems render the axisymmetric model unable to simulate the hip with implant adequately. Therefore, in this section, only the results from the pseudo 3-D models are compared with clinical observations.

From the results of the pseudo 3-D models, the following observations are made:

(a) Calcar resorption is predicted in all cases. The resorption area increases when the stiffness of the implant increases.

(b) Interface resorption, as shown in Figure 25, on both the medial and lateral side is predicted in all cases. The resorption area increases when the coated area of an implant increases.

(c) Humps on the periosteal surface at the location of the distal end of the implant, as shown in Figure 25, are observed. Increasing the initial interference will increase the hump size on the medial side and reduce the hump size on the lateral side, if other conditions are unchanged.

(d) Since interface resorption is predicted in all cases and resorption starts at the very beginning of remodeling, uniformly distributed initial ingrowth and initial interference are not necessary to get the results as predicted in this dissertation, as long as there is enough initial ingrowth and initial interference in both the upper and

lower parts of the bone-implant interface on both medial and lateral sides.

(e) The resorption in the greater trochanter area is predicted in the pseudo 3-D model if the abductor force is not simulated. In the pseudo 3-D model with the simulated abductor force no resorption is predicted in the region of the greater trochanter.

D'Antonio *et al.* (1992) studied 220 patients with implants between January 1988 and December 1989. The implants used were straight titanium-alloy collarless femoral stems with a fifty-micrometer-thick hydroxyapatite coating proximally and stepped macrogrooves on the proximal, anterior and posterior surfaces. In their study, in addition to calcar resorption, subcortical cancellous-bone formation, representing new-bone formation between the implant and the femoral cortex, occurred most commonly at the interface between the hydroxyapatite-coated and the uncoated portions of the stem. This was noted in 51 percent of the implants laterally, 67 percent medially, 28 percent anteriorly and 37 percent posteriorly. Diaphyseal subperiosteal cortical thickening was most commonly observed in zones 3 (12 percent) and 5 (17 percent) of the implants on the anteroposterior radiographs (Figure 52), but no cortical thickening was seen on the lateral radiographs. A typical radiograph is shown in Figure 53.

Engh *et al.* (1992) employed dual-energy x-ray absorptiometry analysis to quantitatively determine the periprosthetic bone-mineral content of five elderly patients who had had an AML (anatomic medullary locking) prosthesis *in situ* for seventeen to eighty-four months. They found that the mean difference in the periprosthetic bone-mineral content between the remodeled femora and the femora in which the prosthesis had been implanted post mortem ranged from 7 to 52 percent, with the bone-mineral

content always less in the remodeled femora. The greatest mean decrease in bone-mineral content (45 percent) occurred adjacent to the proximal one-third of the remodeled femora. The same conclusion was drawn by Turner et al. (1987) and Summer et al. (1990). Their measurement was made over three levels from proximal to distal. Thus comparison of bone remodeling below these levels is impossible. However a comparison of their results of dual-energy x-ray absorptiometry with the appearance of the clinical radiographs provided a clear impression of association between quantitative and qualitative information. For example, the changes visible at the most proximal level in Figure 54b represented a 33 percent decrease in the bone-mineral content compared with that in the same area of the control femur.

The comparison of our numerical results and clinical study shows them to be qualitatively consistent. Calcar resorption is predicted by the numerical models and observed clinically. Both numerical models and clinical studies find that greatest bone resorption occurred in the proximal third and that implants having a more extensive porous coating and a larger-diameter (stiffer) stem cause more extensive resorptive bone remodeling. Although bone resorption near the bone-implant interface has not been measured quantitatively, it is visible from radiographs and is mostly proximal, as in Figure 54. Humps on the periosteal surface or cortical thickening are predicted by the numerical models on both medial and lateral sides distally. The size of these humps depends on the initial condition. If the distal end of an implant initially contacts tightly with the endosteal surface on the medial side, a hump on the periosteal surface on the medial side will be predicted. If the distal end of an implant initially contacts with the

endosteal surface on the lateral side, not necessarily tightly, a hump on the periosteal surface on the lateral side will be predicted. In the Cook *et al.* (1988) study, cortical thickening was found only on the medial side. An explanation based on our numerical model is that there is a tight contact between the distal part of the implant and the endosteal surface on the medial side but not on the lateral side. Cortical thickening was observed in the clinical study, as shown in Figure 55. Due to the lack of knowledge of how the distal part of an implant initially contacts the endosteal surface on the medial and lateral sides, comparison is made based on the final numerical results and clinical observations.

The following are the limitations on the comparison of the numerical results and clinical observations.

(a) The simplified pseudo 3-D models only can simulate the stress distribution in the middle plane in the medial and lateral directions and no out-plane effects can be considered

(b) Homogeneous and isotropic material properties are used in the numerical calculation, while in the femur the material properties are neither homogeneous nor isotropic, especially in the proximal femur.

(c) The load applied on a femur depends on one's activity, and many muscles attached to the femur make the loading more complicated. However, the load applied on the numerical models is only the main part of the walking load.

Due to these factors, the comparison of the numerical results with clinical observations can be made qualitatively.

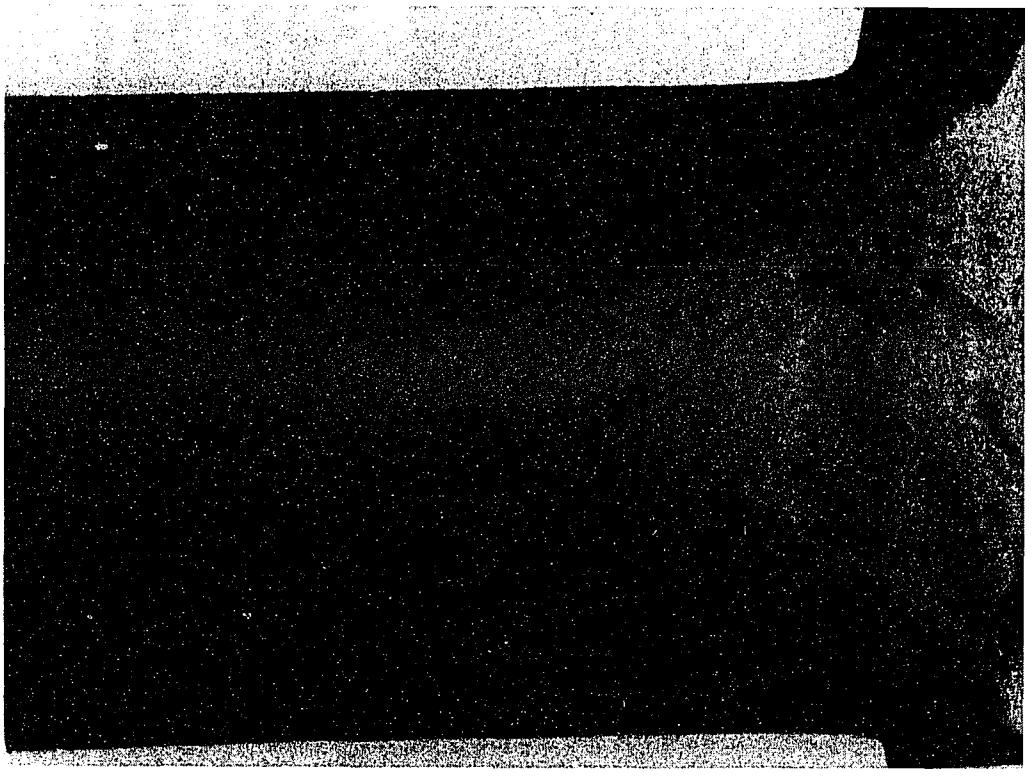

Figure 47. Microradiograph showing bone ingrowth into a 24-week smooth-surfaced specimen. This triangular-shaped area of dense lamellar bone was characteristic of all smooth test groups. (original magnification X83) (from Ricci *et al.* 1991)

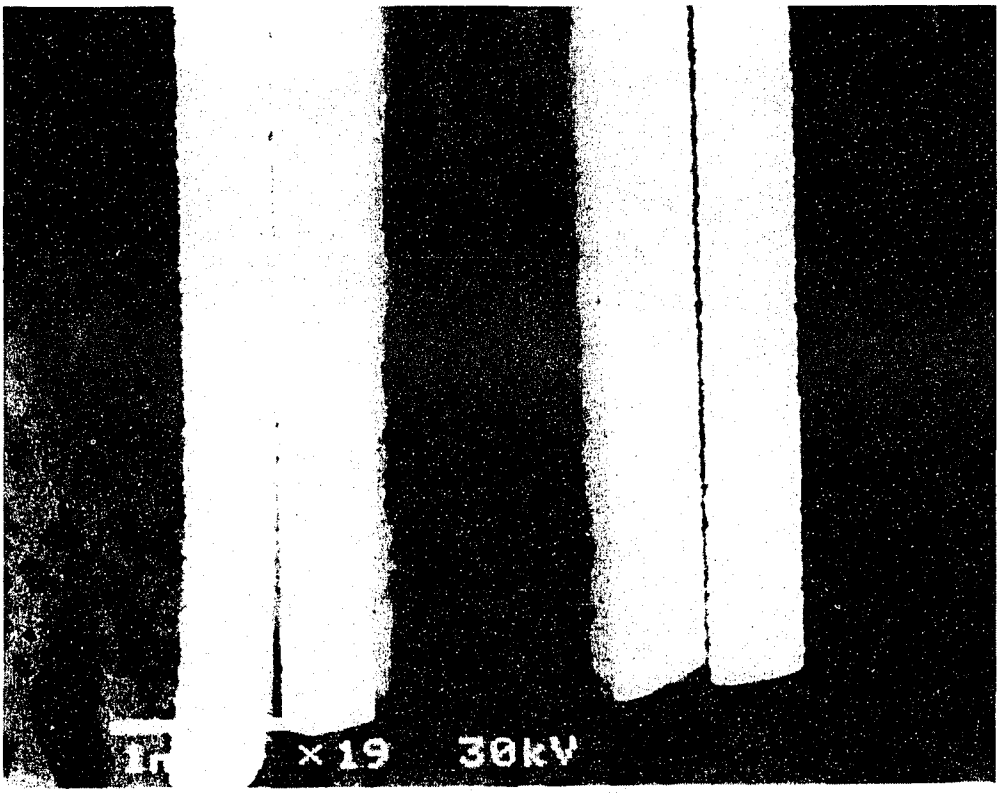

Figure 48. Back-scattered electron image of 12-week bone ingrowth into two rough-surfaced Ti channels (left and right) and one HA-lined channel (center). Channel width is 1 mm. (from Ricci *et al.* 1991)

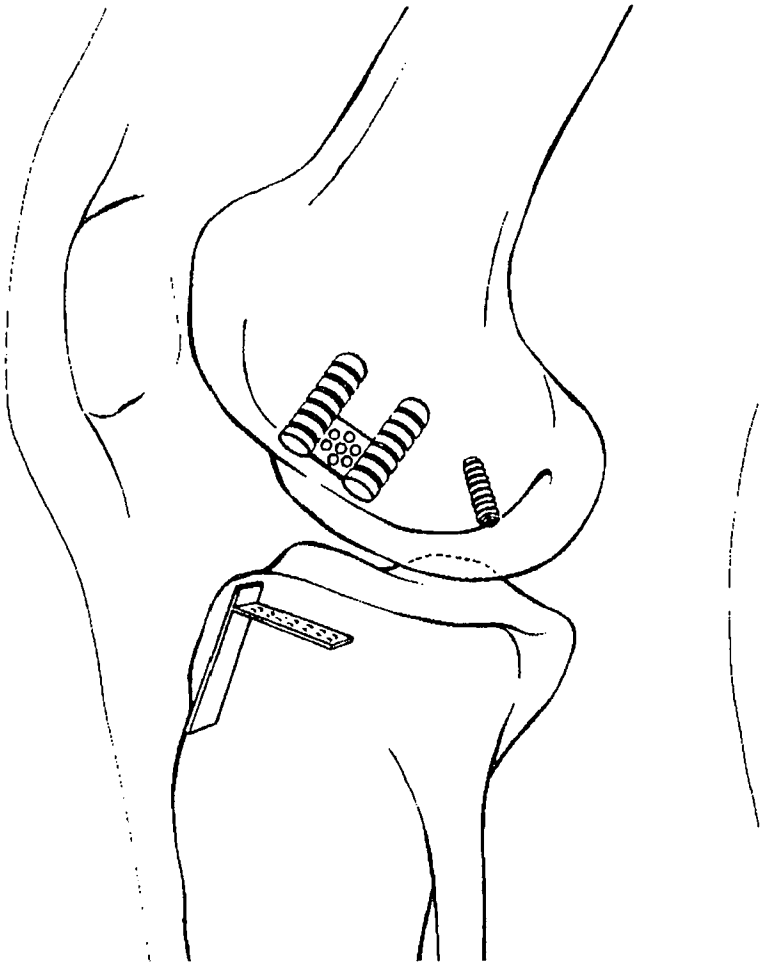

Figure 49. Three implants were used: screw, double cylinder and T-plate (from Carlsson *et al.* 1986)

Figure 50. Direct contact between bone and Titanium (Ti) on all sides of the screw threads. (original magnification X10) (from Carlsson *et al.* 1986)

Figure 51. A 34-year-old man with a PCA stem, removed after 23 months for persistent pain. The histologic sections demonstrated a relatively high degree of bone growth into almost 10% of the available pore volume. The primary area of a bone ingrowth was at the distal lateral portion of the porous coating. (original magnification X24) (from Cook *et al.* 1988)

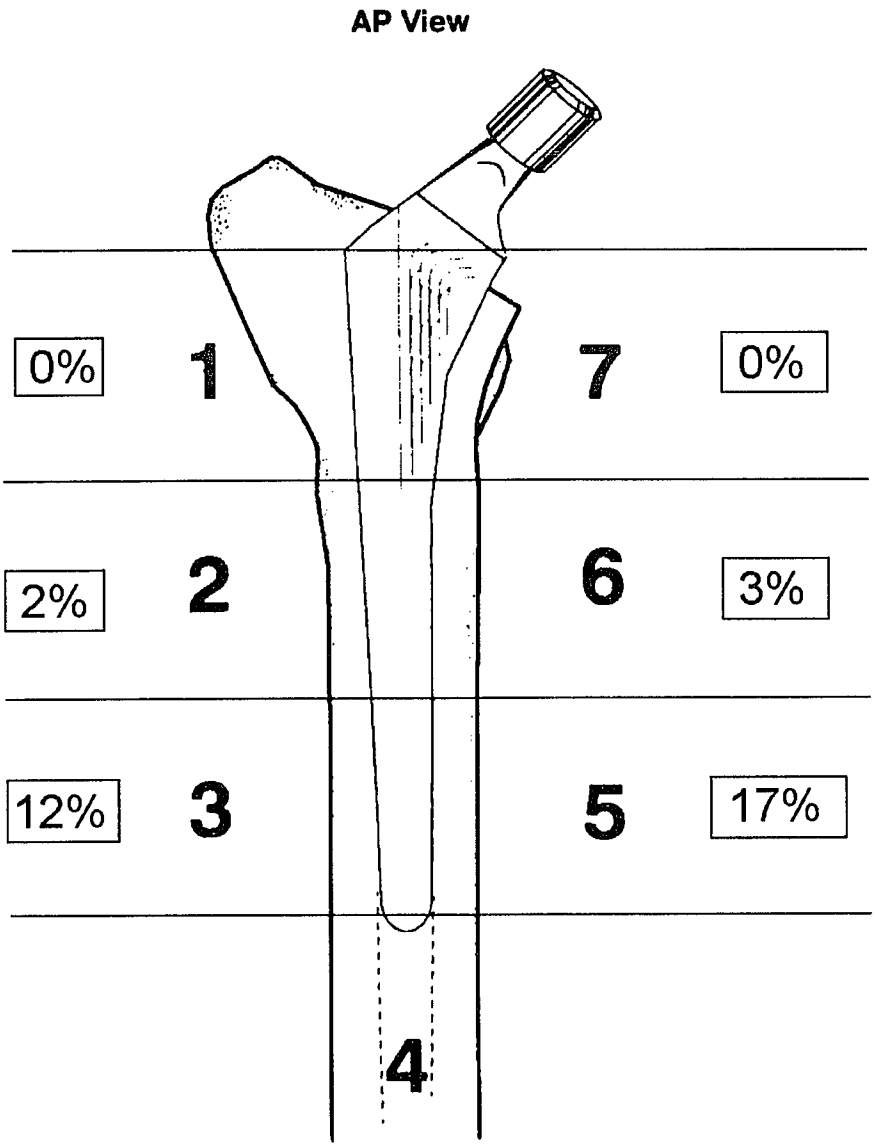

Figure 52. Schematic drawing showing cortical thickening two years postoperatively. Thickening was observed on the anteroposterior but not on the lateral radiographs. The rate was highest in zone 5. (from fig. 10 D'Antonio *et al.* 1992).

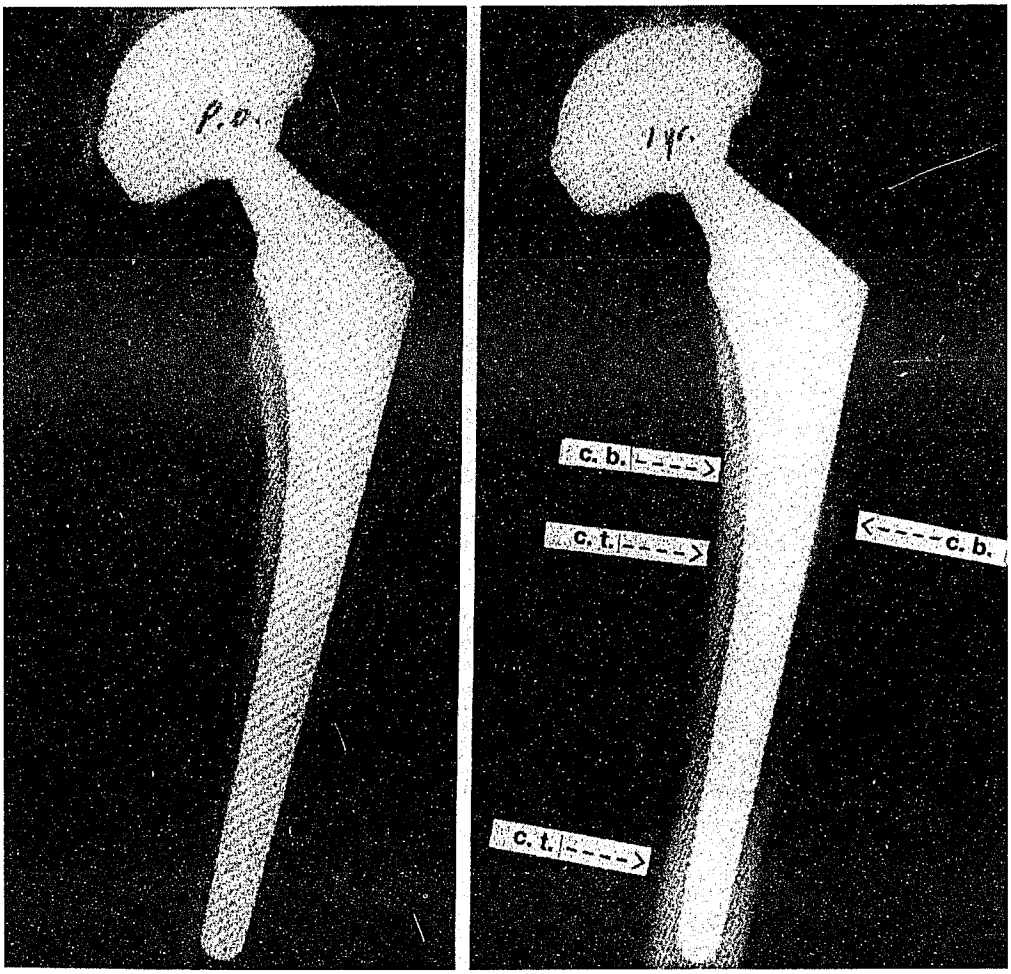

Figure 53. In this patient, cancellous-bone (c.b.) formation is seen both one and two years postoperatively. Cortical thickening (c.t.) is present at the middle and the distal medial portion of the stem at one year and progressed at the two-year follow-up. Radiolucencies (r.l.) are found only around the distal portion of the tip of the stem. (a) and (b): Anteroposterior radiographs made soon postoperatively and one year postoperatively. (from fig. 6, D'Antonio *et al.* 1992).

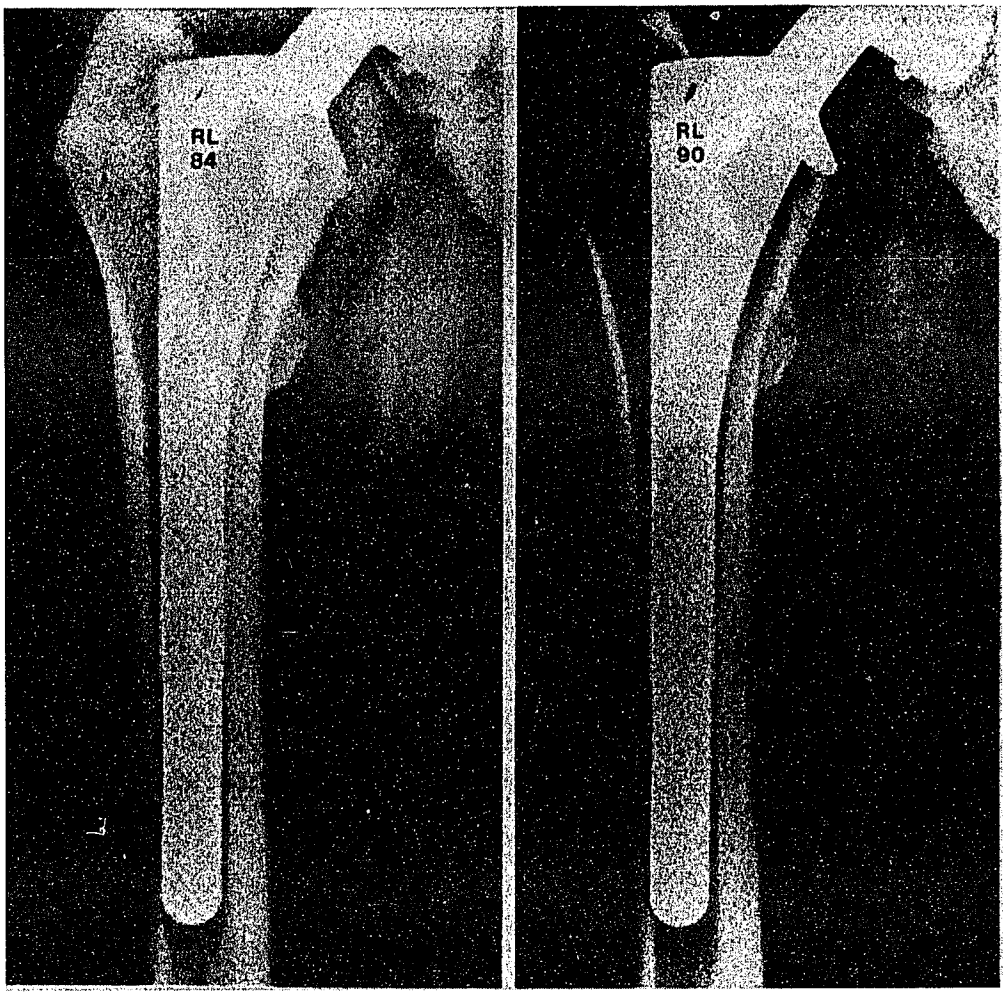

Figure 54. (a) Clinical radiograph made immediately after *in vivo* implantation of the prosthesis, when the patient was sixty-two years old, shows bone of excellent quality. (b) The final radiograph made before the patient's death demonstrates resorptive remodeling of the lateral and medial cortices. (form fig. 2-A and 2-B, Engh *et al.* 1992)

Figure 55. Anteroposterior radiograph made 16 months postoperatively. Cortical thickening is clear on lateral side. (Courtesy of R. Siffert, M.D.)

8. DISCUSSION

The long term stability of the hip implant is studied using a local-global feedback model. The surface bone remodeling theory with strain rate stimulus is used to predict surface bone remodeling for the interface as well as the traction-free surface. The connection between the local model (interface) and the global model (whole bone-implant system) is achieved by passing the stresses and the displacements determined by the global model to the local model and the local model in turn feeds back the surface movement and the Coulomb friction to the global model. The process repeats itself until a criterion for stopping is achieved. The advantages of the local-global model are the following:

(a) Remodeling at both the local level, which is in a scale less than 1 mm, and at the global level, which is in a scale greater than 30 mm, can be considered at the same time.

(b) Due to the creation of databases for the local models, accomplishing the feedback model consumes minimal CPU time. Therefore in a particular calculation, most of the CPU time is consumed by the finite element method, the stress analysis in the global model, and not by the local model calculation.

(c) The local models are interchangeable and a combination of different local models for an implant is easily accomplished. Thus the feedback may be used to design an implant with different interfaces in different locations.

(d) Although the models used in this dissertation are two-dimensional, theoretically

there is no barrier to extend the feedback model to three-dimensional models. However a very powerful computer is needed for three-dimensional calculation.

There are some limitations on the models employed here. The assumptions of isotropy and homogeneity are used in the calculation. The assumptions may be removed if an appropriate model with bulk density and orientation remodeling is employed.

We should stress that the cases we studied are the predictions of remodeling in the middle medial-lateral plane of a femur with an implant. A finite element method study (Verdonschot *et al.* 1992) shows that a three-dimensional model and a two-dimensional model with side plates predict similar stresses and displacement distributions in the middle medial-lateral plane.

Since no bending moment can be applied on an axisymmetric global model, while a real femur is predominantly loaded by a bending moment, the axisymmetric global model is not an appropriate model to study long term stability of a hip implant. The numerical results predicted by the two pseudo 3-D global models with and without abductor force are similar except for the remodeling in the region of the greater trochanter. The pseudo 3-D global model without abductor force does not contain the force of the abductor muscle in the region of the greater trochanter and therefore predicts a great deal of resorption in the region. The pseudo 3-D global model with abductor force predicts no resorption in the region of the greater trochanter. The numerical results show that the axial loads applied at the top of the implant and greater trochanter have no significant influence on bone remodeling. In fact, the axial load creates only less than 10 percent of total normal stress in the bone, and the average

shear stress created by an axial load along the bone-implant interface is less than 1 MPa. In other words, the stresses created by the axial load do not change the bone remodeling process significantly, as long as there is enough initial interference and enough initial bone ingrowth along the bone-implant interface.

Comparison of the numerical results with the animal experimental results at the local level shows that the numerical results are qualitatively consistent with experimental results. Due to the lack of data on the loading history in these experiments, a quantitative comparison is not possible at this time. The comparison of the numerical results with the clinical observation at the global level shows them to be qualitatively consistent. The loading history at the global level is better defined than that at the local level. However, the simplifications, i.e, a two-dimensional model with the assumptions of isotropy and homogeneity, employed in the calculations make the comparison at the global level only qualitatively possible.

The initial interference is assumed to be uniformly distributed in these calculations. Practically, the assumption is not attainable. However similar remodeling results will be predicted if there is enough initial ingrowth and interference along the upper and lower parts of the bone-implant interface. The numerical results show that bone remodeling does not depend highly on the initial ingrowth and initial interference.

The initial ingrowth can be viewed as the effect of wound healing. When an implant is placed in a femur, the initial reaction of bone is filling the cavities of the coated implant. The numerical remodeling process does not start until there is some calcifed bone filling the cavities. As in the case of the interface, the initial ingrowth is

assumed to be uniformly distributed along the bone implant interface. This assumption is made for starting a remodeling process with some of the effect of trauma reaction. The remodeling process results in an inhomogeneous distribution of bone ingrowth into the cavities of an implant. The bone remodeling process predicted does not really depend upon the assumption of a uniformly distributed initial ingrowth.

Although the initial interface, initial ingrowth and initial effective Coulomb friction coefficient are assumed to be uniformly distributed along the bone-implant interface, the local-global model itself does not depend upon that assumption. This assumption is made because the initial distributions of these parameters are unknown. Since the initial distributions must be assumed, the uniform distribution is a reasonable starting point.

The models used in this dissertation are useful for gaining understanding of bone remodeling at both the local and the global levels and for studying the long term stability of hip implants. The models can be used for numerically testing the stability of an implant and as aids in choosing good implant designs. Using numerical models to design animal experiments will be very cost effective, because computer analysis is much cheaper than animal experiments.

REFERENCES

Albrektsson T. and Albrektsson B., (1988) Implant fixation by direct bone anchorage, in Non-cemented total hip Arthroplasty, (editor: Fitzgerald, R.) Raven Press, New York, pp. 87-97.

Banerjee, P.K. and Butterfield, R., (1981) Boundary Element Methods in Engineering Science. McGraw Hill.

Brebbia, C.A., Telles, J.C.F and Wrobel, L.C., (1984) Boundary Element Techniques. Springer Verlag.

Carlsson, L. Rostlund T., Albrektsson, Bjorn, Albrektsson T. and Branemark P., (1986) Osseointegration of Titantium Implants, *Acta Orthop Scand*, **57**, pp. 285-289.

Cook, S. D., Barrack, R. L., Thomas, K. A. and Haddad, R. J., (1988) Quantitaive Analysis of Tissue Growth Into Human Porous Total Hip Components, *J. of Arthroplasty*, Vol. 3, No. 3, September.

Cowin, S.C and Hegedus, D.M., (1976) Bone Remodeling I: A Theory of Adaptive Elasticity, *J of Elasticity*, **6**, pp. 313-325

Cowin, S.C. and Van Buskirk, W.C., (1979) Surface bone remodeling induced by a medullary pin, *J. Biomechanics*, **12**, pp. 269-276

Cowin, S.C., (1981) Continuum models of bone adaptation to stress, The mechanical properties of bone (S.C. Cowin, ed.), ASME AMD **45**, pp. 193-211.

Cowin, S.C., (1985a) The relationship between the elasticity tensor and the fabric tensor, *Mech. Mater.* **4**, 137.

Cowin, S.C., Hart, R.T., Balser. J.R. and Kohn, D.H., (1985b) Functional adaptation in long bones: Establishing in vivo values for surface remodeling rate coefficients. *J. Biomechanics.* **18**, pp. 665-684.

Cowin, S.C., (1989) A resolution restriction for Wolff's law of trabecular architecture, Bulletin of the Hospital for Joint Diseases Orthopaedic Institute, **49**, pp. 206-213.

Cowin, S.C., Sadegh, A.M. and Luo, G.M., (1991) Correction formulas for the misalignment of axes in the measurement of the orthotropic elastic constants, Technical note, *Biomechanics*, **24**, No. 7, pp. 637-641

Cowin, S.C., Sadegh, A. M. and Luo, G.M., (1992) An evolutionary Wolff's law for

trabecular architecture, *J. Biomechanical Engineering*, **114**, pp. 129-136.

Cowin, S.C., Arramon, Y.P., Luo, G.M. and Sadegh, A.M., (1993) Chaos in the discrete-time algorithm for bone density remodeling rate equations, *J. Biomechanics*, **26**, pp. 1077-1089.

D'Antonio J. A., Capello, W. N., Crothers, O. D., Jaffe, W. L. and Manley, M. T. (1992) Early Clinical Experience with Hydroxyapatite-Coated Femoral Implants, *The Journal of Bone and Joint Surgery*, Vol. 74-A, No. 7, Augest.

Ducheyne, P., Radin, S., King, L., Ishikawa, K. and Kim, C., (1991) In vitro dissolution and precipitation of calcium phosphate phases on various bio materials correlates with in vivo bioactivity, *Bioceramics*, **4**, Proceedings of 4th Int. Sym. on Ceramics in Medicine, (edited by Bonfield, W., Hastings, G. and Tanner, E.) pp. 135-144.

Engh, C., Bobyn, J. and Glassman, A., (1987) Porous-coated hip replacement: the factors governing bone ingrowth, stress shielding, and clinical results, *J. Bone Jt. Surg.*, 69-B, pp. 45-55.

Engh, C., Mcgovern, T., Bobyn, J. and Harris, W., (1992) A quantitative evaluation of periprosthetic bone-remodeling after cementless total hip arthroplasty, *J. Bone Jt. Surg.*, 74-A, pp. 1009-1020.

Fitzgerald, R., (1988) Non-cemented total hip arthroplasty, Raven Press, New York.

Fyhrie, D.P. and Carter, D.R., (1986) A unifying principle relating stress to trabecular bone morphology, *J. Orthop. Res.* **4**, pp. 304-371

Haddad, R., Cook, S. and Brinker, M., (1990) A comparison of three varieties of noncemented porous-coated hip replacement, *J. Bone Jt. Surg.*, 72-B, pp. 2-8.

Harrigan, T.P, Jasty, M., Mann, R.W. and Harris, W.H., (1988), Limitations on the continuum assumption in cancellous bone, *J. Biomechanics*, **21**, pp. 269-276.

Harrigan, T.P., and Hamilton, J.J., (1992) An analytical and numerical study of the stability of bone remodeling theories: dependence on microstructural stimulus, *J. Biomechanics* **25**, pp. 477-488.

Harrigan, T. P., and Hamilton, J. J., (1993) Bone strain sensation via transmembrane potential channels in surface osteoblasts: loading rate and microstructural implications. *J. Biomechanics.* **26**, pp. 183-200.

Hart, R.T., Davy, D.T. and Heiple, K.G., (1984) Mathematical modeling and numerical solutions for functionally dependent bone, *Calc. Tissue Int.*, **36**, S11-S18.

Hibbitt, D., Karlsson, B., and Sorensen, P., (1991) The ABAQUS user manual, HKS Inc. Rhode Island.

Hori, R, and Lewis, J., (1982) Mechanical properties of the fibrous tissue found at the bone cement interface following total joint replacement. *J. Biomechanical Mat. Res.*, **16**, pp. 911-927.

Huiskes, R., and Chao, E., (1983) A survey of finite element analysis in orthopedic biomechanics: The first decade, *J. Biomechanics*, **16**, pp. 385-409.

Huiskes, R., Schouten, R., (1983) The effect of interface loosening on the stress distribution in intramedullary fixated artificial joints, Advances in Bioengineering, ASME, pp. 213-216.

Huiskes, R., Weinans, H., Grootenboer, H., Dalstra, M., Fudala, B. and Slooff, T., (1987) Adaptive bone-remodeling theory applied to prosthetic-design analysis. *J. Biomechanics*, **20**, pp. 1135-1150.

Huiskes, R., (1988) Stress patterns, failure modes, and bone remodeling, in Non-cemented total hip Arthroplasty, (editor: Fitzgerald, R.) Raven Press, New York, pp. 283-302.

Huiskes, R., Weinans, H., Summer, D., Fudala, B., Turner, T., Grootenboer and Galante, J., (1989) Stress-shielding, stress-bypassing and bone resorption around press-fit and bone-ingrowth THA, Proc. 35th ORS Ann. Meeting, 529.

Keaveny, T., and Bartel, D., (1991) Comparison of short-term load transfer mechanisms for Moor-type and anatomic-type cementless fixation hip prostheses, ASME AMD, **120**, pp. 89-92.

Keaveny, T., (1991) A finite element analysis of load transfer and relative motion for contemporary cementless hip implants in the short and long-term., Ph. D. Thesis, Cornell.

Kohn, D.H., Ko, C.C. and Hillister, S.J., (1992) Stress analysis of porous coated total joint replacements: coupled global/local modeling, BED-Vol.22, Advances in Bioengineering, ASME.

Lanyon, L.E., (1984) Functional strain as a determinant for bone remodeling. *Calcif. Tissue Int.* **36**, S56-S61.

Lewis, J., 1988, The mechanical state of the bone implant interface, in Non-cemented total hip Arthroplasty, (editor: Fitzgerald, R.) Raven Press, New York, pp. 23-30.

Ling, R., (1986) Observation of the fixation of implants to the bone skeleton, *Clin. Orthop.& Rel. Res.*, **210**, pp. 80-96.

Maniatopoulos, C., Pilliar, R. and Smith, D., (1986) Threaded versus porous-surfaced designs for implant stabilization in bone-endodontic implant model, *J. Biomedical Mat. Res.*, **20**, pp. 1309-1333.

Luo, G.M., Sadegh, A.M. and Cowin, S.C., (1991) The mean intercept length polygons for systems of planar nets, *J. of Materials Science*, **26**, pp. 2389-2396.

Luo, G.M., Cowin, S.C. and Sadegh, A.M., (1994) "Modeling bone ingrowth into implant cavities", in preparation

Luo, G.M., Cowin, S.C., Sadegh, A.M. and Arramon Y.P, (1994) "Implementation of strain rate as a bone remodeling stimulus", Submitted to *J. Biomechanics.*

Mann, K., (1991) Finite element analysis of cemented hip prostheses, Ph.D. Thesis, Cornell.

Mann, K., Bartel, D., and Wright, T., (1991) Cement stresses in a femoral hip component with Coulomb friction at the stem-cement interface, Proc. 37th ORS Ann. Meeting, 107.

Mann, K., Bartel, D., Wright, T. and Ingraffea, A., (1990) The role of friction at the stem PMMA cement interface. Proc. 36th ORS Ann. Meeting, 231.

McLeod, K.J. and Rubin, C.T., (1993) Strain oscillations in functionally loaded bone: A species independent determinant of skeletal morphology, *J. Biomechanics*, in press

Oh, I., (1988) Design rationale of interference-fit total hip prostheses, in Non-cemented total hip Arthroplasty, (editor: Fitzgerald, R.) Raven Press, New York, pp. 365-382.

Pilliar, R., Lee, J., and Manitopolous, C., (1986) Observations on the effect of movement on bone ingrowth into porous-surfaced implants, *Clin. Orthop. & Rel. Res.*, **208**, pp. 108-113.

Ricci, J.L., Spivak, J.M, Blumenthal, N.C. and Alexander, H., (1991) Modulation of bone ingrowth by surface chemistry and roughness, The Bone-Biomaterial Interface, (J.E. Davies, Ed.) University of Toronto Press, Toronto, Ontario, Canada, pp. 334-349.

Rohlmann, A., Cheal, E., Hayes, W. and Bergmann, G., (1988) A non-linear finite element analysis of interface conditions in porous coated hip end prostheses, *J. Biomechanics.*, **21**, pp. 605-611.

Rubin, C.T. and Lanyon, L.E., (1984) Regulation of bone formation by applied dynamic loads. *J. Bone Jt. Surg.* 66A, pp. 397-410.

Rubin, C.T. and Lanyon, L.E., (1987) Osteoregulatory nature of mechanical stimuli: function as a determinant for adaptive bone remodeling. *J. Orth. Res.*, **5**, pp. 300-307.

Sadegh, A.M., Cowin, S.C. and Luo, G.M., (1991) Inversions related to the stress-strain-fabric relationship, *Mechanics of Materials*, **11**, pp. 323-336

Sadegh, A.M., Luo, G.M. and Cowin, S.C., (1993) Bone ingrowth; an application of boundary element method to bone remodeling at the implant interface, *J. Biomechanics* **26**, No. 2, pp. 167-182.

Salzstein, R.A., Pollack, S.R., Mak, A. F. T., and Petrov, N., (1987) Electromechanical potentials in cortical bone-I. A continuum approach. *J. Biomech.* **20**, pp. 261-270.

Spivak, J., Blumenthal, N., Ricci, J. and Alexander, H., (1990) A new canine model to evaluate the biological effects of implant materials and surface coatings on intramedullary bone ingrowth, *J. Biomaterials*, **11**, pp. 79-82.

Stone, J., Beaupre, G. and Hayes, W., (1983) Multiaxial strength characteristics of trabecular bone, *J. Biomechanics.*, **16**, pp. 743-752.

Summer, D., Turner, T., Urban, R. and Galante, J., (1990) Bone remodeling two years after a cementless THE with proximally porous coated stem, Proc. 36th ORS Ann. Meeting, 207.

Turner, T., Summer, D., Urban, R. and Galante, J., (1987) Femoral remodeling associated with uncoated and porous coated cementless total hip arthroplasty., Proc. 33th ORS Ann. Meeting, 408.

Vaillancourt, H., and Johnson, W. R., (1990) A finite element model for porous implants, in Development and Design with Advanced Materials, Sih, G.C., Hoa, S.V., and Pindera, J.T., Eds., Elsevier, pp. 207-218.

Vanderby, R., Lewis, J. and Chapman, S., (1985) Biphasic modeling of fibrous tissue at the bone-prosthesis interface in total joints. 1985 Advances in Bioengineering, ASME, pp. 22-23.

Verdonschot, N., Huiskes, R., (1992) A comparison of anatomic, symmetric and 2-dimensional FEM models of femoral THA, personal communication.

Weinans, H., Huiskes, R. and Grootenboer, H., (1988) The mechanical effects of fibrous

tissue interposition at the cement-bone interface in THE, Proc. 33th ORS Ann. Meeting, 502.

Weinans, H., Huiskes, R. and Grootenboer, H., (1990a) Trends of mechanical consequences and modeling of a fibrous membrane around femoral hip prostheses, *J. Biomechanics*, **23**, pp. 991-1000.

Weinans, H., Huiskes, R. and Grootenboer, H.J., (1990b) Numerical comparisons of strain-adaptive bone-remodeling theories. Trans. First World Congress of Biomechanics. II, 75.

Weinans, H., (1991) Mechanically induced bone adaptation around orthopaedic implants, thesis, Nijmegen.

Weinans, H., Huiskes, R., Van Rietbergen, B., Summer, D., Turner, T. and Galante, J., (1992a) Adaptive bone remodeling analysis around bonded non cemented total hip arthroplasty: A comparison between animal experiments and computer simulation, *J. Orthop. Res.* **11**, No. 4, pp. 500-513.

Weinans, H., Huiskes, R. and Grootenboer, H., (1992b) Effects of material properties of femoral hip components on bone-remodeling, *J. Orthop. Res.* **11**, No. 6, pp. 845-853.

Weinans, H., Huiskes, R. and Grootenboer, H., (1992c) Effect of fit and bonding characteristics of femoral stems on adaptive bone-remodeling, to appear in *J. Arthroplasty.*

Weinans, H., Huiskes, R. and Grootenboer, H. J., (1992d) The behavior of adaptive bone-remodeling simulation models, *J. Biomechanics*, **25**, No. 12, pp. 1425-1441.

Weinans, H., Huiskes, R. and Grootenboer, H., (1993) Quantitative analysis of bone reactions to relative motions at implant-bone interfaces, *J. Biomechanics.* **26**, No. 11, pp. 1271-1281.

Wolfarth, D., Filiaggi, M. and Ducheyne, P., (1990) Parametric analysis of interfacial stress concentrations in porous coated implants, *J. Appl. Biomaterials*, **1**, pp. 3-12.

Weinbaum, S., Cowin, S.C., and Zeng, Yu, (1991) A model for the fluid shear stress excitation of membrane ion channels in osteocytic processes due to bone strain, Advances in Bioengineering (edited by R. Vanderby, Jr.), ASME, pp. 317-320.

Weinbaum, S., Cowin S.C. and Zeng, Yu, (1994) Excitation of osteocytes by mechanical loading-induced bone fluid shear stresses, *J. Biomechanics.* **27**, pp. 339-360.